



Norwegian University of
Science and Technology

Mechanical properties of bainitic and martensitic high strength steels in the hardened and untempered state

Åsne Salte Håland

Materials Science and Engineering (MTMT)

Submission date: June 2018

Supervisor: Ida Westermann, IMA

Co-supervisor: Erlend Sølvsberg, Kverneland Group Operations Norway AS
Morten I. Onsøyen, SINTEF

Norwegian University of Science and Technology
Department of Materials Science and Engineering

Preface

This master thesis has been conducted at the Norwegian University of Science and Technology (NTNU) in Trondheim, at the Department of Materials Science and Engineering during the spring of 2018. The work is a result of a cooperation between the Department of Materials Science and the RoHard project.


Åsne Salte Håland

Trondheim, June 2018
Åsne Salte Håland

Acknowledgments

I would like to thank my supervisors Associate Professor Ida Westermann (NV-IMA), Erlend Sølberg (Kverneland Group Operations Norway AS) and Morten I. Onsøyen (SINTEF) for feedback and guidance during the master thesis.

Further, I want to thank Tore Andre Kristensen and Hans Iver Lange at SINTEF for help with charpy testing, Pål Christian Skaret for help with tension testing, Morten Myren for sample machining, Yingda Yu for SEM training and Trygve Lindahl Schanche for lab training.

Finally, I would like to thank RoHard, represented here by the companies Kverneland Group, Trygg Nøsted Kjetting AS and Sintef Raufoss Manufacturing, which made this thesis possible.

Abstract

The objective of the research project named RoHard, is to increase the understanding of the interaction between the quality of the incoming materials, the hardening process and the resulting mechanical properties of the products [1]. In relation to that work, it was interesting to investigate the mechanical properties of bainitic and martensitic high strength steel with varying alloy content, in the hardened and untempered state. The steel alloys 42M13B, 50CrMo4, 100Cr6, 100CrSiMn6-5-4, 11M13CB, 18MnCrSiMoVB6, 27MnSiCrVB6 and 35MnCrMoVB5 were looked at.

This work has looked at the possibility to use steel austempered to a lower bainitic microstructure for purposes where martensite are used today. According to the literature, austempered steels should have benefits like less internal stresses, superior toughness and ductility at equivalent hardness, less distortion and no need for subsequent tempering [2, p. 485].

Three main hardening procedures have been performed. These are direct hardening, martempering and austempering. Before hardening, samples were austenitized at a higher temperature of 1200 °C followed by one lower temperature between 840-900 °C, or only at one lower temperature. Direct hardening was performed by quenching the samples in a salt bath at 180 °C directly from the austenitizing temperature. Martempering and austempering were performed by holding the samples a given time in the quenching bath, at a temperature 25 °C below M_s and just above M_s after austenitizing.

The hardening procedures were adjusted to the alloys based on alloy content, feedback from the steel producer Ascometal and the RoHard companies, in addition to performed experiments. This was done to be able to investigate mechanical properties of bainite vs. martensite at similar hardnesses. Steels with hardnesses around 700 and 400 HV were tested. The effect of prior austenite grain size on mechanical properties of bainite vs. martensite, in addition to the tendency of mechanical properties for different hardness categories and the effect of silicon on austempered steel was also investigated. The mechanical properties of the steels were found by use of hardness testing, notch-impact testing and tensile testing. In addition, examination of microstructure, prior austenite grain size determination and studying of fracture surfaces have been performed.

For a hardness of about 700 HV, read total energy from charpy testing was higher for direct hardened 42M13B than for austempered 100Cr6 and 100CrSiMn6-5-4. Stress at offset yield was higher for austempered 100Cr6 and 100CrSiMn6-5-4 than for direct hardened 42M13B and 50CrMo4. For a hardness of about 400 HV, austempered 18MnCrSiMoVB6, 27MnSiCrVB6 and 35MnCrMoVB5 showed a considerable lower read total energy from charpy testing than direct hardened 11M13CB, but the total area under the stress-strain curves were higher. Peak stress was higher for austempered 27MnSiCrVB6 and 35MnCrMoVB5 than for the direct hardened samples. And the austempered 18MnCrSiVB6 showed a slightly lower value of peak stress compared to direct hardened 11M13CB. All these samples were austenitized at only one lower temperature between 840-900 °C.

For austempered 100Cr6 and 100CrSiMn6-5-4 austenitized at 1200 °C followed by a lower austenitizing temperature between 840-900 °C and austenitized only at one lower temperature, the read total energy from charpy testing and stress-strain properties were decreasing with increasing prior austenite grain size. Direct hardened and martempered 42M13B and 50CrMo4 austenitized at 1200 °C followed by a lower austenitizing at 870 °C and austenitized only at one lower temperature, showed higher read total energy values for the fine grained samples of

42M13B compared to the coarser grained samples of this alloy. For 50CrMo4 the energy values were quite equal for all grain sizes. Stress at offset yield was increasing with decreasing grain size. All these samples had a hardness around 700 HV.

Direct hardening, martempering and austempering of 18MnCrSiMoVB6, 27MnSiCrVB6 and 35MnCrMoVB5, showed a trend where the values for hardness, stress at offset yield and peak stress were highest for the direct hardened samples, lower for the martempered samples and lowest for the austempered samples. Read total energy values from charpy testing of 18MnCrSiMoVB6 and 27MnSiCrVB6 were highest for the martempered samples, lower for the direct hardened samples and lowest for the austempered samples. The values for read total energy of 35MnCrMoVB5, were quite equal for all heat treatments. The ductility was highest for the austempered samples, lower for the martempered samples and lowest for the direct hardened samples.

Austempered 100CrSiMn6-5-4 showed poorer mechanical properties compared to austempered 100Cr6. A considerable difference between these alloys was the higher content of silicon in 100CrSiMn6-5-4.

Samandrag

Formålet med RoHard-prosjektet er å gje auka forståing av samspelet mellom kvaliteten på inngåande material, herdeprosessen og dei mekaniske eigenskapane til det resulterande produktet [1]. I forbindelse med dette arbeidet er det interessant å sjå på mekaniske eigenskapar for bainittiske og martensittiske høgstyrkestål med varierende legeringsinnhald, i herda og uanløpt tilstand. Legeringane som har blitt undersøkt er 42M13B, 50CrMo4, 100Cr6, 100CrSiMn6-5-4, 11M13CB, 18MnCrSiMoVB6, 27MnSiCrVB6 og 35MnCrMoVB5.

Dette arbeidet har sett på moglegheita for å kunne bruke stål herda til ein bainittisk mikrostruktur til formål der martensitt i dag blir brukt. Ifølge litteraturen har austempererte stål fordeler som mindre indre spenningar, betre seigheit og duktilitet ved lik hardleik, mindre kast og etterfølgjande anløping er ikkje nødvendig [2, p. 485].

Dei tre herdeprosessane direkteherding, martemperering og austemperering har blitt utført. Før herding blei prøvane austenittisert ved ein høg temperatur på 1200 °C etterfølgd av ein lågare temperatur mellom 840-900 °C, eller berre ved ein lågare temperatur. Direkteherding har blitt utført ved å kjøle stålet i eit 180 °C saltbad etter austenittisering. Martemperering og austemperering har blitt utført ved å halde prøvane ei viss tid i badet ved ein temperatur 25 °C under M_s og rett over M_s etter austenittisering.

Herdeprosessane har blitt tilpassa legeringane basert på legeringsinnhald, innspill frå stål produsenten Ascometal og prosjektbedrifter i RoHard, i tillegg til utførte eksperiment. Dette blei gjort for å kunne sjå på mekaniske eigenskapar for bainitt samanlikna med martensitt for stål med omtrent same hardleik. Testing vart utført på stål med ein hardleik omkring 700 og 400 HV. Effekten av tidlegare austenittkornstorleik på mekaniske eigenskapar til bainitt samanlikna med effekten for martensitt, i tillegg til tendensar i resultatata ved samanlikning av stål i forskjellige hardleiksområder og effekten av silisium på austemperert stål har blitt undersøkt. Dei mekaniske eigenskapane til ståla har blitt funne ved bruk av hardleiksmåling, slagpendelprøving og strekktesting. I tillegg har det blitt sett på mikrostruktur, tidlegare austenittkorgrenser og brotflater.

Slagpendelprøving ved ein hardleik på ca. 700 HV viste høgare energi for direkteherda 42M13B samanlikna med austemperert 100Cr6 og 100CrSiMn6-5-4. Flytespenninga var høgare for austemperert 100Cr6 og 100CrSiMn6-5-4 enn for direkteherda 42M13B og 50CrMo4. Energien etter slagpendelprøving av austemperert 18MnCrSiMoVB6, 27MnSiCrVB6 og 35MnCrMoVB5 ved ein hardleik på ca. 400 HV var betydeleg lågare enn for direkteherda 11M13CB, men det totale arealet under spenning-tøynings-kurva var høgare. Brotstyrken var høgare for austemperert 27MnSiCrVB6 og 35MnCrMoVB5 enn for dei direkteherda 11M13CB, medan den var noko lågare for austemperert 18MnCrSiVB6. Alle desse prøvane var austenittisert ved berre ein lågare temperatur mellom 840-900 °C.

For austemperert 100Cr6 og 100CrSiMn6-5-4 austenittisert ved 1200 °C etterfølgd av ein lågare austenittiseringstemperatur mellom 840-900 °C og austenittisering ved berre ein lågare temperatur, viste mekanisk testing at energien etter slagpendelprøving og spenning-tøynings-eigenskapane blei lågare eller dårlegare ved aukande tidlegare austenittkornstorleik. Direkte herda og martemperert 42M13B og 50CrMo4 austenittisert ved 1200 °C etterfølgd av ein lågare austenittiseringstemperatur på 870 °C og austenittisert ved berre ein lågare temperatur, viste betre slagpendelenergi-verdiar for prøver av 42M13B med liten kornstorleik, enn for prøver med større kornstorleik av denne legeringa. For 50CrMo4 var energi verdiane tilnærma like for alle kornstorleikar. Flytespenninga auka med minkande kornstorleik. Alle desse prøvane hadde ein

hardleik på omkring 700 HV.

Direkteherding, martemperering og austemperering av 18MnCrSiMoVB6, 27MnSiCrVB6 og 35MnCrMoVB5 viste ein trend der hardleiksverdiane, flytespenninga og brotstyrken var høgast for dei direkteherda prøvane, lågare for dei martempererte prøvane og lågast for dei austempererte prøvane. Dei målte slagpendelverdiane for 18MnCrSiMoVB6 og 27MnSiCrVB6 var høgast for dei martempererte prøvane, lågare for dei direkteherda prøvane og lågast for dei austempererte prøvane. For 35MnCrMoVB5 var desse verdiane tilnærma like for alle dei utførte varmebehandlingane. Duktiliteten var høgast for dei austempererte prøvane, lågare for dei martempererte prøvane og lågast for dei direkteherda prøvane.

Austemperert 100CrSiMn6-5-4 gav dårlegare mekaniske eigenskapar enn austemperert 100Cr6. Ein betydelig skilnad mellom desse to legeringane, var det høge innhaldet av silisium i 100CrSiMn6-5-4.

Contents

Preface	i
Acknowledgments	iii
Abstract	v
Samandrag	vii
1 Introduction	1
2 Theory	3
2.1 The iron - iron carbide phase diagram	3
2.2 Phase transformation hardening of steel	4
2.2.1 Strengthening mechanisms	4
2.2.2 Transformation diagrams	5
2.2.3 Martensite transformation	5
2.2.4 Bainite transformation	7
2.2.5 Retained austenite	9
2.2.6 Quenching stress and quench cracking	9
2.2.7 Quenching media	9
2.3 Hardening processes	10
2.3.1 Direct hardening	10
2.3.2 Martempering	10
2.3.3 Austempering	11
2.4 Effect of alloying elements	12
2.5 Grain growth kinetics	15
2.6 Effect of grain size	16
2.6.1 Grain size determination	16
2.7 Mechanical test methods	16
2.7.1 Notch - impact test	16
2.7.2 Tension test	17
2.8 Inspection of microstructure	18
2.9 Electron fractography	19
3 Materials and experimental techniques	21
3.1 Chemical composition	21
3.2 Condition at delivery	24
3.3 Macro etching for investigation of segregations	24
3.4 Sampling	24
3.5 Naming of samples	25
3.6 Hardening	28
3.6.1 M_s and austempering temperatures	28
3.6.2 Direct hardening	33
3.6.3 Martempering	33
3.6.4 Austempering	34
3.7 Investigation of microstructure and prior austenite grains	35
3.7.1 Sample preparation	35
3.7.2 Etching	36

3.7.3	Inspection of microstructure	36
3.7.4	Measuring of prior austenite grain size	37
3.7.5	EBSD	37
3.8	Notch-impact test	37
3.8.1	Specimen geometry	37
3.8.2	Charpy testing	38
3.8.3	Data processing	39
3.8.4	Inspection of fracture surfaces	39
3.9	Tension test	40
3.9.1	Specimen geometry	40
3.9.2	Tensile testing	41
3.10	Hardness testing	41
4	Results	43
4.1	Grain size determination	43
4.2	Microstructure	48
4.2.1	EBSD	54
4.3	Notch-impact test	55
4.3.1	Key data	55
4.3.2	Fracture surfaces	56
4.4	Tension test	63
4.4.1	Stress-strain curves	63
4.4.2	Key data	68
4.5	Hardness testing	70
4.5.1	Microhardness testing	73
5	Discussion	75
5.1	Mechanical properties of bainite vs. martensite at similar hardness	75
5.1.1	700 HV	75
5.1.2	400 HV	77
5.2	Effect of prior austenite grain size on mechanical properties of bainite vs. martensite	79
5.2.1	Prior austenite grain sizes	79
5.2.2	Bainite	81
5.2.3	Martensite	81
5.2.4	Comparison	83
5.3	Tendency of mechanical properties for different hardness levels	83
5.4	The effect of silicon on austempered 100Cr6 and 100CrSiMn6-5-4	85
6	Conclusion	87
7	Further work	89
8	Reference	91
9	Appendix	93
A	Converting weight percent to atomic percent	93
B	Control measurement of notch-impact samples	94
C	Key data for all tested notch-impact samples	95
D	Fracture surfaces	96

1 Introduction

Kverneland Group, Trygg Nøsted Kjetting AS and SINTEF Raufoss Manufacturing are together with other companies involved in a joint industry research project called RoHard (Robust and advanced steel quenching processes). The project runs over four years and is founded by the Research Council of Norway. The goal of this project is to increase the understanding of the interaction between the quality of the incoming materials, the hardening process and the resulting mechanical properties of the products. In addition, they are working for a better understanding of how variations of incoming materials, process changes and process variations, at hardening, define the resulting material- and product properties. This will contribute to minimised scrap production, optimised cost and increased speed to market for new product developments [1].

This work is a continuation of the project work *Mechanical properties of steels for quenching and tempering in the hardened and untempered state* [3], performed at NTNU autumn 2017 in collaboration with Kverneland Group. During the project work, mechanical testing of the two alloys 42M13B and 50CrMo4 in the hardened and untempered state were performed. The purpose is now to continue the same kind of work, with the main focus on bainite instead of martensite. Several of the companies involved in RoHard are interested in investigating if bainite can be used as an alternative to martensite. The three hardening procedures direct hardening, martempering and austempering have therefore been discussed.

Before hardening, samples were austenitized at a higher temperature of 1200 °C followed by one lower temperature between 840-900 °C, or only at one lower temperature. Direct hardening was performed by quenching the samples in a salt bath at 180 °C directly from the austenitizing temperature. Martempering and austempering were performed by holding the samples for a given time in the quenching bath, at a temperature 25 °C under M_s and just above M_s after austenitizing.

The steel alloys 42M13B and 50CrMo4 were in the project work direct hardened and martempered to approximately 700 HV. These alloys have in this work been compared with austempered 100Cr6 and 100CrSiMn6-5-4, in the same range of hardness. Direct hardening of 11M13CB have also been performed, which should give a hardness around 400 HV. The bainitic alloys 18Mn-CrSiMoVB6, 27MnSiCrVB6 and 35MnCrMoVB5 were austempered to function as comparison at the same range of hardness. 700 HV are relevant for plough shears produced by Kverneland and Trygg are interested in chains with a hardness around 400 HV. The plough shears are today verified by hardness and geometrical measurements. Characterizing of mechanical properties of the shears were performed in the project work and is in this work given by the properties of direct hardened 42M13B. Minimum hardness for current plough shears are 615 HV. The mechanical properties of the chains are not fully characterized, but should have a minimum hardness between 350-400 HV and the ultimate tensile strength are one of the most important properties.

The effect of prior austenite grain size on mechanical properties of bainite vs. martensite have been investigated for 42M13B, 50CrMo4, 100Cr6 and 100CrSiMn6-5-4 hardened from 1200 °C followed by a lower austenitizing temperature between 840-900 °C and hardened from only one lower austenitizing temperature, with a hardness of about 700 HV. This is interesting because of the benefits of bainite and since reducing the required number of austenitizing treatments to only one time, will be beneficial in the production of plough shears. This would lead to reduced production time, less energy consumption and require less manufacturing storage area.

In addition, different tendencies in results by comparing direct hardened, martempered and austempered 18MnCrSiMoVB6, 27MnSiCrVB6 and 35MnCrMoVB5 in different hardness categories were studied. Finally, the effect of silicon on austempered steel were looked at.

The main advantage with using bainite compared to martensite, is probably that hardening to bainite results in less internal stresses in the material, due to isothermal transformation [2, p. 485]. Internal stresses, which are a result of phase transformation and temperature gradients in steel, gives risk for cracking. By using austempering and also martempering, the idea is to separate those stress-raisers and thus reduce the brittleness. Martempering is here a variant of tempered martensite. The lower bainite is more ductile and tougher than tempered martensite at equivalent hardness [2, p. 485]. However, the lower bainite has a lower yield strength owing to that the bainite sheaf is larger than the tempered martensite plate [4]. Austempering lead to less distortion and no subsequent tempering is required [2, p. 485].

If it should be applicable to use bainite instead of martensite, it is important that the mechanical properties are sufficient, i.e about as good as those today achieved for martensite. The mechanical properties of the steels were found by use of hardness testing, notch-impact testing and tensile testing. In addition, examination of microstructure, grain size determination and studying of fracture surfaces have been performed.

2 Theory

2.1 The iron - iron carbide phase diagram

The metastable Fe-Fe₃C phase diagram is shown in Figure 1. The part of the phase diagram that is applicable for steel, is the part with low carbon content up to 2 wt. %. At higher carbon content cast iron is represented [5, p. 2-3]. The eutectoid point in the phase diagram is found where the carbon content is 0.76 wt. % and the temperature is 723°C (A₁). Based on the eutectoid point, one can distinguish between hypoeutectoid alloys, with a carbon content between 0.022 and 0.76 wt. % and hypereutectoid alloys with a carbon content between 0.76 and 2 wt. %.

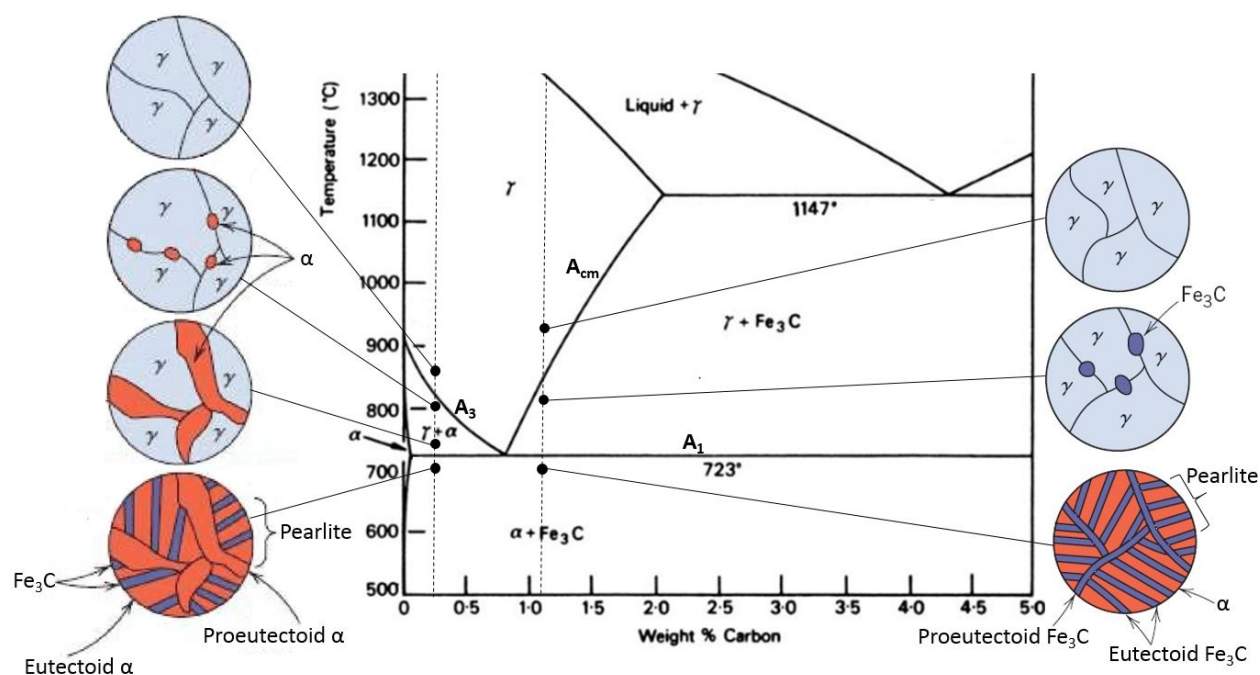


Figure 1: The metastable Fe-Fe₃C phase diagram [6, p. 40] with schematic representations of the microstructures for an iron-carbon hypoeutectoid composition (left) and hypereutectoid composition (right) [7, 324-327].

By heating to above A₃ (the boundary line between austenite (γ) and austenite + ferrite (α)), the microstructure consists of austenite with FCC (face-centered cubic) structure. With slow cooling of an alloy with hypoeutectoid composition from this area, precipitation of ferrite with BCC (body-centered cubic) structure will start when the temperature decreases below A₃. The steel is now in the $\alpha + \gamma$ area and both ferrite and austenite will coexist in the microstructure. Precipitation of ferrite takes place mainly on the original austenite grain boundaries. When cooling through the two-phase region, the carbon content in the ferrite and austenite will change, depending on the phase boundary lines. The amount of ferrite will increase with reduced temperature in the two-phase region. When the temperature decreases below A₁, all the austenite will transform to pearlite. The microstructure will then consist of a mixture between pearlite (Fe₃C and eutectoid ferrite) and proeutectoid ferrite [7, p. 324-325]. The microstructure of an iron-carbon hypoeutectoid composition are schematically illustrated on the left side in Figure 1.

If a hypereutectoid alloy is slowly cooled from the austenite area, cementite will be formed along the initial austenite grain boundaries, when A_{cm} is crossed. This cementite is called proeutectoid cementite and the composition remains constant as the temperature changes. When the temperature decreases below A_1 the austenite is converted into pearlite and the resulting microstructure consists of pearlite and proeutectoid cementite [7, p. 327]. The microstructure for an iron-carbon hypereutectoid composition are schematically illustrated on the right side in Figure 1.

2.2 Phase transformation hardening of steel

Hardening is the process used to create a microstructure consisting of martensite or bainite. The purpose of the hardening process is to increase the hardness or strength of the steel. Briefly, the process involves heating the steel to a temperature in the austenite region (austenitizing). When the whole material has reached the austenitizing temperature, the steel is quenched in a suitable quenchant [2, p. 359].

Hardenability tells how easy it is for a steel to harden to a fully martensitic microstructure. When the hardenability is poor, fast cooling rates are required to harden the steel. In the case of good hardenability, slower cooling rates may be applied [5, p. 45]. The necessary quenchant depends on the hardenability of the steel and the dimensions of the material being hardened.

Austenite grain size and chemical composition are the two most important variables that influence hardenability. The hardenability increases with increasing austenite grain size. When the austenite grain size increases, the grain boundary area per volume decreases and therefore it is a reduced amount of sites for nucleation of ferrite and pearlite. The transformation of ferrite and pearlite will slow down, and the hardenability therefore increases. All alloying elements that slow down this transformation will increase the hardenability [6, p. 176].

2.2.1 Strengthening mechanisms

Strengthening by hardening is the dominating strengthening mechanism, but steel can also be strengthened by work hardening, solid solution strengthening, refinement of grain size, dispersion strengthening, order hardening and size and shape effects.

Work hardening is an important strengthening process in steel. Strengthening arises from creation of crystal defects, primarily dislocations, during plastic deformation.

Solid solution strengthening occurs when the strain fields around misfitting solutes interfere with the motion of dislocations. The strengthening will depend on the difference in atomic size between the solute and iron atoms. Solid solution strengthening by interstitial atoms is caused by the addition of small impurity atoms between the iron atoms, like carbon and nitrogen. Substitutional solution strengthening is when solute or impurity atoms replace or substitute for the host atoms [8, p. 24-54]. Most of the strengthening in martensitic steels comes from carbon in solid solution. Since carbon atoms are positioned in non-regular octahedral sites and will interact strongly with dislocations. In bainite this effect is less, since carbon is precipitated as cementite or it is partitioned into the austenite [9].

One of the most important strengthening routes in the heat treatment of steel is the refinement of grain size of ferrite. This effect is given by the Hall-Petch equation, which will be further explained in Section 2.6.

Steels are further strengthened by controlling the precipitation of other phases in the microstructure like carbides, nitrides and intermetallic compounds. Most dispersion lead to strengthening, but they can have adverse effect on ductility and toughness [8, p. 24-54].

2.2.2 Transformation diagrams

A TTT diagram (Time-Temperature-Transformation diagram) can be looked at when the hardenability of a steel is going to be examined. But, they are only rough guides since the kinetics of transformation of austenite is carried out isothermally [6, p. 168]. It holds when the material is taken very rapidly from a certain starting point to the relevant temperature and is held there isothermally [2, p. 63]. The isothermal TTT diagrams have limitations for situations involving cooling rates through the transformation temperature range. Therefore the more representative CCT diagram (continuous cooling transformation diagram) has been developed. In these diagrams the process of the transformation with increasing temperature for series of cooling rates are recorded [6, p. 168-169]. An illustration of a CCT diagram for steel is shown in Figure 2. From the figure it can be seen that the microstructure formed is dependant on the cooling rate from the austenite region. The two cooling lines show a faster cooling rate of the surface than for the core of the material.

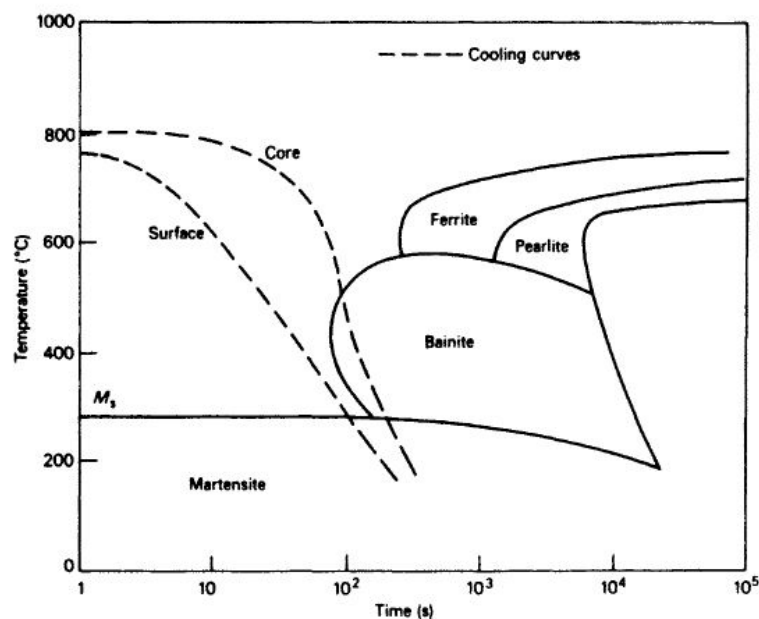


Figure 2: Illustration of a CCT diagram for steel. The microstructure formed depends on the cooling rate. The cooling rate of the surface is faster than for the core [6, p. 170].

2.2.3 Martensite transformation

Martensite is generally formed when an austenitized steel is rapidly cooled to a relatively low temperature. When the super cooling is sufficient, plates and/ or needles will grow from austenite boundaries. This metastable phase is the martensite [5, p. 31-32]. Because martensite is a non-equilibrium phase, it does not appear in the iron-iron carbide phase diagram. The transformation of austenite to martensite is, however represented on the isothermal transformation diagram [7, p. 363]. Martensite is a very hard phase and carbon that was in solid solution in the

austenite remains in solution in the new phase. The microstructure is formed by a deformation of the austenite lattice and there are no diffusion of atoms. The change in the shape when BCT (body-centered tetragonal) martensite is formed, causes large shear deformation and a volume expansion [6, p. 95].

Since the formation of martensite is a diffusionless transformation, there exists no lower temperature boundary. The transformation requires continuous cooling for the transformation process to be continued. There are two important temperatures for matensite transformation, and that are the martensite start temperature, M_s , and the martensite finish temperature, M_f . M_f is defined at the point where 95 % of the martensitic transformation is completed. With quenching from the austenite area, the temperature have to decrease to M_s before the super-cooling is large enough for the martensite transformation to start. Continuous cooling from this temperature is required, if not, carbon will start move to the dislocations and the transformation of austenite to matensite will stop [5, p. 31-32].

The M_s temperature can be found from empirical formulas as:

$$M_s (^{\circ}C) = 539 - 423 C - 30.4 Mn - 17.7 Ni - 12.1 Cr - 7.5 Mo \text{ (wt.\%)} \quad (1)$$

$$M_s (^{\circ}C) = 561 - 474 C - 33 Mn - 17 Ni - 17 Cr - 21 Mo \text{ (wt.\%)} \quad (2)$$

The equations are taken from two different sources, Equation 1 from [8, p. 159] and Equation 2 from [2, p. 60]. They show the effect of different alloying elements on the M_s temperature. Most alloying elements which enter into solid solution in austenite lower the M_s . Exceptions are cobolt and aluminum. Carbon is the alloying element having the largest influence on the M_s temperature and manganese the second largest. The uncertainty of the equations such as Equation 1 and 2 are about $\pm 20^{\circ}C$ [8, p.159]. The validity is limited with regards to alloy content. For Equation 1 the limit of data are given in Table 1. Equation 2 is available for low-alloy carbon steel [2, p. 60]. CCT or TTT diagrams can also be used for determination of M_s .

Table 1: *The limit of the data on witch Equation 1 is based [8, p. 159]*

	C	Mn	Si	Ni	Cr	Mo
Minimum [wt. %]	0.11	0.20	0.11	0.00	0.00	0.00
Maximum [wt. %]	0.55	1.67	1.74	5.04	3.34	1.00

The effect of carbon content on M_s and M_f is shown in Figure 3. M_s and M_f are decreasing with increasing carbon content. At a carbon content of 0.7 wt. %, M_f is equal to $0^{\circ}C$. Deep cooling is therefore needed for the transformation of austenite to be continued.

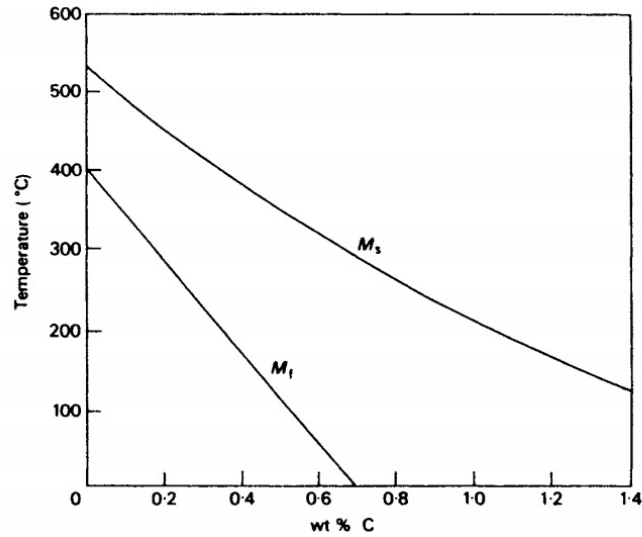


Figure 3: The effect of carbon on M_s and M_f [6, p. 116].

2.2.4 Bainite transformation

The microstructure of bainite consists of plates or needles that grow from austenite grain boundaries at high super-cooling. The structure can be formed under continuous rapid cooling from the austenite area. Not so rapid that martensite is formed, but fast enough to avoid formation of pearlite and ferrite. The bainite that occurs during continuous cooling transformation, is called granular bainite [8, p. 194-195]. Bainite can also be formed isothermally after quenching from an austenitizing temperature [5, p. 27]. Bainite is a hard structural constituent with hardness close to that of martensite [2, p. 485]. Figure 4 illustrates the sequence of transformations expected at varying isothermal transformation temperature.

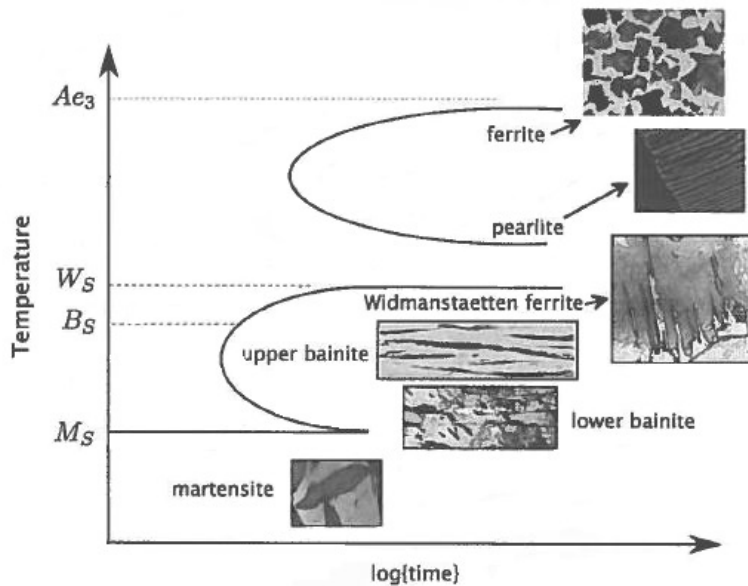


Figure 4: An illustration of microstructures that can be generated during the isothermal transformation of austenite [8, p. 180].

Bainite is often divided into two main types, upper and lower bainite, depending on the transformation temperature and resulting microstructure. Upper bainite appears in the temperature range between 550-400°C and lower bainite in the temperature range between 400-250°C [6, p. 129-132].

Upper bainite is formed in two distinct stages. The first stage involve formation of fine plates of ferrite, that nucleates on the austenite grain boundaries. The plates eventually retain little carbon in solid solution (<0.02 wt.%). The remaining austenite is therefore enriched in carbon [8, p. 180-183]. Due to the relatively high formation temperature, the carbon has time to diffuse to the interface between the plates, here cementite particles are formed [5, p. 27].

Lower bainite has a microstructure which are very similar to upper bainite. The major distinction is that the transformation temperature is lower, so the carbon particles also precipitate inside the plates of ferrite. The carbides precipitated in upper bainite are cementite and in lower bainite the carbides are either cementite or ϵ - carbides [5, p. 27-28]. The mechanism of bainite reaction is illustrated in Figure 5, for upper and lower bainaite.

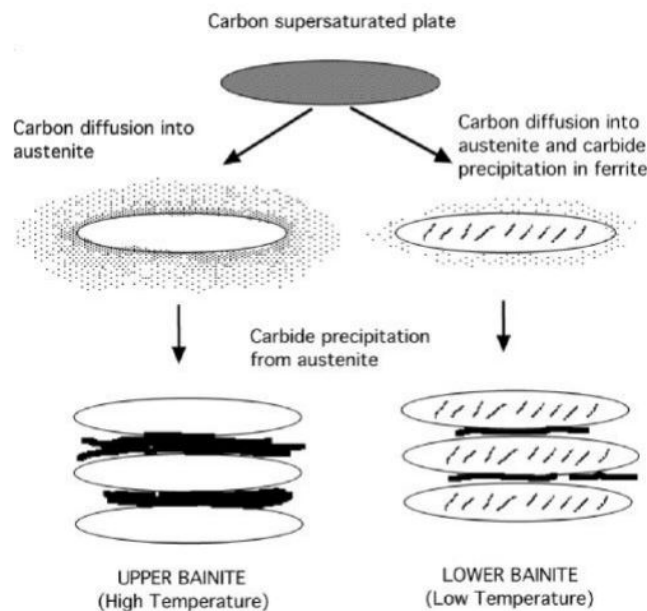


Figure 5: *The mechanism of bainite reaction [8, p. 193].*

The carbides in lower bainite are extremely fine and because they precipitate within the ferrite, a smaller amount of carbon is left into the residual austenite. This means that fewer and finer cementite particles precipitate between the ferrite plates, compared to the microstructure for upper bainite. This is why lower bainite with its highly refined microstructure is much tougher than upper bainite, in spite of the fact that it also tends to be stronger [8, p. 185].

In a mixed microstructure, when bainite forms it enriches the residual austenite with carbon, so that the strength of the subsequent martensite increases. In addition, during its deformation, the strength of the bainite is enhanced via plastic constraint by the surrounding stronger martensite. So bainite in an mixed structure with martensite, will have higher strength than 100 % pure bainite [9].

2.2.5 Retained austenite

Retained austenite is austenite that does not transform to martensite upon quenching. The microstructure occurs when the steel is not quenched to M_f , and 100 % martensite is not formed. The amount of retained austenite is a function of carbon content, alloy content (especially nickel and manganese), quenchant temperature and subsequent thermal and/or mechanical treatments [10].

The presence of retained austenite influence the mechanical properties in steel. Martensite is hard, strong and brittle while austenite is soft and tough. Surface hardness and compressive residual stresses decrease with increasing amount of retained austenite. The good ductility in the austenite phase prevents propagation of cracks and stress gradients is leveled out [2, p. 388]. Retained austenite itself is a ductile face but the fact that it can transform into martensite during deformation can alter the mechanical behaviour of the microstructure as a whole [11, p. 314].

2.2.6 Quenching stress and quench cracking

During quenching, red-hot samples of steel are being plunged into a lower temperature fluid. The instant effect is evaporation of the fluid near/on the sample surface. During evaporation, the cooling rate is slow because the vapour shields the sample from the fluid. Once the vapour film has collapsed, the heat transfer rate increases dramatically. This is due to the rapid removal of heat, while the liquid that touches the sample is boiling off. Heat transfer slows down, when the sample reaches a temperature less than the boiling temperature of the fluid. This is because the heat transfer primarily occurs by conduction and convection [8, p. 228]. This contributes to varying cooling rate and therefore distortion.

While quenching steels, there are always a risk for distortion and even serious cracking. These problems arise because of internal stresses in the material developed during quenching. The internal stresses come from thermal stresses and transformation stresses. Thermal stresses arise because of the different temperature gradient from the surface to the core. Transformation stresses appear due to the volume change when austenite transforms to other phases. The residual stress in the material at room temperature increases with increasing cooling rate because the temperature difference between the core and the surface increases with more rapid quenching [6, p. 179]. Distortion can therefore be reduced by using a less drastic quenching media. The transformation stresses depend on the hardenability of the steel and on whether the transformation at surface and core start simultaneously. The change in volume during the transformation increases with reduced M_s temperature and higher transformation stresses are developed [6, p. 179-181].

2.2.7 Quenching media

It is important to quench the steel sufficiently fast to get the desired microstructure and hardness, but not faster than needed so that the amount of thermal stresses is as small as possible. There are many types of quenchants available with different cooling capacities. The most commonly used are water, quenching oils, polymer quenchants, salt baths and certain gases [2, p. 559].

A salt bath contains a combination of nitrite and nitrate salts. Quenching in this medium normally results in little distortion. This is a consequence of the slow cooling rate below the martensite transformation temperature, and that all heat transfer when quenching in salt occurs by convection. The salt bath usually consists of a mixture of sodium nitrite and potassium nitrate and the quenchant temperatures is normally 180-200°C, but can be up to 500°C [2, p. 576]. To regulate the cooling efficiency, water can be added to the bath. A small addition of water to a salt bath increases its quench severity significantly. It should be noted that water will evaporate if the system is not closed. The degree of agitation will also regulate the cooling efficiency and it is necessary to disperse the water uniformly in the salt.

2.3 Hardening processes

2.3.1 Direct hardening

Direct hardening refers to quenching directly from the austenitizing temperature. The quenching has to be done rapidly enough to prevent transformation from austenite to pearlite, ferrite and bainite. Martensite is the desired microstructure [2, p. 489-490]. Figure 6 shows an illustration of direct hardening and martempering (modified) where a martensitic microstructure is formed and austempering where a bainitic microstructure is formed as function of time and temperature.

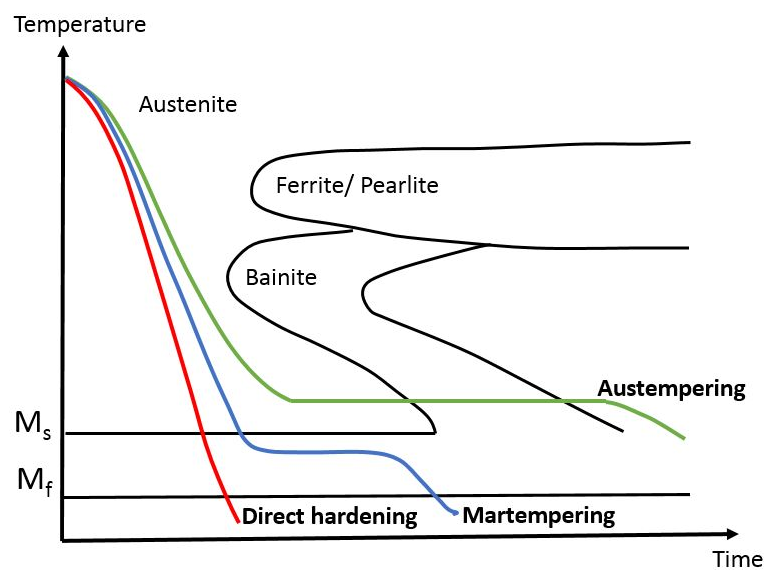


Figure 6: Illustration of cooling rate during direct hardening, martempering (modified) and austempering as function of time and temperature.

2.3.2 Martempering

When martempering is performed, the steel is first cooled from the austenitizing temperature to a martempering temperature, usually just above M_s in a suitable quenchant, as shown in Figure 7 (a). The material is held in the quenchant until the steel temperature is approximately uniform. The time in the martempering bath depends on section thickness, type of steel, temperature and degree of aggregation in the bath. After this, the steel is cooled to room

temperature, usually in air. Here moderate cooling rate is required to prevent large differences in temperature between the surface and the core of the material. This heat treatment gives mainly a microstructure consisting of untempered and brittle martensite through the material.

The advantages with martempering compared to conventional quenching is the reduction in the thermal gradient between the surface and the center of the material. This reduction occurs because the material is quenched to an isotherm temperature followed by air-cooling to room temperature. The residual stress developed during martempering is reduced. This happens because the greatest thermal variations occurs when the steel is austenitic and because the final transformation and thermal changes occur throughout the material at approximately the same time.

Modified martempering is nearly the same as martempering, except for a different temperature in the quenching bath. The temperature in the bath is in this case just below the M_s temperature, as shown in Figure 7 (b). This reduction in temperature is important for steels with low hardenability, because the quenching effect is improved. This is why modified martempering can be used to a greater range of steel compositions than the standard process [12, p. 137-151]. Modified martempering is also illustrated in Figure 6.

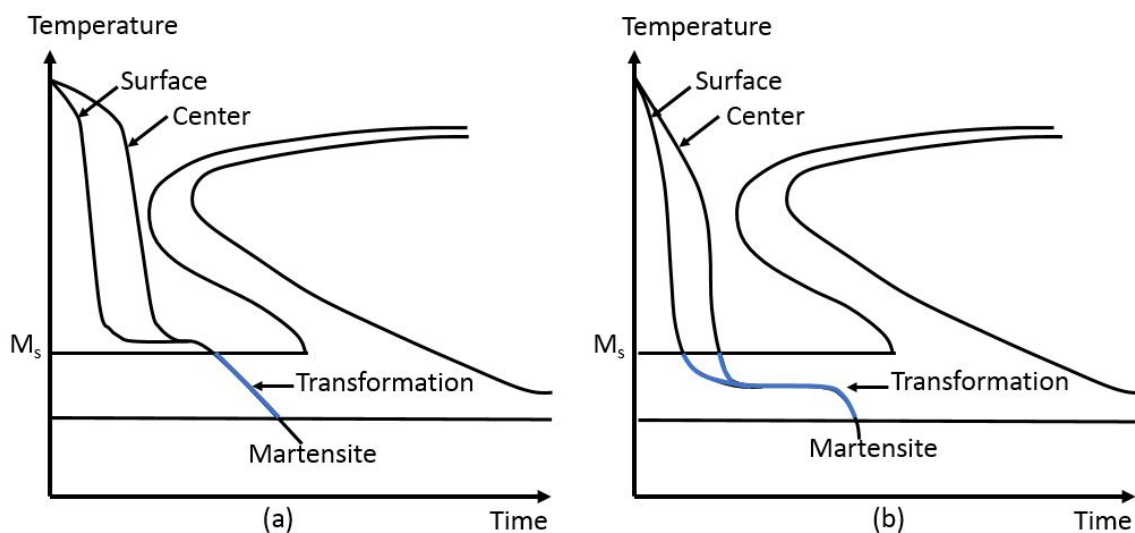


Figure 7: Temperature sequences for Martempering (a) and Modified martempering (b) [12, p. 137].

2.3.3 Austempering

The cooling process where austenite transforms to a bainitic microstructure is called austempering. Bainite transformation has the character of diffusion controlled transformation, which is to say that it takes some time since diffusion of carbon is required [2, p. 485]. During austempering the steel is heated to required austenitizing temperature, as for direct hardening and martempering. The material is then quenched. To achieve a homogeneous microstructure, the material quality and the quenching ability of the quenchant must be sufficient to allow the cooling curves to pass the pearlite and bainite noses by isothermal quenching [13, p. 24]. Transformation of bainite occurs isothermally at lower temperatures than pearlite, but above the M_s temperature. The holding time in the salt bath is usually longer than for martempering.

The process has several advantages over martensitic hardening. The main advantage is probably that hardening to bainite result in less internal stresses in the material, due to isothermal

transformation. The bainite formed is more ductile and tougher than martensite with the same hardness, which gives greater usable strength. Formation of an bainitic microstructure lead to less distortion than with martensitic hardening. There is therefor less need for subsequent machining. Austempered parts have no residual tensile stresses in the surface, which are seen for through hardened martensitic parts. The residual tensile stress can lead to worsening of the mechanical properties and entails a risk for cracking. I addition, austempering requires no subsequent tempering. [2, p. 485].

Disadvantage with austempering are that the dwell time might be very long and therefore the process might get uneconomical. The process parameters have to be carefully adjusted to the material and the parts geometry. In addition the austempered material usually does not achieve the same maximum hardness as martensitic hardened material [13, p. 25].

2.4 Effect of alloying elements

The influence carbon has on the martensite hardness is shown in Figure 8. At approximately 0.7 wt. % C, the M_f temperature of the steel is 0 °C. For a higher carbon content, retained austenite will be formed, as previously mentioned, if water is used as cooling agent. This causes reduction in hardness, as shown by the split line for martensite in Figure 8. Increased carbon content increases the hardness. But the increase also results in lack of toughness, more difficult fabrication, increased probability of distortion and cracking during heat treatment and welding [6, p. 178]. Bainite has hardness values which lies between the two graphs in Figure 8 [5, p. 38], increasing linearly with carbon content.

Carbon have a large effect on the temperature range over which upper and lower bainite occur. B_s , the maximum temperature for bainite, is reduced by alloying elements such as manganese, nickel, chromium and molybdenum, but carbon has the greatest influence. An increase in carbon content makes it easier for lower bainite to form. The reason for that is that it becomes more difficult for plates of supersaturated bainitic ferrite to decarburize before the onset of cementite precipitation [6, p. 146-147].

Manganese is added in order to increase the hardenability of a steel, and it has the ability to absorb sulphur impurities. Hot shortness is a phenomenon that may occur when there is too much sulphur in a steel. Then continuous films are formed on the grain boundaries that lead to embrittlement at high temperatures. Formation of MnS particles prevent this type of embrittlement [5, p. 82]. Manganese is a powerful austenite stabilizer and will therefore increase the hardenability by slowing down the growth of pearlite and ferrite.

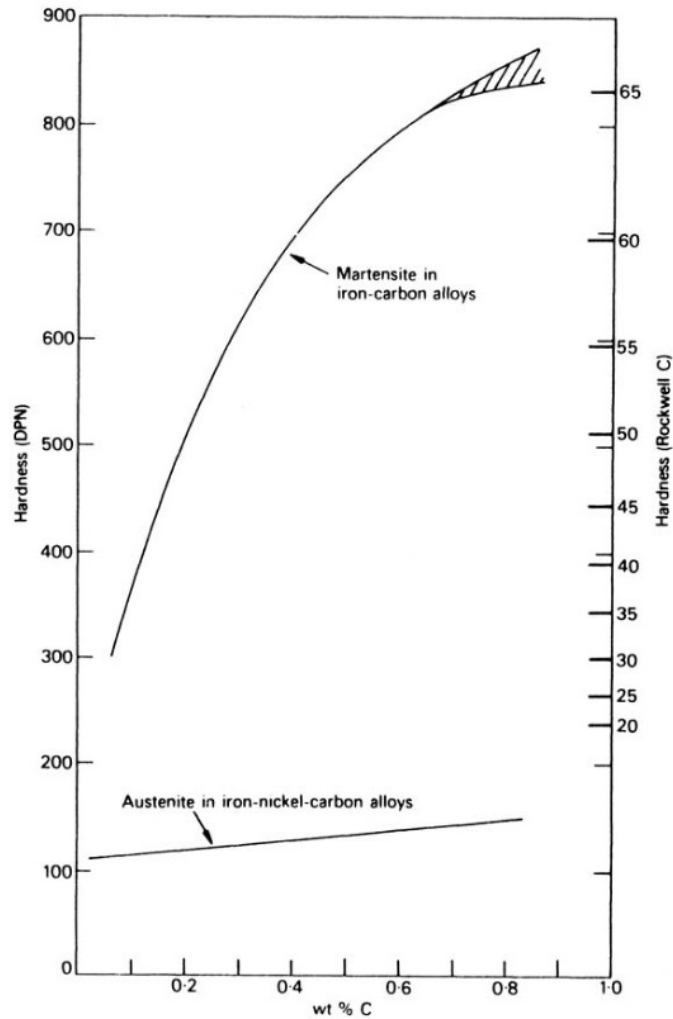


Figure 8: *The hardness in martensite as function of carbon content [6, p. 121].*

Silicon is usually added in contents of 0.3-0.5 % as a deoxidizing agent for the oxygen dissolved in the steel melt. Silicon has greater affinity to oxygen than carbon, and forms oxide particles that stays in the steel. Gas formation and bobbles that leads to pores are therefore prevented [2, p. 105].

Silicon provide solid solution strengthening, in addition to help to achieve a different morphology of bainite. Bainite usually have lower toughness than martensite, due to the precipitation of cementite. The lack of toughness can in principle be eliminated by using steels with a high silicon concentration (e.g. 1.5 wt %). Silicon has a negligible solubility in cementite and hence greatly retards its precipitation [14]. The addition of silicon enhances the toughness because the carbon that is usually precipitated as brittle cementite instead partitions into the residual austenite, allowing the latter to be retained [15, p. iii].

Boron is an interstitial element with high diffusivity in austenite. Before the austenite to ferrite transformation, boron will precipitate on the austenite grain boundaries during cooling. A small amount of boron will dramatically increase the hardenability of a steel [16]. It is a relatively cheap alloying element and makes the steel less susceptible to quench cracking and distortion during heat treatment. To achieve the hardenability effect from boron, it is important that

boron does not combine with nitrogen. To prevent the formation of BN, titanium is added to the steel which has greater affinity to nitrogen than boron [17]. Boron is effective in retarding proeutectoid ferrite formation, but has a negligible effect on the bainite reaction. This allows bainitic microstructure to be obtained over a wider range of cooling rates [11, p. 303].

The hardenability effect from boron comes from the mentioned grain boundary segregation. This segregation lowers the interfacial energy at the austenite grain boundary and therefore the transformation of austenite to ferrite is retarded. It is found that addition of boron together with molybdenum remarkably increases the hardenability. The same effect has been seen for boron in combination with chromium. However, microstructural evolution and hardness measurement has shown that molybdenum is a more effective alloying element for the enhancement of hardenability in boron-steels than chromium [16].

Microalloying elements that are mostly used in steels are niobium, vanadium and titanium. They lead to refinement of the structure and partly to produce precipitation hardening. The refinement of the structure takes place through retarded grain growth during the heating process as well as during the recrystallization and related grain growth after forging [2, p. 226]. Figure 9 shows the solubility product of some important combinations of elements as function of temperature [5, p. 104].

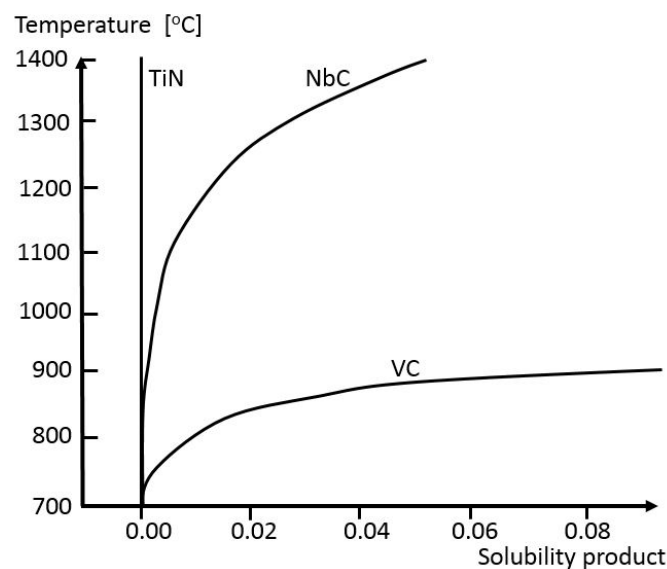


Figure 9: Solubility product of TiN , NbC and VC in austenite, based on [5, p. 104].

Elements like molybdenum, chromium and tungsten are strong carbide-forming elements. Cementite will be replaced by the appropriate alloy carbides, often at relatively low element concentrations [8, p. 120]. Particles can be precipitated or be barriers on the grain boundaries, they will therefore reduce the grain boundary area and prevent grain growth [5, p. 73]. The tendency of alloying elements to form carbides are illustrated in Figure 10.

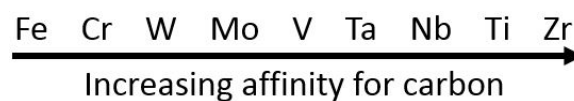


Figure 10: The tendency of alloying elements to form carbides [2, p. 110].

In general, all alloying elements, except of vanadium, increase the hardenability of steel. The reason why alloying elements have this effect, is that they enter into the two phases ferrite and cementite with different distribution. For transformation of austenite to ferrite and cementite a redistribution of alloying elements through diffusion is required. Alloying elements are mostly substitutional solved and the diffusion is therefore slower than for alloying elements as carbon that is interstitial solved. The redistribution will therefore delay the reaction. The curve for ferrite and pearlite transformation in the CCT diagram will be displaced towards longer time, and the cooling rate can therefore be reduced while martensite can still be formed. This leads to increased hardenability [5, p. 46-47].

The austenite stabilizing alloying elements increase the hardenability by displacing the transformation curves for ferrite, pearlite and bainite towards longer times. The carbide forming alloying elements or ferrite stabilizers displace the pearlite transformation curve towards longer time in addition to the part of the ferrite curve that is below 600°C. But they have a reduced effect on the bainite curve [2, p. 118].

2.5 Grain growth kinetics

Austenite grain growth during hot working of materials is an important factor when determining the final microstructure and mechanical properties. The growth kinetics of austenite grains are dependent on austenitizing temperature and holding time.

$$d = A * e^{\frac{-Q}{R*T}} * t^n \quad (3)$$

Equation 3 shows the relation between austenite grain growth and austenitizing conditions. Here d is the grain size in micrometer, A a constant, Q activation energy (J/mol) for grain growth, R the gas constant (8.314 J/(mol*K)), T the austenitizing temperature in Kelvin, t the austenitizing time in seconds and n a time exponent [18]. From this equation it is seen that grain size increase with increasing temperature and time in the austenite area.

It has been seen that a reduction in austenite grain size causes reduction of the M_s temperature. This is because the size of the largest martensite plate that can form, is related to the austenite grain size [8, p. 164]. The relationship between M_s temperature and austenite grain size is shown in Figure 11.

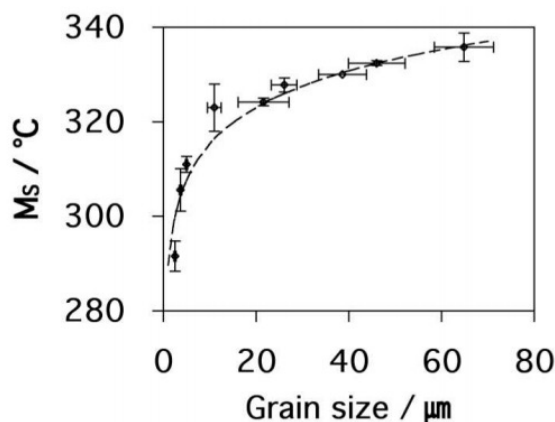


Figure 11: Martensite start temperature as function of austenite grain size [8, p. 165].

2.6 Effect of grain size

The Hall-Petch equation given in Equation 4, shows the relation between grain diameter d and yield stress σ_y . Here σ_0 and k_y are material constants. This equation can be applied for a wide variety of iron and steels, in addition to many nonferrous metals and alloys. The equation shows that the yield strength decreases with increasing grain size.

$$\sigma_y = \sigma_0 + k_y \frac{1}{\sqrt{d}} \quad (4)$$

The grain size effect can be explained based on movement of dislocations from dislocation sources. The dislocations will pile-up at the grain boundary and cause generation of stress in the neighbor grain. When this stress reaches a critical value, a new dislocation source will be formed in that grain. This is how the yield process is propagated between the grains [6, p. 28-30]. It leads to a large amount of piled-up dislocations in front of grain boundaries in big grains. The amount of stress needed to create a brittle fracture is therefore small. In small grains the amount of piled-up dislocations is low and the stress needed for brittle fracture is high [5, p. 67-68]. The grain boundary hardening mechanism has interesting characteristics compared to other hardening mechanisms. A decrease in grain size raises the strength in the material and at the same time, the steel becomes tougher [2, p. 78]. In addition, a reduction in the austenite grain size lead to an increase in the rate of transformation, because of the greater number density of grain boundary nucleation sites [11, p. 167].

2.6.1 Grain size determination

The size of the grains is important because it has a great effect on the mechanical properties of a steel. Small grains are usually preferred since fine grained material normally possesses better characteristics than coarse grained. ASTM E112 *Standard Test Methods for Determining Average Grain Size* [19] describes different methods that can be used for grain size determination. Grain size can be indicated in ASTM *Grain size*, G. A high values of G indicates a small grain size and a low value a bigger grain size. Table 2 lists the average grain size in μm compared with G [2, p. 193] [19].

Table 2: Average grain size in μm compared with G.

μm	508	359	254	180	127	90	64	45	32	23	16	11	8
G	00	0	1	2	3	4	5	6	7	8	9	10	11

2.7 Mechanical test methods

2.7.1 Notch - impact test

Charpy V is a mechanical test method where notched samples are broken by a swinging pendulum. The swinging pendulum is released from a given height h and cause impact load on the sample. After fracturing the sample, the pendulum continues its swing, until it reaches a maximum height h' , which is lower than h . The energy absorption is computed from the difference in potential energy for the two heights [7, p. 251]. This gives a measure of the impact

energy of the material. Fracture toughness is the measure of a material's resistance to fracture when a crack is present [7, Appendix E].

For many materials, this energy varies with temperature. It is therefore important to specify the temperature used during performing of the test. If the temperature differs from ambient temperature, the specimen should be heated or cooled to the given temperature under controlled conditions. It is also important to notice that not all separate notch-impact tests can be compared. By comparison, the test has to be performed under equal conditions. As an example, the radius of the swinging pendulum has to be equal and the specimens should have equal geometry, as described in NS-EN ISO 148-1:2016, *chapter 5 Principles of the test* [20].

2.7.2 Tension test

During tension testing, a sample of a material is slowly stretched with an axial force until fracture occurs. The test specimen usually have either a circular or a rectangular cross section. The cross section at the ends of the specimen is usually enlarged to provide extra area for gripping. This is done to avoid the sample breaking where it is being gripped [21, p. 123-124]. Screw-threads can be used to attach the test specimen in the machine. From a tensile test one can find the relationship between the stress and the level of deformation. The area under the stress - strain curve can be used to consider toughness. Toughness of a material is its ability to absorb energy in the plastic range. The size of the area is an indication of the amount of work per unit volume which can be done on the material without causing it to rupture. A greater total area under the curve means a tougher material, since toughness is a parameter that comprises both strength and ductility [22, p. 282-283].

Formation of a neck in the tension specimen introduces a complex triaxial state of stress in that region. The necked region can function as a mild notch. A notch exposed to tension produces radial and transverse stresses, which raise the value of longitudinal stress required to cause plastic flow [22, p. 292].

The conditions during the performance is important, the temperature shall, as an example, be between 10-35°C, as given in EN ISO 6892-1:2016, *chapter 5 Principle* [23]. The dimensions of the test specimen is dictated by the material dimensions in the delivery condition. A typical engineering stress-strain curve and the geometry of the deformed specimen at various points are illustrated in Figure 12.

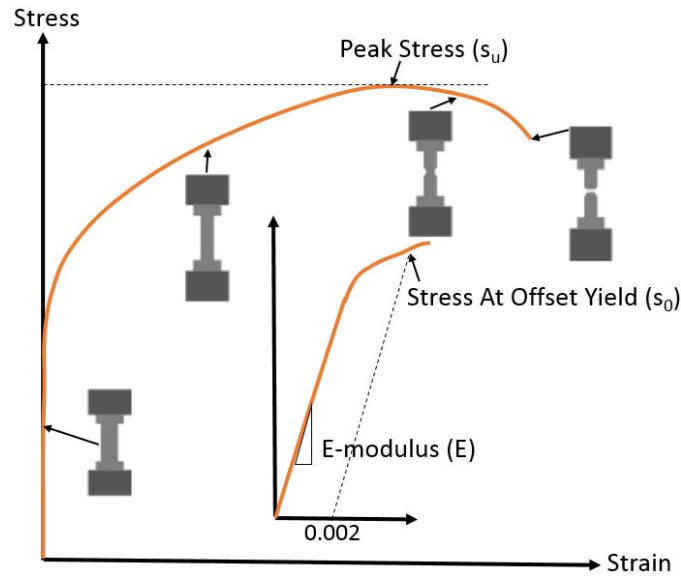


Figure 12: Typical engineering stress-strain behavior to fracture. The geometry of the deformed specimen at various points are illustrated along the curve [7, p. 164-145].

2.8 Inspection of microstructure

If a microstructure is consisting of martensite and bainite, the two structures can be distinguished as long as both phases are present in the microstructure. This can be illustrated by looking at optical micrographs of a nital etched medium carbon steel, as shown in Figure 13 and 14. The bainite etches dark because it is a mixture of ferrite and cementite, and the upper bainite/cementite interfaces are easily attacked by the nital etchant used. The residual light phase is untempered martensite, which etches lighter because of the absence of carbide precipitates.

The straight edges between the dark etched bainite and the light etching areas of martensite, are shown by the black arrows in Figure 14. This is a typical characteristic of a mixed microstructure of martensite and bainite, because bainite forms on specific crystallographic planes of austenite. If the brown etched phase was pearlite, the edges would be less straight [24].

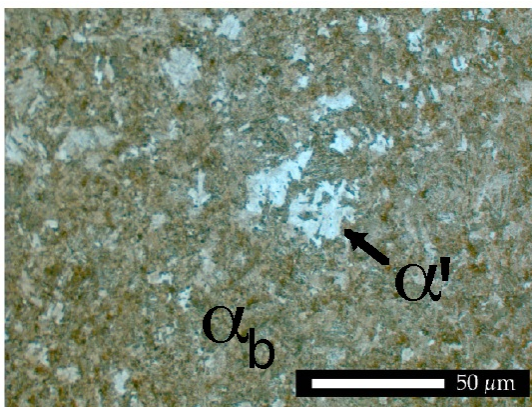


Figure 13: Optical micrograph of a mixture of bainite and martensite etched with nital. The dark etched areas are upper bainite (α_b) and the lighter areas are martensite (α').

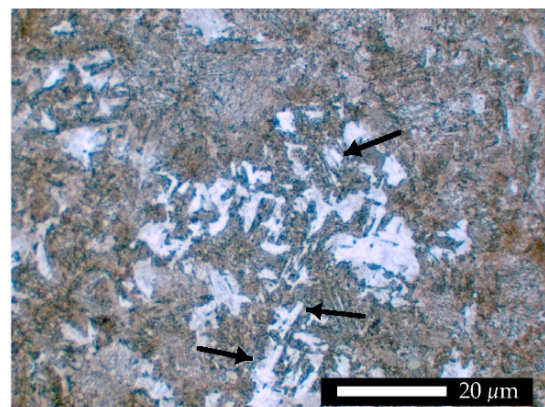


Figure 14: Characteristic microstructure of a mixture of dark etched bainite and light etched martensite. The arrows shows straight edges between the two microstructures.

2.9 Electron fractography

Fractography is studies of the mechanism of fracture by microscopic examination, normally using scanning electron microscopy (SEM). The scanning electron microscope is preferred for fractographic examinations because it has a much better resolution and depth of field than the optical microscope, these characteristics are necessary to reveal the topographical features of fracture surfaces [7, p. 238].

The most common features associated with ductile fracture are dimples, which are formed by plastic deformation as part of the fracture process [25, p. 90-91]. For most brittle crystalline materials, crack propagation corresponds to the successive and repeated breaking of atomic bonds along specific crystallographic planes, that process is termed cleavage. Here the fracture pass through the grains, and the fracture is said to be transcrystalline. In some alloys crack propagation is along grain boundaries, this fracture is termed intercrystalline [7, p. 240-241]. Characteristic of dimples, intercrystalline fracture and cleavage fracture are shown in Figure 15.

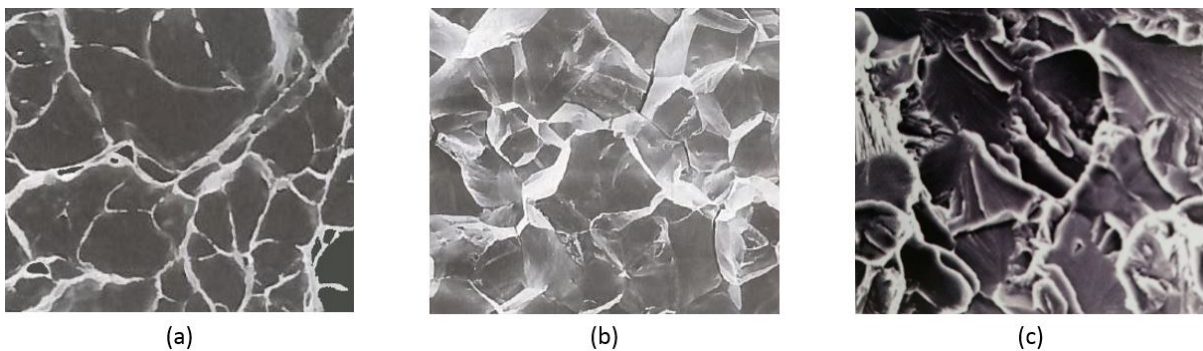


Figure 15: Scanning electron microscope images showing dimples characteristic of ductile fracture (a) [7, p. 238], intercrystalline fracture surface (b) [7, p. 241] and cleavage fracture (c) [2, p. 83].

3 Materials and experimental techniques

In this chapter the materials investigated and the experimental techniques that have been used will be presented. Since the materials investigated are classified into two different categories (700 HV for plough shares and 400 HV for chains), it has been natural to present the categorized alloys separately. One category for 42M13B, 50CrMo4, 100Cr6 and 100CrSiMn6-5-4 and one for 11M13CB, 18MnCrSiMoVB6, 27MnSiCrVB6 and 35MnCrMoVB5.

3.1 Chemical composition

Table 3 shows the chemical composition in weight and atomic percent of 42M13B, 50CrMo4, 100Cr6 and 100CrSiMn6-5-4. These alloys were hardened to about 700 HV, which is relevant for plough share production. 100CrSiMn6-5-4 contains 4.877 wt.% alloying elements and is the highest alloyed steel in the table. The alloy contains e.g 0.995 wt.% C and 1.216 wt.% Si. 42M13B is the lowest alloyed steel and contains 2.285 wt.% alloying elements, but it is alloyed with boron which have effect on the hardenability. The atomic percent was calculated as shown in Appendix A.




Table 3: Chemical composition of 42M13B, 50CrMo4, 100Cr6 and 100CrSiMn6-5-4 in weight and atom percentage.

Alloying elements		42M13B	50CrMo4	100Cr6	100CrSiMn6-5-4
C	[wt.%]	0.417	0.4917	1.0444	0.9945
	[at.%]	1.904	2.2397	4.6583	4.4060
Si	[wt.%]	0.192	0.263	0.31	1.216
	[at.%]	0.375	0.512	0.59	2.303
Mn	[wt.%]	1.26	0.769	0.315	0.954
	[at.%]	1.26	0.766	0.307	0.924
P	[wt.%]	0.014	0.0085	0.0104	0.0129
	[at.%]	0.025	0.0150	0.0180	0.0222
S	[wt.%]	0.0024	0.0157	0.00212	0.0036
	[at.%]	0.0041	0.0268	0.00354	0.0060
Cr	[wt.%]	0.32	0.835	1.466	1.366
	[at.%]	0.34	0.878	1.510	1.398
Ni	[wt.%]		0.171	0.113	0.122
	[at.%]		0.159	0.103	0.111
Mo	[wt.%]		0.156	0.021	0.034
	[at.%]		0.089	0.012	0.019
V	[wt.%]		0.0125	0.0102	0.0038
	[at.%]		0.0134	0.0107	0.0040
Ti	[wt.%]	0.03	0.0275	0.0031	0.0024
	[at.%]	0.03	0.0314	0.0035	0.0027
Cu	[wt.%]		0.1887	0.1782	0.138
	[at.%]		0.1624	0.1502	0.116
Al	[wt.%]	0.043	0.0202	0.0273	0.0221
	[at.%]	0.087	0.0410	0.0542	0.0436
Nb	[wt.%]		0.0015	0.0011	0.0015
	[at.%]		0.0009	0.0006	0.0009
B	[wt.%]	0.0025	0.00015	0.00005	
	[at.%]	0.0127	0.00076	0.00025	
N	[wt.%]	0.0038	0.01029	0.01062	0.0058
	[at.%]	0.0149	0.04018	0.04061	0.0220

Table 4 shows the chemical composition in weight and atomic percent of 11M13CB, 18MnCrSi-MoVB6 (Metasco 1200), 27MnSiCrVB6 (Metasco MC2) and 35MnCrMoVB5 (Metasco BAE75). These alloys were hardened to about 400 HV, which is relevant for chain production. 18MnCr-SiMoVB6 contains 4.996 wt.% alloying elements and is the highest alloyed steel in the table. The alloy contains e.g only 0.178 wt.% C, but 1.502 wt.% Mn and 1.485 wt.% Cr. 11M13CB is the lowest alloyed steel, containing 2.859 wt.% alloying elements. All these alloys contain a substantial part of boron. The atomic percent was calculated as shown in Appendix A.

Table 4: Chemical composition of 11M13CB, 18MnCrSiMoVB6, 27MnSiCrVB6 and 35MnCrMoVB5 in weight and atom percentage.

Alloying elements		11M13CB	18MnCrSiMoVB6	27MnSiCrVB6	35MnCrMoVB5
C	[wt.%]	0.11	0.1781	0.2634	0.3365
	[at.%]	0.51	0.8139	1.1965	1.5410
Si	[wt.%]	0.28			
	[at.%]	0.55			
Mn	[wt.%]	1.3			
	[at.%]	1.3			
P	[wt.%]	0.009			
	[at.%]	0.016			
S	[wt.%]	0.006			
	[at.%]	0.010			
Cr	[wt.%]	0.87			
	[at.%]	0.93			
Ni	[wt.%]				
	[at.%]				
Mo	[wt.%]				
	[at.%]				
V	[wt.%]				
	[at.%]				
Ti	[wt.%]	0.04			
	[at.%]	0.05			
Cu	[wt.%]	0.2			
	[at.%]	0.2			
Al	[wt.%]	0.03			
	[at.%]	0.06			
Nb	[wt.%]				
	[at.%]				
B	[wt.%]	0.0027			
	[at.%]	0.0138			
N	[wt.%]	0.0111			
	[at.%]	0.0439			

3.2 Condition at delivery

Table 5 shows the condition at delivery for the tested alloys. Half of the steel alloys were delivered as round bars, the other half as hot rolled plates.

Table 5: *Condition at delivery for the tested alloys.*

Alloy	Condition at delivery
42M13B	Hot rolled 9 mm plate
50CrMo4	Hot rolled 12 mm plate
100Cr6	Hot rolled 9 mm plate
100CrSiMn6-5-4	Round bar, 38 mm in diameter
11M13CB	Hot rolled 30 mm plate
18MnCrSiMoVB6	Round bar, 60 mm in diameter
27MnSiCrVB6	Round bar, 37 mm in diameter
35MnCrMoVB5	Round bar, 88.3 mm in diameter

3.3 Macro etching for investigation of segregations

Macro etching for investigation of segregations in the four alloys delivered as round steel bars were performed. This was done as a decision basis before sampling of the bars. A one centimeter thick disc from each cylinder was cut off, ground and polished to a shiny surface. Then the discs were immersed in a 5 % nital etch, for 15 min. Afterwards the surfaces were cleaned with soap and water, then dried. The surfaces were studied with the naked eye and with a stereo microscope. Figure 16 shows images taken of the etched surfaces for 100CrSiMn6-5-4 (a), 18MnCrSiMoVB6 (b), 27MnSiCrVB6 (c) and 35MnCrMoVB5 (d). They all showed traces of segregation in the middle of the discs. 35MnCrMoVB5 showed indication of a bigger homogeneous squared segregation area.

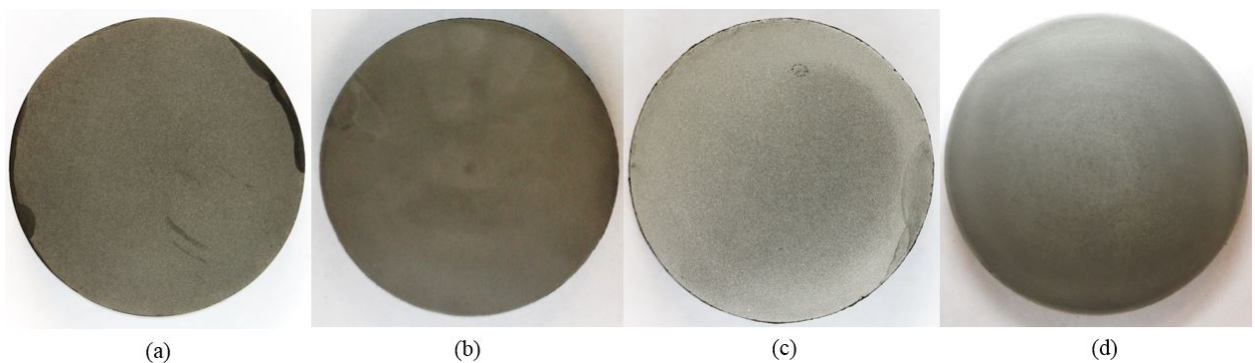


Figure 16: *The inspected surfaces of 100CrSiMn6-5-4 (a), 18MnCrSiMoVB6 (b), 27MnSiCrVB6 (c) and 35MnCrMoVB5 (d) after 15 min etching in 5 % nital.*

3.4 Sampling

Based on the results from the performed macro etching, it was decided to do sampling of the round bars as illustrated in Figure 17 and 18. The gray vertical and horizontal lines indicates the material waste during machining of three millimeter and the white rectangles (8.5 x 11

mm²) are cross sections for samples for notch-impact testing. There were taken eight samples per length from the material with the largest diameter (88.3 mm), as illustrated in Figure 17 and four samples per length for the other diameters (37 mm, 38 mm and 60 mm), as illustrated in Figure 18. This was done to achieve as homogeneous samples as possible. The same kind of sampling was performed for the tension rods.

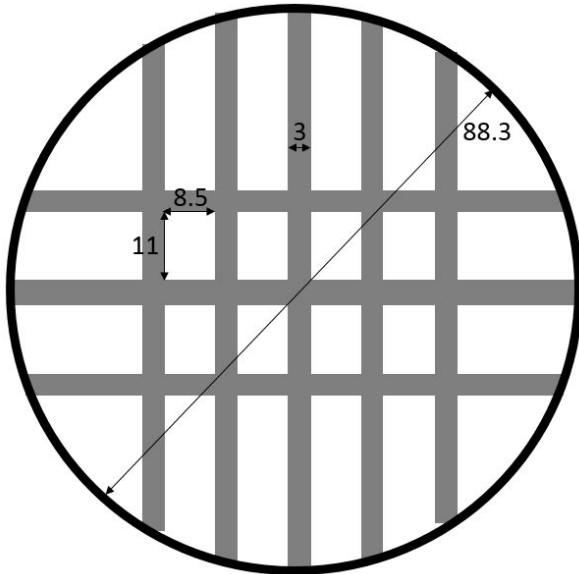


Figure 17: Illustration of sampling of the round bar with diameter of 88.3 mm. The image shows the cross section of the round bar. All dimensions are given in millimeter.

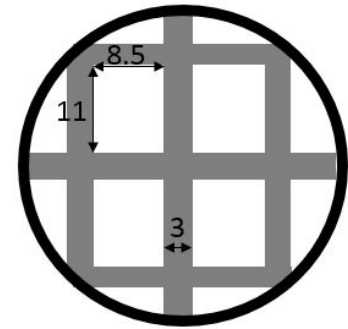


Figure 18: Illustration of sampling of the round bars with diameters of 37 mm, 38 mm and 60 mm. The image shows the cross section of the round bars. All dimensions are given in millimeter.

For the alloys delivered as plates, samples were taken out of the delivered material as illustrated in Figure 19. The figure shows the rolling direction (RD) and how the specimens for notch-impact testing and tensile testing were taken out from the plate materials. The samples were taken out in the middle of the plate thickness.

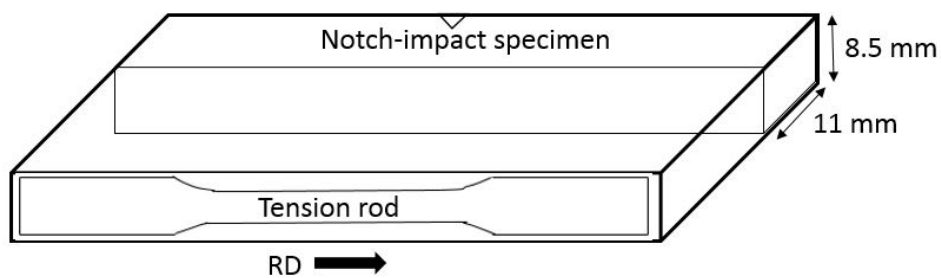


Figure 19: Rolling direction (RD) and the direction of notch-impact specimen and tension rod. The position of the notches are illustrated with a triangle in the middle of the notch-impact specimen.

3.5 Naming of samples

Naming of samples are given in Table 6 and 7 based on alloy and type of hardening performed. There are four parallels of each type. The listed samples were made once with geometry for

notch-impact testing as described in Section 3.8.1 and once with geometry for tensile testing as described in Section 3.9.1. The different heat treatments mentioned in the tables are described in Section 3.6.2, 3.6.3 and 3.6.4.

Table 6: Naming of samples for tension test and notch-impact test. 1.: 42M13B, 2.: 50CrMo4, 3.: 100Cr6 and 4.: 100CrSiMn6-5-4. N: direct hardening, M: martempering and B: austempering.

* These samples have first been austenitized 30 min at 1200 °C, then 10 min at a temperature between 840-900 °C before cooling.

Alloy	Type of hardening	Sample name
42M13B (1)	Direct hardening	1.N1 1.N2 1.N3 1.N4
	Direct hardening*	1.N1* 1.N2* 1.N3* 1.N4*
	Martempering*	1.M1* 1.M2* 1.M3* 1.M4*
50CrMo4 (2)	Direct hardening	2.N1 2.N2 2.N3 2.N4
	Direct hardening*	2.N1* 2.N2* 2.N3* 2.N4*
	Martempering*	2.M1* 2.M2* 2.M3* 2.M4*
100Cr6 (3)	Austempering	3.B1 3.B2 3.B3 3.B4
	Austempering*	3.B1* 3.B2* 3.B3* 3.B4*
100CrSiMn6-5-4 (4)	Austempering	4.B1 4.B2 4.B3 4.B4
	Austempering*	4.B1* 4.B2* 4.B3* 4.B4*

Table 7: Naming of samples for tension test and notch-impact test. 5.: 11M13CB, 6.: 18MnCrSiMo VB6, 7.: 27MnSiCr VB6 and 8.: 35MnCrMo VB5. N: direct hardening, M: martempering and B: austempering.

Alloy	Type of hardening	Sample name
11M13CB (5)	Direct hardening	5.N1
		5.N2
		5.N3
		5.N4
18MnCrSiMoVB6 (6)	Direct hardening	6.N1
		6.N2
		6.N3
		6.N4
	Martempering	6.M1
		6.M2
		6.M3
		6.M4
	Austempering	6.B1
		6.B2
		6.B3
		6.B4
27MnSiCrVB6 (7)	Direct hardening	7.N1
		7.N2
		7.N3
		7.N4
	Martempering	7.M1
		7.M2
		7.M3
		7.M4
	Austempering	7.B1
		7.B2
		7.B3
		7.B4
35MnCrMoVB5 (8)	Direct hardening	8.N1
		8.N2
		8.N3
		8.N4
	Martempering	8.M1
		8.M2
		8.M3
		8.M4
	Austempering	8.B1
		8.B2
		8.B3
		8.B4

3.6 Hardening

Three main types of heat treatments have been performed, which are direct hardening, martempering and austempering. The heat treatments have been done on samples as described in Table 6 and 7 for both geometries for notch-impact testing and tensile testing.

Wire was used to tie around specimens during heat treatment. This was done because the specimens were small and would therefore suffer a rapid heat loss if tongs were used. In addition, it was much easier to handle the samples while moving them between furnaces and salt bath. Two or four samples were hardened simultaneously. They were all attached together two and two, as shown in Figure 20 (a) for notch-impact samples and (b) for tension rods.

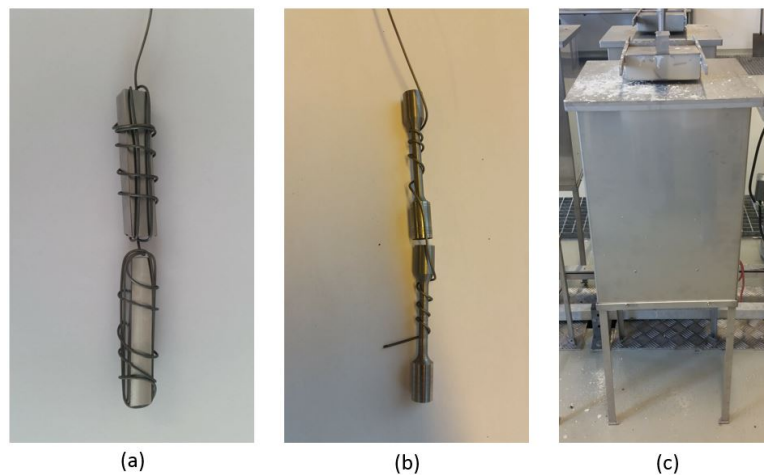


Figure 20: Wire tied around two specimens for notch-impact testing (a) and two tension rods (b) before hardening. Image (c) shows the salt bath used for hardening.

Heating the samples to desired austenitizing temperatures were done in Nabertherm N17/HR furnaces. To reduce the amount of distortion during quenching, the specimens were vertically immersed in the cooling bath. The quenching has mainly been performed in a salt called AS 135. The salt bath used for hardening had an inner cylindrical form with a relatively small volume and no agitation. At maximum, the bath's salt height was approximately 250 mm and the cylindrical diameter was 85 mm. The salt bath is shown in Figure 20 (c).

3.6.1 M_s and austempering temperatures

When hardening steel, it is important to know the M_s temperature of the steel to be able to decide the cooling rate or the isothermal transformation temperature, which give the wanted microstructure and hardness. Data from different sources have therefore been collected to be able to determine the M_s temperature as exact as possible.

A pre-test of the austempering procedure was performed. This made it possible to make adjustments to increase the likelihood of being in the wanted hardness range of approximately 400 and 700 HV. This was done on an approximately five millimeter slice of each alloy for austempering. The hardness was measured as an average from five indentations per sample measured by Struers Duramin-A2500 hardness machine in the core of the samples.

42M13B

The chemical composition satisfy the limitation for Equation 1. M_s was calculated to 320 °C. In the project work, M_s was determined based on average calculation from Equation 1 and 2. Equation 2 is not sufficient at this high carbon concentration, but it did not affect the result much. The M_s used was 318 °C.

50CrMo4

For 50CrMo4, some dilatometer measurements have been performed by SINTEF on order from Kvernelend. The measurements showed an average M_s temperature of 275 °C. The temperature from the dilatometer measurements was in the project work assumed to be most accurate and was therefore used as the M_s temperature.

The chemical composition satisfy the limitation for Equation 1, and M_s was calculated to be 293 °C. The Ovako's steelnavigator for 50CrMo4 gave a M_s temperature of 289 °C [26]. These temperatures are approximately in the same order of magnitude as the used M_s temperature.

100Cr6

100Cr6 is usually used for martensitic hardening, but function well for austempering. The alloy is mainly used for austempering when dimensions are important. According to the CCT diagram in Figure 21, M_s is approximately 220 °C. The 100Cr6 alloy used in this work is between the upper and lower limits of chemical composition, as given in Table 8.

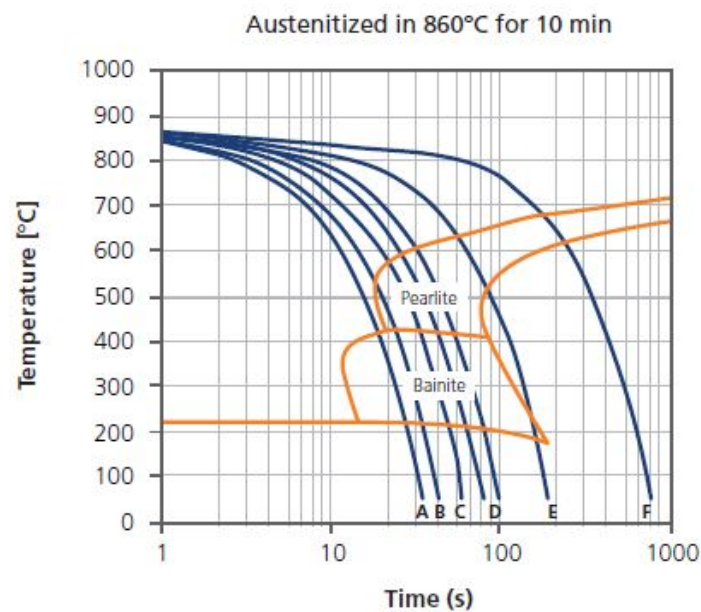


Figure 21: CCT diagram for 100Cr6 austenitized in 860 °C for 10 min [27].

Table 8: Upper and lower limits of chemical composition for 100Cr6.

Alloying elements [wt. %]	C	Si	Mn	Cr	Mo
min	0.93	0.015	0.25	1.35	0
max	1.05	0.35	0.45	1.6	0.1

M_s for 100Cr6 with an alloy content as given in Table 9, has also been found by dilatometer measurements. The alloy content is similar as the content for the 100Cr6 alloy used in this work. The measurements gave a M_s temperature of 155 °C [28, p. 197].

Table 9: Chemical composition of 100Cr6 used for material investigation in article *Influence of Si and Prior Heat Treatment on Long-Term Thermal Stability of 100Cr6-Type Bearing Steels* [28, p. 194].

Alloying elements [wt. %]	C	Si	Mn	Cr	Mo	Cu	Ni
100Cr6	0.94	0.24	0.31	1.38	0.04	0.16	0.13

The austempering temperature used was chosen to be 230 °C, which are above the found M_s temperatures.

100CrSiMn6-5-4

This alloy was made for martempering, but function well for austempering. M_s for 100CrSiMn6-5-4 with an alloy content as given in Table 10 has been found by dilatometer measurements. The alloy content is similar as the content for the 100CrSiMn6-5-4 alloy used in this work. The measurements gave a M_s temperature of 137 °C [28, p. 197].

The austempering temperature was decided to be 220 °C.

Table 10: Chemical composition of 100CrSiMn6-5-4 used for material investigation in article *Influence of Si and Prior Heat Treatment on Long-Term Thermal Stability of 100Cr6-Type Bearing Steels* [28, p. 194].

Alloying elements [wt. %]	C	Si	Mn	Cr	Mo	Cu	Ni
100CrSiMn6-5-4	1.00	1.25	0.96	1.39	0.03	0.13	0.12

11M13CB

The chemical composition satisfy the limitation for Equation 1 and Equation 2, and M_s was calculated to 442.4 °C and 451.1 °C, respectively. M_s was decided based on the average from these equations, which is 447 °C. The hardenability of this alloy is poor, especially do to the low carbon content. Martempering was therefore not performed, since it would have resulted in a too low hardness. Direct hardening with water as quenchant was performed to create a martensitic microstructure.

18MnCrSiMoVB6 (Metasco 1200)

The chemical composition satisfy the limitation for Equation 1 and Equation 2, and M_s was

calculated to 396.2 °C and 395.6 °C, respectively. M_s was decided based on the average from these equations, which is 396 °C.

Recommendations for austempering of this alloy were given by Thomas Sourmail (R&D Section Manager Metallurgy) in Ascometal. He recommended austempering at 380-400 °C to reach approximately 400 HV, but should not exceed much. Before hardening, a pre-test of the hardening procedure was performed. Then 400 °C was used as the austempering temperature. This gave a hardness value lower than 400 HV. It was decided to use 385 °C as the austenitizing temperature, to hopefully reach a greater hardness value.

27MnSiCrVB6 (MC2)

The chemical composition satisfy the limitation for Equation 1 and 2, and M_s was calculated to 373.6 °C and 373.0 °C, respectively. M_s was calculated based on the average from these equations, which is 373 °C. Figure 22 shows the TTT diagram for 28MnSiCrVB6. The M_s temperature is approximately 355 °C and was assumed to be more accurate than the temperature calculated by the equations.

Recommendations for austempering of this alloy were given by Thomas Sourmail (R&D Section Manager Metallurgy) in Ascometal. He recommended austempering at 400-425 °C to reach a hardness of 400 HV or more. A pre-test with austempering temperature of 420 °C was performed. The following hardness testing gave a hardness of 398 HV. This temperature was therefore chosen as the austempering temperature.

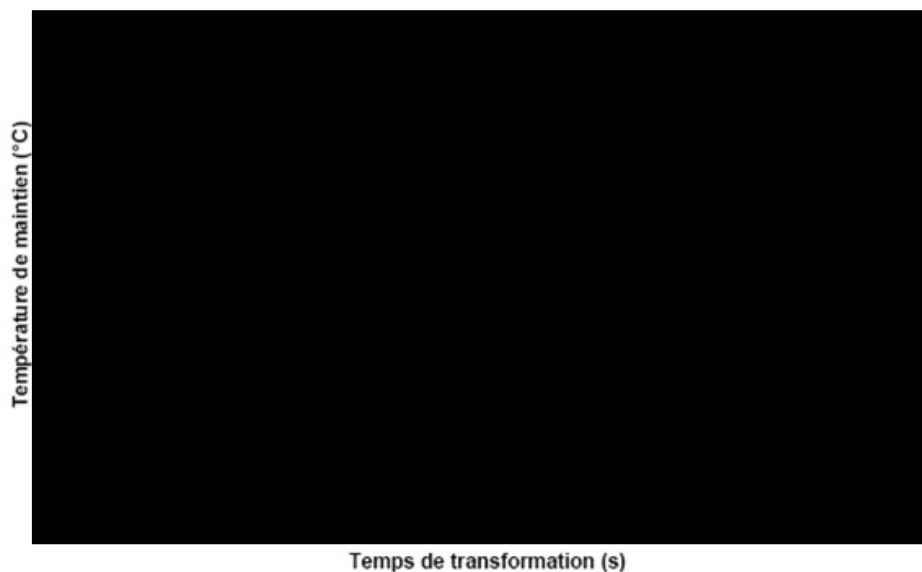


Figure 22: *TTT diagram for 27MnSiCrVB6 [29].*

Figure 23 shows isothermal transformation temperature against hardness for 27MnSiCrVB6. An austempering temperature of 420 °C will give a hardness in the range of 400 HV.

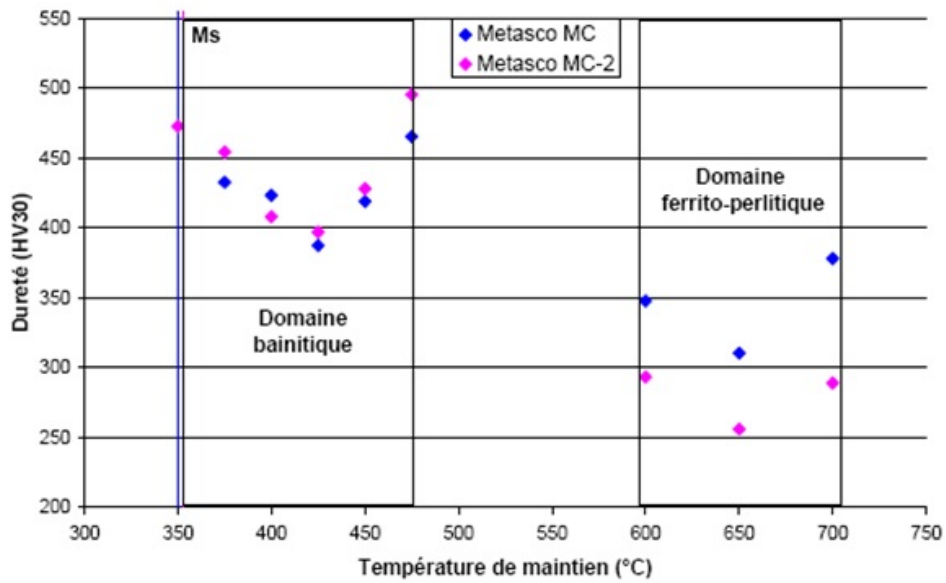


Figure 23: Hardness against isothermal transformation temperature for MC2 [29].

35MnCrMoVB5 (Metasco BAE75)

The chemical composition satisfy the limitation for Equation 1, and M_s was calculated to 347 °C. According to the TTT diagram in Figure 24, M_s of the alloy is 310 °C and was assumed to be more accurate than the temperature calculated by the equation.

Recommendations for austempering of this alloy were given by Thomas Sourmail (R&D Section Manager Metallurgy) in Ascometal. He recommended austempering around 380 °C to probably reach 400 HV, but this was based on few data. A pre-test with austempering temperature of 360 °C was performed. The following hardness testing gave a hardness of 395 HV. A temperature of 360 °C was therefore chosen as the austempering temperature.

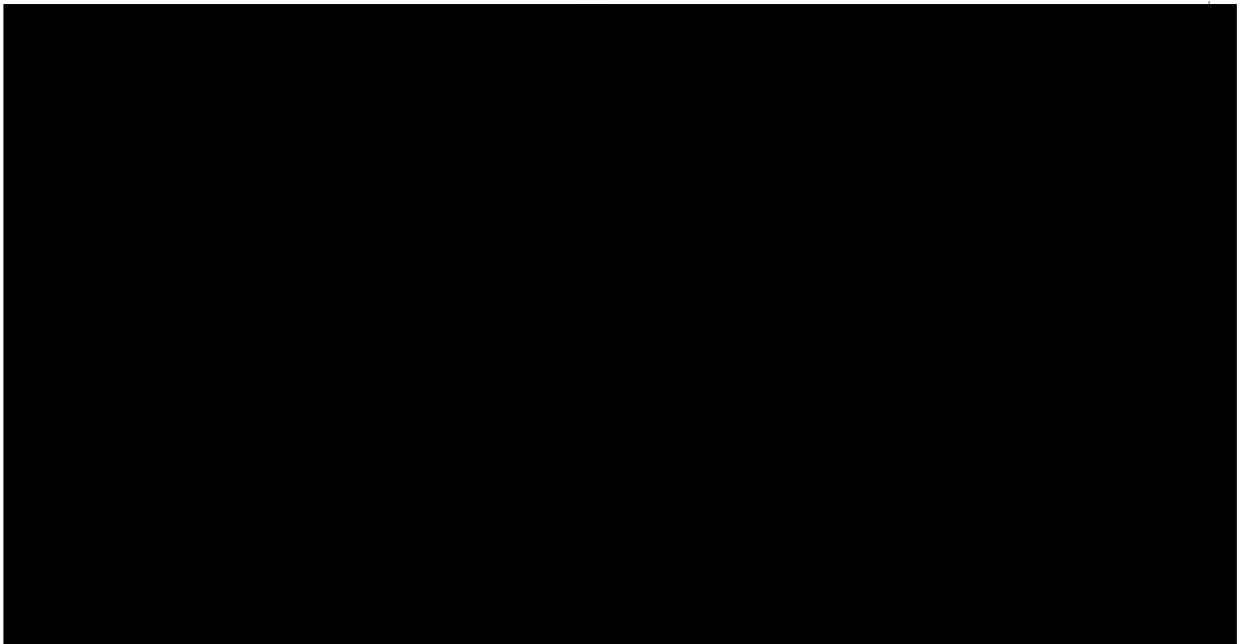


Figure 24: TTT diagram for 35MnCrMoVB5 [29].

3.6.2 Direct hardening

Direct hardening has been performed as described in Table 11. All samples were placed in a furnace preheated to the austenitizing temperature. Some of the samples were then directly moved to a furnace preheated to a second lower austenitizing temperature. Afterwards the samples were quenched. All samples except of those made of 11M13CB, which were quenched in water, were cooled in salt bath. Approximately 2 vol. % of room tempered water was poured into the salt bath around one to two minutes before hardening, while some manual agitation was done. The cover was then put on until the samples were hardened. The samples were further cooled in water.

Table 11: *Temperature and time for performance of direct hardening for given alloys.*

* *The samples were austenitized at 1200 °C followed by a lower austenitizing temperature before quenching.*

Alloy	Sample name	Austenitizing		Cooling	
		Temp. [°C]	Time [min]	Temp. [°C]	Time [min]
42M13B	1.N	870	20	180	1
	1.N*	1200 870	30 10	180	1
50CrMo4	2.N	870	20	180	1
	2.N*	1200 870	30 10	180	1
11M13CB	5.N	900	30	about 25 (water)	
18MnCrSiMoVB6	6.N	900	30	180	1
27MnSiCrVB6	7.N	880	30	180	1
35MnCrMoVB5	8.N	860	30	180	1

3.6.3 Martempering

Modified martempering has been performed as described in Table 12. All samples were placed in a furnace preheated to the austenitizing temperature. Some of the samples were then directly moved to a furnace preheated to a second lower austenitizing temperature. Afterwards the samples were quenched in salt bath for exactly one minute. It was assumed that one minute holding time was sufficient to achieve uniform temperature in the specimens. The salt temperature was set to 25°C under M_s for the alloys. The samples were further cooled in air. The remaining salt on the specimen surface was then washed away with water after room temperature was reached.

Table 12: *Temperature and time for performance of martempering for given alloys.*

* The samples were austenitized at 1200 °C followed by a lower austenitizing temperature before quenching.

Alloy	Sample name	Austenitizing		Cooling	
		Temp. [°C]	Time [min]	Temp. [°C]	Time [min]
42M13B	1.M*	1200	30	293	1
		870	10		
50CrMo4	2.M*	1200	30	250	1
		870	10		
18MnCrSiMoVB6	6.M	900	30	371	1
27MnSiCrVB6	7.M	880	30	330	1
35MnCrMoVB5	8.M	860	30	285	1

3.6.4 Austempering

Austempering has been performed as described in Table 13. All samples were placed in a furnace preheated to the austenitizing temperature. Some of the samples were then directly moved to a furnace preheated to a second lower austenitizing temperature. Afterwards the samples were quenched in salt bath, with temperature and holding time as given in the table. The samples were further cooled in air. The remaining salt on the specimen surface was then washed away with water after room temperature was reached.

Table 13: *Temperature and time for performance of austempering for given alloys.*

* The samples were austenitized at 1200 °C followed by a lower austenitizing temperature before quenching.

Alloy	Sample name	Austenitizing		Cooling	
		Temp. [°C]	Time [min]	Temp. [°C]	Time [min]
100Cr6	3.B	900	30	230	600 (10 t)
	3.B*	1200	30	230	600 (10 t)
900		10			
100CrSiMn6-5-4	4.B	840	30	220	960 (16 t)
	4.B*	1200	30	220	960 (16 t)
840		10			
18MnCrSiMoVB6	6.B	900	30	385	10
27MnSiCrVB6	7.B	880	30	420	10
35MnCrMoVB5	8.B	860	30	360	10

The performed heat treatments are summarized in Figure 25. The figure shows schematically the temperature-time curves for the performed direct hardening, martempering and austempering. The lower austenitizing and M_s temperature varies with alloy content. The austempering temperature and time are also dependent on alloy content.

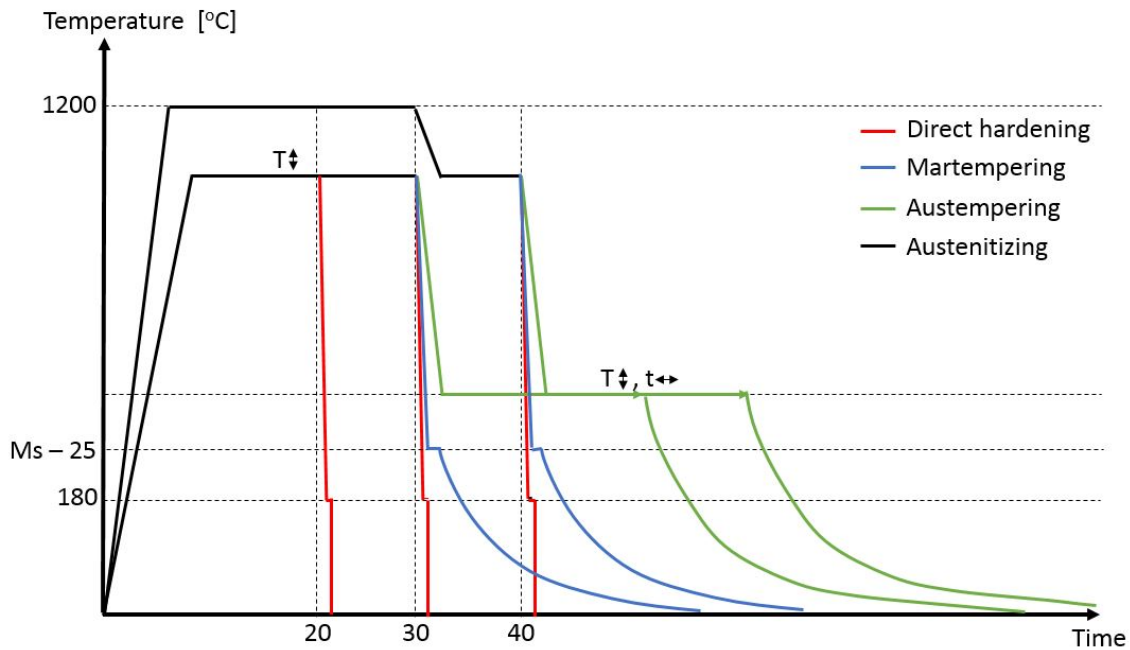


Figure 25: Illustration of temperature-time curves for the performed direct hardening, martempering and austempering. M_s temperature, lower austenitizing temperature and austempering temperature and time varies with alloy content.

3.7 Investigation of microstructure and prior austenite grains

3.7.1 Sample preparation

A small piece from the edge of the tension rods were cut off with Struers Labotom-5, as illustrated in Figure 26. The samples were then molded two and two together as shown in Figure 27, so that the microstructure could be looked at transverse to the rolling direction. Warm molding, using Struers LaboPress-1 machine and molding mass DuroFast, was performed to make sure the top and bottom became parallel and because a hard mold was wanted. This gave better results for the following hardness tests and curved sample edges were avoided during grinding and polishing. Afterwards the samples were ground and polished to $1\ \mu\text{m}$ according to the steps in Table 14, using a Struers Tegramin-30 machine.



Figure 26: Cutting of tension rod. The part to the right was warm molded with cutting side down.



Figure 27: Pieces from tension rods, warm molded.

Table 14: *The steps for grinding and polishing used on the molded samples before etching.*

	Grinding/ Polishing disk	Water	Liquid [μm]	Force [N]	RPM (rounds per min)	Time [min]
Step 1	Piano 220	Yes	-	90	300	To plane
Step 2	MD-Allegro	No	DiaPro 9	90	150	2
Step 3	MD-Dac	No	DiaPro 3	50	150	2
Step 4	MD-Nap	No	DiaPro 1	30	150	2

3.7.2 Etching

For investigation of the microstructure, 2 % Nital etch was used, with an etching time less than 10 seconds.

During etching of prior austenite grains a lot of different etchants were tried. In the ASTM E407-07(2015) *Standard Practice for Microetching Metals and Alloys* [30], there are etchants recommended for prior austenite grain boundary etching of martensitic and bainitic steels. Here etchant number 82 was tried. The two other recommended etchants could not be tried because picric acid can not be used at NTNU. In addition, Fe (m6) [31] and Marble's etch were tried, without great success. Table 15 shows the different etchants that successfully revealed the austenite grain boundaries. The etchant named *Kverneland* has been used on 42M13B; with an etching time less than 30 seconds. Viellas etchant etched coarse prior austenite grains in 50CrMo4 and 2 % nital made coarse grains visible in 100CrSiMn6-5-4. Since Viellas etchant contains picric acid, the etching was performed with help from SINTEF Industry at Department of Materials Integrity and Welding. This was the only picric acid containing etchant available for use at SINTEF.

Table 15: *The etchants successfully used to reveal of the prior austenite grain boundaries.*

Etchant	Composition	Alloy
<i>Kverneland</i>	4 ml hydrogen peroxid 28 ml oxalic acid (10%) 80 ml water	42M13B
Vrellas	1 g picric acid 100 ml ethanol 5 ml HCl	50CrMo4
2 % Nital	2 ml HNO ₃ 98 ml ethanol	100CrSiMn6-5-4

3.7.3 Inspection of microstructure

Micrographs of the hardened alloys were taken using Leica MEF4M with magnification of 200x for the samples austenitized at 1200 °C and 500x for the remaining samples. The images were taken in the core area of the samples.

3.7.4 Measuring of prior austenite grain size

Prior austenite grain size determination after hardening have been tried on the alloys with hardness around 700 HV, which were 42M13B, 50CrMo4, 100Cr6 and 100CrSiMn6-5-4. Heat treatments for equal alloys with the same temperatures and time in the austenitizing area were assumed to have equal grain size. Grain size determination of the 1.M* and 2.M* samples were therefore not performed, since the prior austenite grain size were equal to 1.N* and 2.N*.

The prior austenite grain size was measured using the Heyn Lineal Intercept Procedure according to the ASTM E112 *Standard Test Methods for Determining Average Grain Size* [19]. A number of micrographs were the basis of the determination in order to make sure that more than 50 grains were counted, as described in the standard. Light microscopy images using Leica MEF4M were taken with a suitable magnification.

3.7.5 EBSD

EBSD (electron back scatter diffraction) was performed on austempered 27MnSiCrVB6 (7.B) and 35MnCrMoVB5 (8.B). The molded samples were ground, so that the steel was visible both on the top and the bottom of the mold. This was done to ensure electrical contact between sample and sample holder. The samples were then polished to 1 μm and further polished in VibroMet 2 using MasterMet 2 polishing for 24 hours. Then it was tried to do a EBSD scan using FESEM (Hitachi SU-6600), but the pattern was not clear enough to get a usable phase map. The samples were then electropolished in Struers LectroPol-5 using A3. Another EBSD scan was tried without good results. The samples were then finally prepared using Hitachi IM3000 ION MILL. Then the pattern was good enough for indexing and a phase scan could be made. Acceleration voltage of 20 kV, working distance of 25 mm, tilt angle of 70 $^{\circ}$, magnification of 400x and step size of 0.5 μm were used.

3.8 Notch-impact test

3.8.1 Specimen geometry

Before hardening, the samples were rough machined to a length of 56 mm and a cross section of 8.5 x 11 mm², as shown in Figure 28. The hardening process was then performed. The samples were then precision machined to 7.5 x 10 mm² cross sections and a length of 55 mm. A notch in the middle of the specimens with an angle of 45 $^{\circ}$, depth of 2 mm and bottom radius of 0.25 mm were also made according to the NS-EN ISO 148-1:2016 section 6.2.1 V-notch [20]. The notches were made with a WEDM-Wire electrical discharge machining. Figure 29 shows the final sample geometry after precision machining. Precision machining was done after hardening to reduce the effects of decarburization and distortions. All the dimensions were checked before testing. This was done by using a micrometer screw and light microscope was used for checking the notches, as shown in Figure 104, Appendix B.

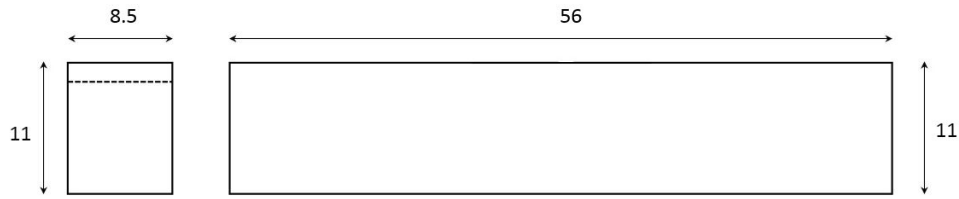


Figure 28: *The dimensions of notch-impact specimens after rough machining given in millimeters.*

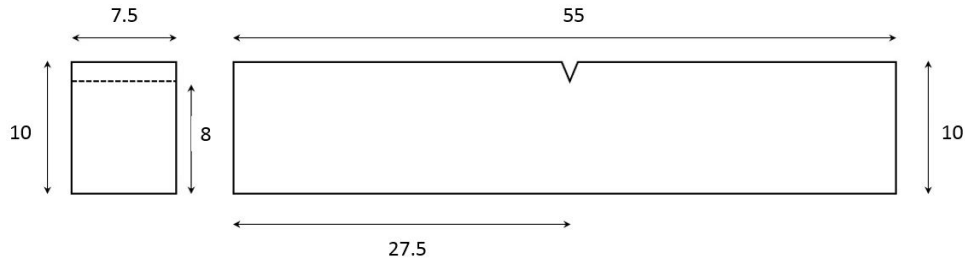


Figure 29: *The dimensions of notch-impact specimens after precision machining given in millimeters.*

3.8.2 Charpy testing

The test was performed at SINTEF according to NS-EN ISO 148-1:2016 *Metallic materials–Charpy pendulum impact test–Part 1: Test method* [20] and NS-EN ISO 14556:2015 *Metalliske materialer–Charpy V-notch pendulum impact test–Instrumented test method* [32]. The LOS, Losenhausenwerk 15/30 mkg, charpy testing machine used is shown in Figure 30.

The machine was inverted with the striking edge fixed in contact with the sample as shown in Figure 31. To reduce wear of the machine due to the hard samples, lead was fastened to the sample in the positions illustrated with arrows in Figure 31. Before use, the lead was pressed to a thickness of 1.1 mm. On the outer part of the samples, lead was positioned with a distance of 43 mm to make sure the swinging pendulum was hitting the lead.



Figure 30: The charpy testing machine used during testing.

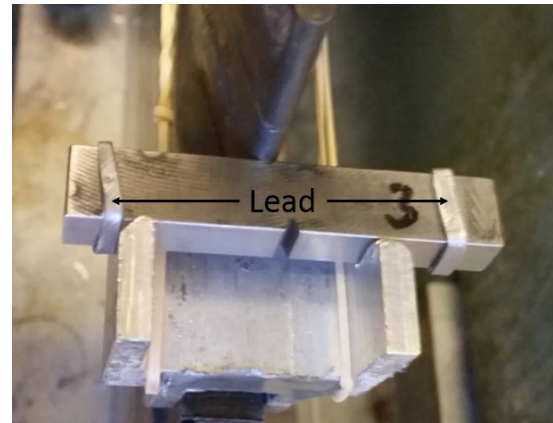


Figure 31: Sample for charpy testing placed in contact with the striking edge. Lead was fastened to the sample to reduce wear of the testing machine.

3.8.3 Data processing

Read total energy [J] was calculated from Equation 5. Here F [kgm] was subtracted due to air, bearing and pointer friction, the value was 0.2 kgm for 42M13B and 50CrMo4, and 0.16 kgm for the remaining alloys. 1.05 is a calculation factor. Dial value [kgm] is the value directly read on the pointer during notch-impact testing.

$$ReadTotalEnergy[J] = (DialValue - F)[kgm] * 9.81m/s^2 * 1.05 * \frac{100}{7.5mm * 10mm} \quad (5)$$

3.8.4 Inspection of fracture surfaces

Images of fracture surfaces after notch-impact testing were taken using LVFESEM, Zeiss Supra, 55VP with magnifications of 100x, 500x, 5000x and 10000x. The images were taken in the core area of the samples, with the use of secondary electrons. The working distance was about 24 mm and accelerating voltage was 10-15 kV.

3.9 Tension test

3.9.1 Specimen geometry

The tension rods were first rough machined before hardening, as shown in Figure 32 and then precision machined after hardening, as shown in Figure 33. This was done to avoid any negative effects of decarburization and distortion due to the heat treatment. The threads were machined after heat treatment to avoid misalignments between sample and holders. Some of the samples got a shorter threaded part than in the draft due to difficult machining. The sample geometry is according to NS-EN ISO 6892-1: 2016 (E) [23].

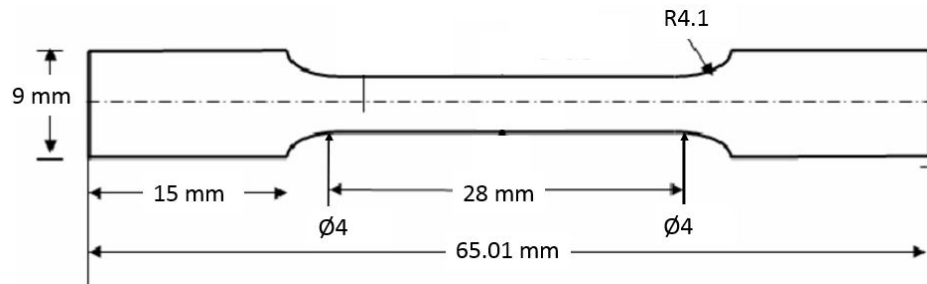


Figure 32: *The dimensions of tension rod after rough machining given in millimeters.*

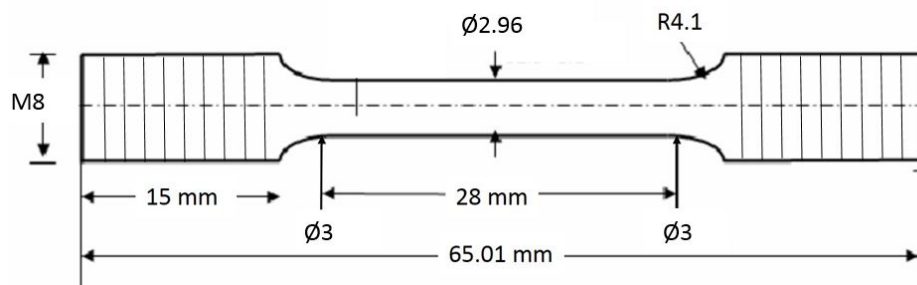


Figure 33: *The dimensions of tension rod after precision machining given in millimeters.*

The geometry of the holders were cylindrical with a length of 25 mm and a diameter of 13.5 mm as shown in Figure 34. The inner threaded part was fitted to the threads on the samples.

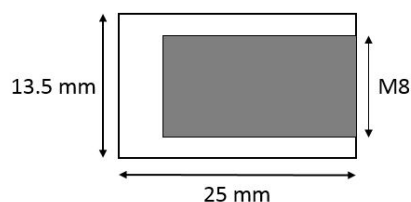


Figure 34: *The geometry of the cylindrical holders.*

Some improvements on the sample geometry that was used for tension testing of 42M13B and 50CrMo4 during the project work have been done. Optimizations were done to avoid misalignments between sample and holders and to make sure there was sufficient space for

the extensometer. The middle part was elongated three millimeters and the threaded part was elongated approximately 8.5 mm. In addition, the threads were machined after hardening, instead of before. The test results from the new sample geometry were assumed to be comparable with the results from the project work.

3.9.2 Tensile testing

The machined samples were attached with threads to holders as shown in Figure 36. Thread tape was used on some samples for better adjustment between the holders and samples. The holders were placed in clips in the MTS 810 Hydraulic tension test machine (100 kN) as shown in Figure 35. Testing was performed according to NS-EN ISO 6892-1:2016 *Metallic materials–Tensile testing–Part 1: Method of test at room temperature* [23]. The smallest cross section area of the tension rods were measured with slide caliper before testing and in the neck after testing. Based on this, the change in cross section diameter and percent reduction in area were measured [7, p. 167].



Figure 35: *Tension rod in the testing machine with attached extensometer.*



Figure 36: *Tension rod screwed together with sample holders before testing.*

3.10 Hardness testing

Hardness testing of the heat treated samples was performed after notch-impact testing and tensile testing. For the tension tested samples, the hardness testing was done on the molded, ground, polished and etched samples. The indentations for notch-impact tested samples were done on the cross section on cutted, molded and slightly ground samples. Zwick/Roell ZHV30 hardness machine was used to determine the hardness in Vickers [HV]. The hardness was determined as an average from five indentations in the first sample in each set. To be able to measure the bulk hardness, a relatively high load of 10 kg was used. The distance between the centres of two indentations were at least three times the diagonal length of the indentation.

Microhardness measurements with varying load were performed using Leica Vmht Mot test machine. This was done in sample 3.B* for investigation of the different phases observed from the light optical micrographs.

4 Results

In this chapter the results from the experimental work are presented. The chapter contains determination of prior austenite grain sizes, micrographs, notch-impact test results, tensile test results and measured hardness values. Since the materials investigated are classified into two different categories (700 HV for ploughshares and 400 HV for chains), it has been natural to present the categorized alloys separately.

4.1 Grain size determination

Table 16 gives prior austenite grain sizes for the successfully etched samples, with a hardness of about 700 HV. These are interesting for Kverneland. If these processes are going to be used in the production of plough shares, the samples marked with * requires only one austenitizing cycle, while the others require two. Reducing the required number of austenitizing cycles to only one time would be beneficial to Kverneland.

A review of the grain size determinations for 42M13B, 50CrMo4, 100Cr6 and 100CrSiMn6-5-4 follows. Heat treatments for equal alloys with the same temperature and time in the austenite area were assumed to have equal grain size. Grain sizes were therefore assumed to be equal for sample 1.N* and 1.M*, in addition to 2.N* and 2.M*.

Table 16: *Prior austenite grain sizes for direct hardening (N), martempering (M) and austempering (B) of 42M13B (1), 50CrMo4 (2), 100Cr6 (3) and 100CrSiMn6-5-4 (4). Samples 2.N, 3.B, 3.B* and 4.B could not be adequately etched for grain size determination.*

Sample	Grain size [$\mu\text{m}/$ grain]
1.N	8.3
1.N*	118.9
1.M*	118.9
2.N	-
2.N*	54.3
2.M*	54.3
3.B	-
3.B*	-
4.B	-
4.B*	547.8

42M13B

Table 17 gives that the resulting grain size determined from four micrographs of direct hardened 42M13B (1.N) austenitized at 870 °C was 8.3 μm/grain. Figure 37 shows one of the four micrographs. The intercepted grains are marked with dotted lines. The closest integer is G=11 in ASTM Grain size.

Table 17: The average grain size for direct hardened 42M13B (1.N).

Micrograph	Line length [μm]	# intercepted grains
1	111.6	18
	117.9	16
2	108.7	13
	120.4	14
3	114.2	12
	116	13
4	109.2	14
	119.2	13
Total	917.2	111
Average	8.3 μm/grain	

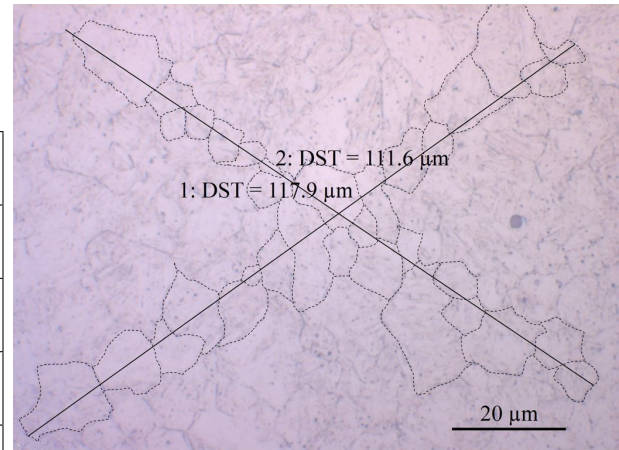


Figure 37: Micrograph 1, direct hardened 42M13B (1.N). Etched with Kvernland etchant. Magnification: 1000x.

Table 18 gives that the resulting grain size determined from six micrographs of direct hardened 42M13B (1.N*) austenitized at 1200 °C followed by 870 °C was 118.9 μm/grain. Figure 38 shows one of the six micrographs, the intercepted grains are marked with dotted lines. The closest integer is G=3 in ASTM Grain size. The grain size of martempered 42M13B (1.M*) is also G=3 in ASTM Grain size, due to equal austenitizing temperature, time and alloy content.

Table 18: The average grain size for direct hardened 42M13B (1.N*).

Micrograph	Line length [μm]	# intercepted grains
1	1121	12
	1123	11
2	470.2	7
	494.2	8
3	1081	7
	1117	9
4	1054	7
	1070	8
5	1066	8
	1088	10
6	1120	7
	1222	7
Total	12004.4	101
Average	118.9 μm/grain	

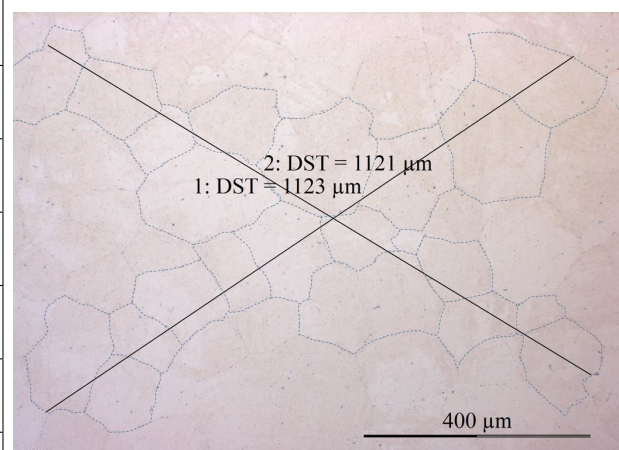


Figure 38: Micrograph 1, direct hardened 42M13B (1.N*). Etched with Kvernland etchant. Magnification: 100x.

50CrMo4

Figure 39 shows a micrograph of direct hardened 50CrMo4 (2.N) austenitized at 870 °C and etching in Viellas etchant. This was the etchant that gave the best results, but the prior austenite grains were not clear enough for determination of the grain size.

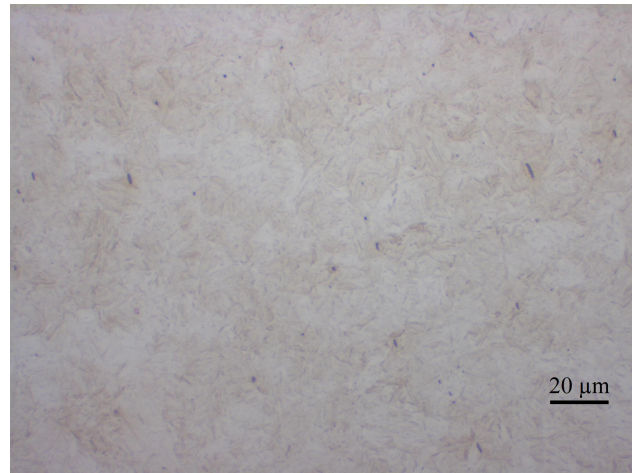


Figure 39: Micrograph of direct hardened 50CrMo4 (2.N). Etched with Viellas etchant. Few prior austenite grains were visible. Magnification: 500x.

Table 19 gives that the resulting grain size determined from four micrographs of direct hardened 50CrMo4 (2.N*) austenitized at 1200 °C followed by 870 °C was 54.3 μm/grain. Figure 40 shows one of the four micrographs. The intercepted grains are marked with dotted lines. The closest integer is G=6 in ASTM Grain size. The grain size of martempered 50CrMo4 (2.M*) is also G=6 in ASTM Grain size, due to equal austenitizing temperature, time and alloy content.

Table 19: The average grain size for direct hardened 50CrMo4 (2.N*).

Micrograph	Line length [μm/grain]	# intercepted grains
1	1003	18
	985.9	21
2	917.7	15
	1070	18
3	1085	19
	891.3	18
4	996.4	19
	985.1	18
Total	7934.4	146
Average	54.3 μm/grain	

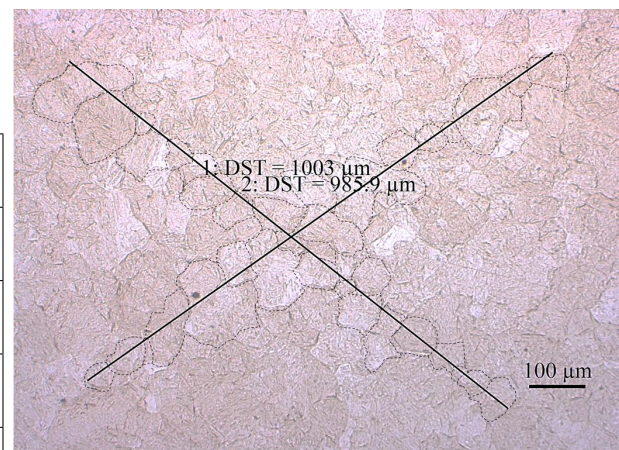


Figure 40: Micrograph 1, direct hardened 50CrMo4 (2.N*). Etched with Viellas etchant. Magnification: 100x.

100Cr6

Figure 41 shows a micrograph of austempered 100Cr6 (3.B) austenitized at 900 °C and etching in Viellas etchant. This was the etchant that gave the best results, but the prior austenite grains were not clear enough for determination of the grain size.



Figure 41: Micrograph of austempered 100Cr6 (3.B). Etched with Viellas etchant. Few prior austenite grains were visible. Magnification: 500x.

Figure 42 shows a micrograph of austempered 100Cr6 (3.B*) austenitized at 1200 °C followed by 900 °C and etching in Viellas etchant. This was the etchant that gave the best results, but the prior austenite grains were not clear enough for determination of the grain size. The fracture surface of this sample is shown in Figure 43, which indicates coarse facets on the surface and, hence, large grain size.

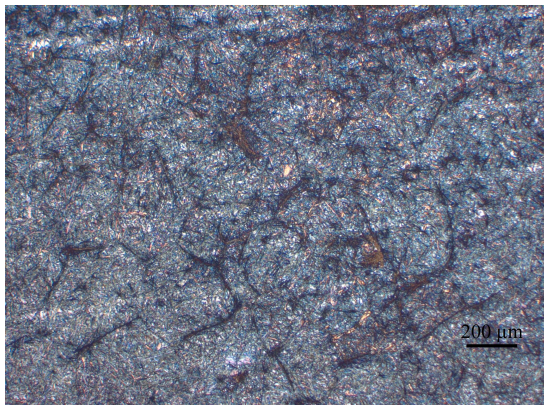


Figure 42: Micrograph of austempered 100Cr6 (3.B*). Etched with Viellas etchant. Few prior austenite grains were visible. Magnification: 50x.



Figure 43: Fracture surface of austempered 100Cr6 (3.B*). The sample was austenitized 30 min at 1200 °C, then 10 min at a lower austenitizing temperature before quenching.

100CrSiMn6-5-4

Figure 44 shows a micrograph of austempered 100CrSiMn6-5-4 (4.B) austenitized at 840 °C and etching in Viellas etchant. This was the etchant that gave the best results, but the prior austenite grains were not clear enough for determination of the grain size.



Figure 44: Micrograph of austempered 100CrSiMn6-5-4 (4.B). Etched with Viellas etchant. Few prior austenite grains were visible. Magnification: 500x.

Table 20 gives that the resulting grain size determined from four micrographs of austempered 100CrSiMn6-5-4 (4.B*) austenitized at 1200 °C followed by 840 °C was 547.8 μm/grain. Figure 45 shows one of the four micrographs. The closest integer is G=00 in ASTM *Grain size*. Fracture surface of this sample is shown in Figure 46, which indicates very coarse facets on the surface and, hence, large grain size.

Table 20: The average grain size for austempered 100CrSiMn6-5-4 (4.B*).

Micrograph	Line length [μm]	# intercepted grains
1	4364	8
	4812	11
2	4298	8
	4320	7
3	4836	8
	4016	9
4	4797	9
	4710	6
Total	36153	66
Average	547.8 μm/grain	

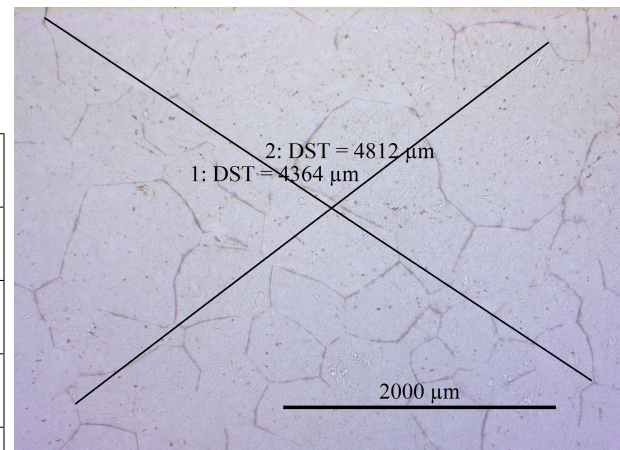


Figure 45: Micrograph 1, austempered 100CrSiMn6-5-4 (4.B*). Etched with 2 % Ni-tal etchant. Magnification: 25x.



Figure 46: Fracture surface of austempered 100CrSiMn6-5-4 (4.B*). The sample was austenitized 30 min at 1200 °C, then 10 min at a lower austenitizing temperature before quenching.

4.2 Microstructure

Micrographs of direct hardening, martempering and austempering of 42M13B, 50CrMo4, 100Cr6, 100CrSiMn6-5-4, 11M13CB, 18MnCrSiMnVB6, 27MnSiCrVB6 and 35MnCrMoVB5 are shown in Figure 47 to 66. Micrographs of the samples austenitized at 1200 °C followed by a lower austenitizing temperature were taken with a magnification of 200x. The remaining images were taken with 500x magnification.

42M13B

Figure 47 to 49 show plates and/or needles, which are typical for a martensitic microstructure. Some prior austenite grains and relatively large needles can be seen in Figure 48 and 49. Figure 47 shows smaller needles compared to the other samples.

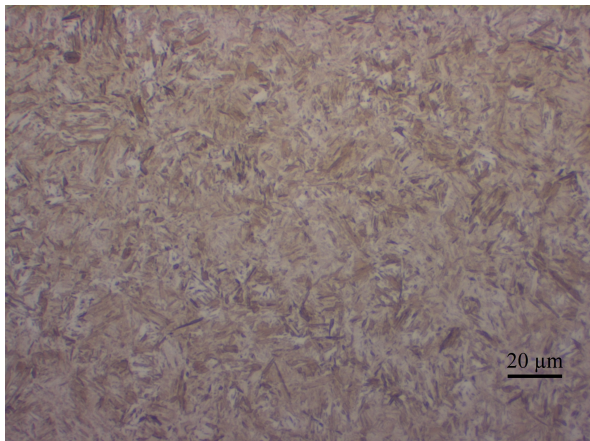


Figure 47: Direct hardened 42M13B (1.N). Etched with 2 % Nital. Magnification: 500x.

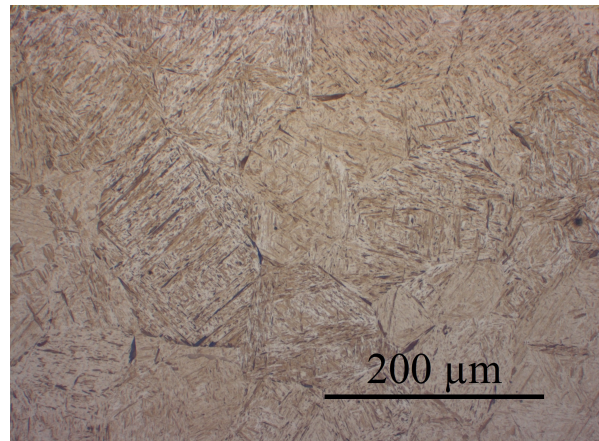


Figure 48: Direct hardened 42M13B (1.N*). Etched with 2 % Nital. Magnification: 200x.

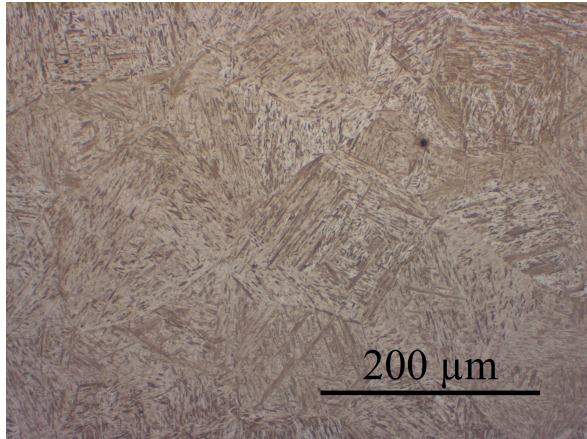


Figure 49: *Martempered 42M13B (1.M*). Etched with 2 % Nital. Magnification: 200x.*

50CrMo4

Figure 50 to 52 show plates and/or needles which are typical for a martensitic microstructure. Some prior austenite grains and relatively large needles can be seen in Figure 51 and 52. Figure 50 shows smaller needles compared to the other samples.

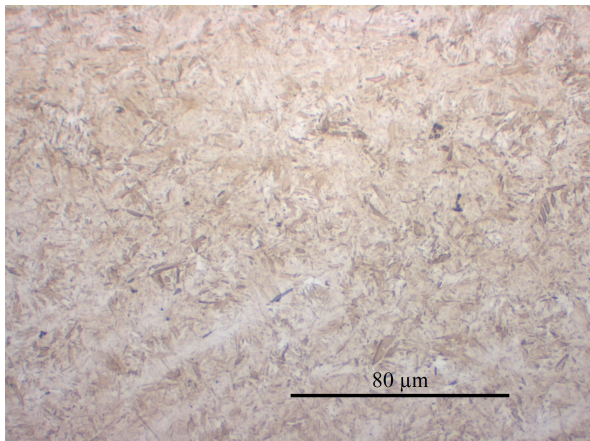


Figure 50: *Direct hardened 50CrMo4 (2.N). Etched with 2 % Nital. Magnification: 500x.*

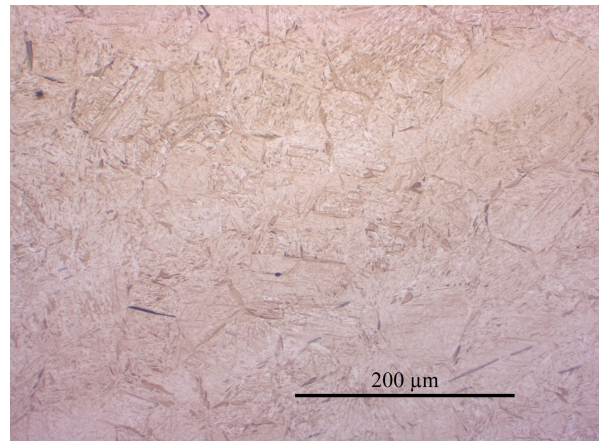


Figure 51: *Direct hardened 50CrMo4 (2.N*). Etched with 2 % Nital. Magnification: 200x.*

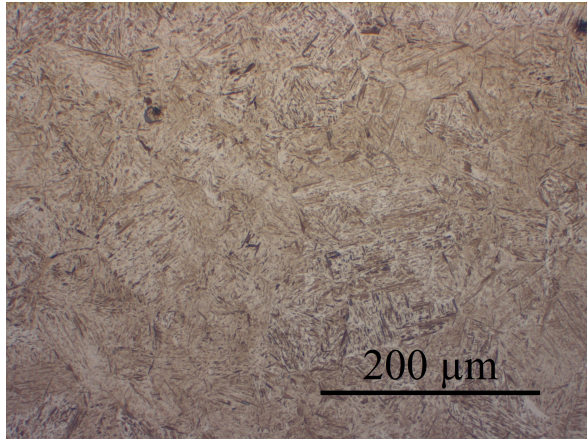


Figure 52: *Martempered 50CrMo4 (2.M*). Etched with 2 % Nital. Magnification: 200x.*

100Cr6

Figure 53 and 54 probably show a bainitic microstructure. The dark needles in Figure 54 are probably plates or needles of bainite, while the light areas can be martensite. Figure 53 shows smaller needles compared to the other sample.

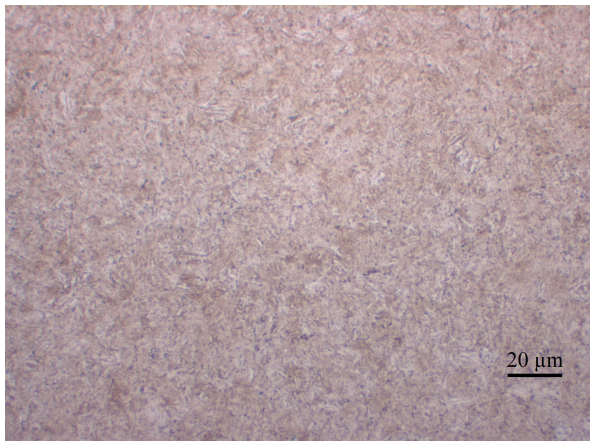


Figure 53: *Austempered 100Cr6 (3.B). Etched with 2 % Nital. Magnification: 500x.*

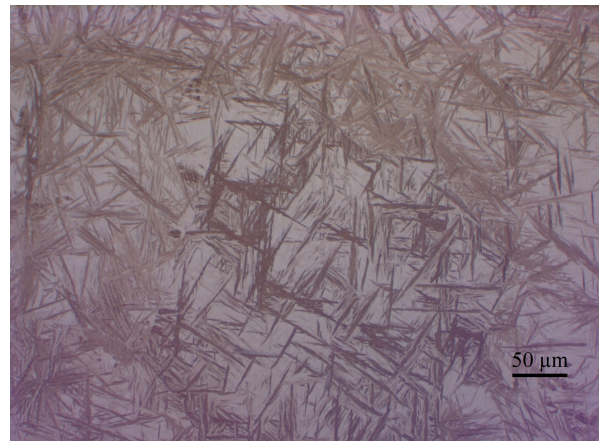


Figure 54: *Austempered 100Cr6 (3.B*). Etched with 2 % Nital. Magnification: 200x.*

100CrSiMn6-5-4

Figure 55 and 56 probably show a bainitic microstructure. The dark needles in Figure 56 are probably plates or needles of bainite, while the light areas can be martensite. The needles of bainite seems to be most frequent along prior austenite grains. Figure 55 shows smaller needles compared to the other sample.

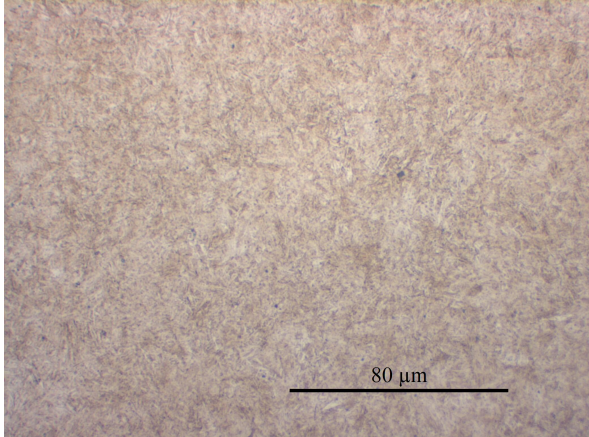


Figure 55: *Austempered 100CrSiMn6-5-4 (4.B). Etched with 2 % Nital. Magnification: 500x.*

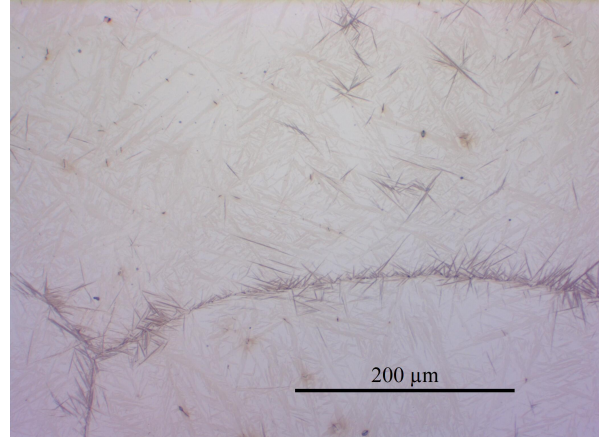


Figure 56: *Austempered 100CrSiMn6-5-4 (4.B*). Etched with 2 % Nital. Magnification: 200x.*

11M13CB

Figure 57 probably shows plates and/or needles of a martensitic microstructure.

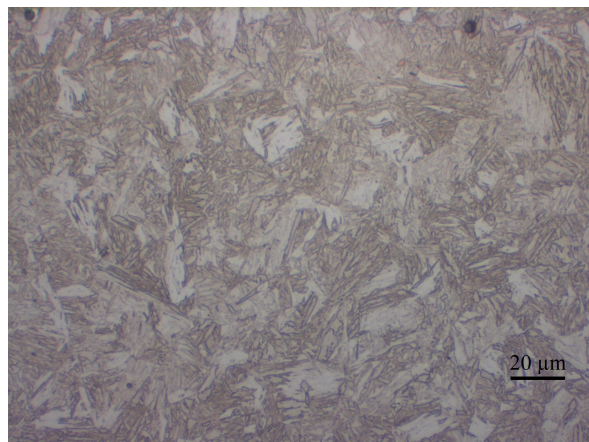


Figure 57: *Direct hardened 11M13CB (5.N). Etched with 2 % Nital. Magnification: 500x.*

18MnCrSiMoVB6

Figure 58 and 59 probably show plates and/or needles of a martensitic microstructure. These microstructures are likely predominantly martensite, while Figure 60 probably mainly contains bainite. The light areas can be retained austenite.

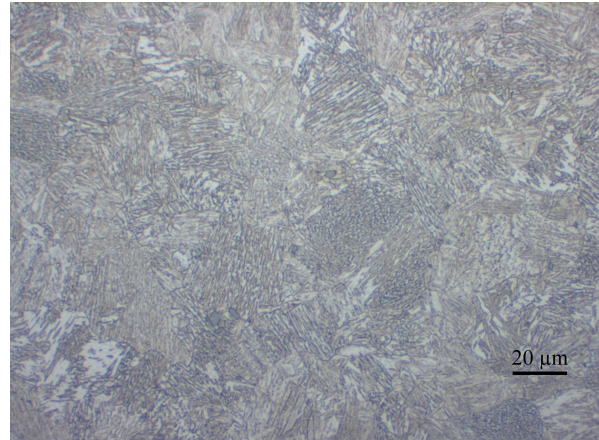
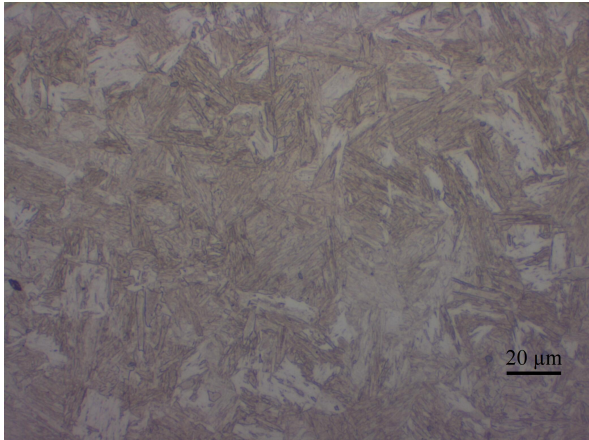


Figure 58: *Direct hardened 18MnCrSiMoVB6 (6.N). Etched with 2 % Nital. Magnification: 500x.* **Figure 59:** *Martempered 18MnCrSiMoVB6 (6.M). Etched with 2 % Nital. Magnification: 500x.*

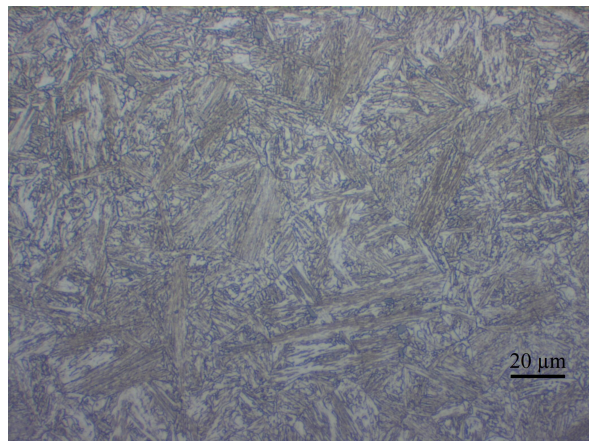


Figure 60: *Austempered 18MnCrSiMoVB6 (6.B). Etched with 2 % Nital. Magnification: 500x.*

27MnSiCrVB6

Figure 61 and 62 probably show plates and/or needles of a martensitic microstructure. These microstructures are likely predominantly martensite, while Figure 63 probably mainly contains bainite. The light areas can be retained austenite.

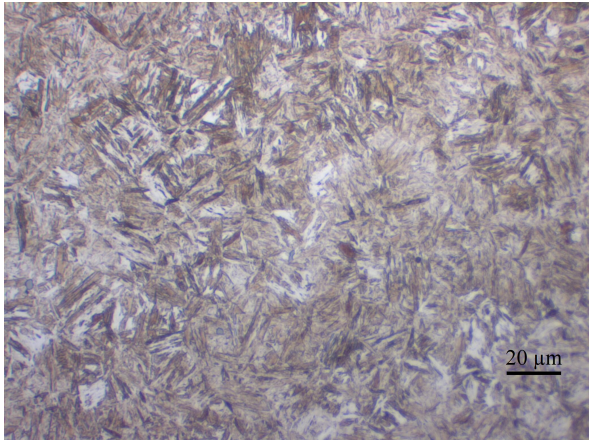


Figure 61: Direct hardened 27MnSiCrVB6 (7.N). Etched with 2 % Nital. Magnification: 500x.

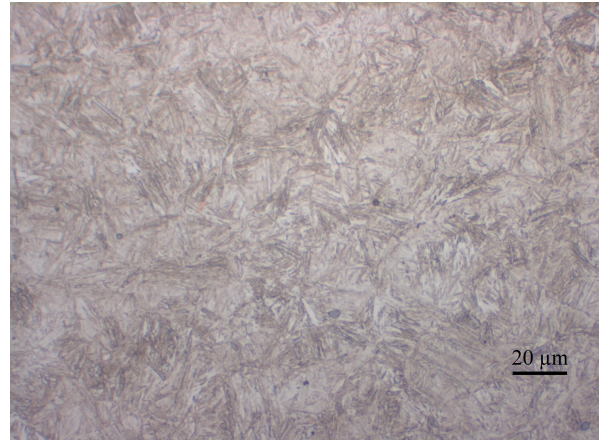


Figure 62: Martempered 27MnSiCrVB6 (7.M). Etched with 2 % Nital. Magnification: 500x.

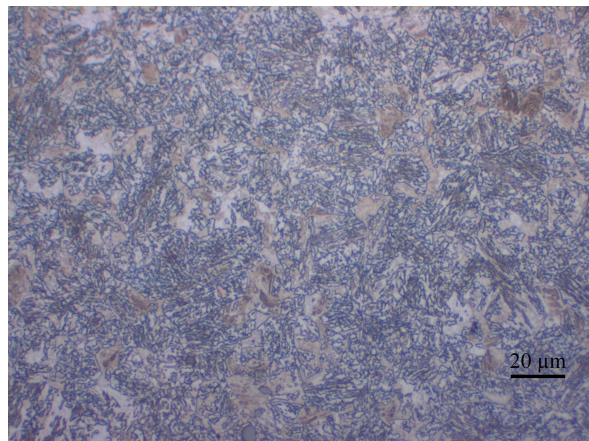


Figure 63: Austempered 27MnSiCrVB6 (7.B). Etched with 2 % Nital. Magnification: 500x.

35MnCrMoVB5

Figure 64 and 65 probably show plates and/or needles of a martensitic microstructure. These microstructures are likely predominantly martensite, while Figure 66 probably mainly contains bainite. The light areas can be retained austenite.

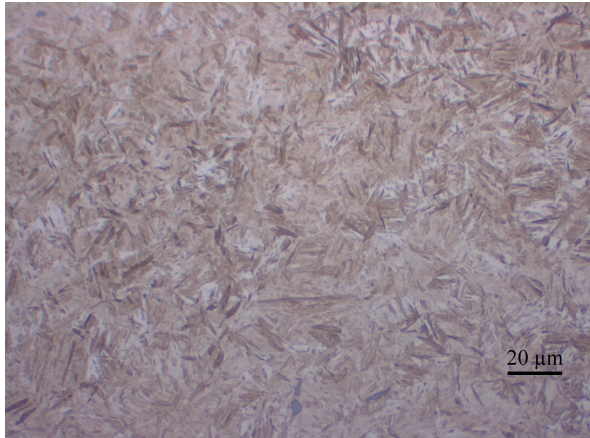


Figure 64: Direct hardened 35MnCrMoVB5 (8.N). Etched with 2 % Nital. Magnification: 500x.

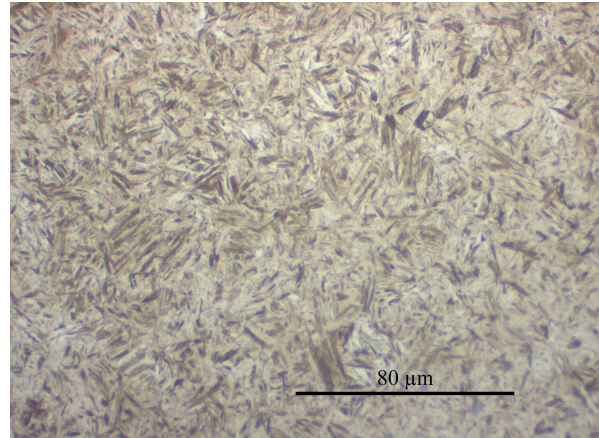


Figure 65: Martempered 35MnCrMoVB5 (8.M). Etched with 2 % Nital. Magnification: 500x.

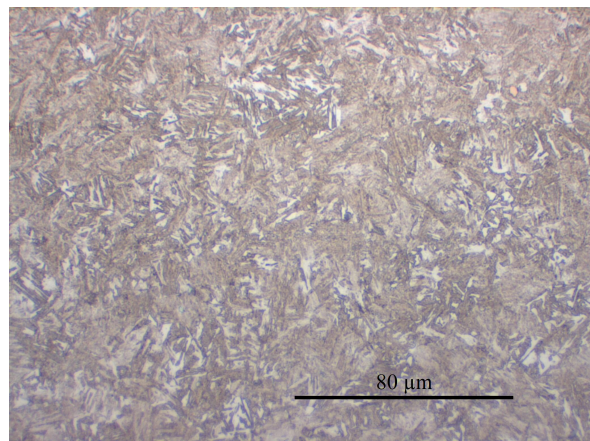


Figure 66: Austempered 35MnCrMoVB5 (8.B). Etched with 2 % Nital. Magnification: 500x.

4.2.1 EBSD

EBSD was performed on austempered 27MnSiCrVB6 (7.B) and 35MnCrMoVB5 (8.B) to be able to determine the amount of α (bainite, martensite or ferrite) and γ (austenite) phase in the microstructure. The results can show how the phase distribution affects the mechanical properties. Figure 67 and 68 show orientation maps after EBSD scan of austempered 27MnSiCrVB6 and 35MnCrMoVB5. The green phase is α/α' (BCC/ BCT) and the red phase is γ (FCC). For austempered 27MnSiCrVB6, the measured fraction of α was 0.773 and the fraction of γ was 0.189. For austempered 35MnCrMoVB5 the fraction of α was 0.588 and the fraction of γ was 0.341. The dark spots are likely particles like carbides and nitrides.

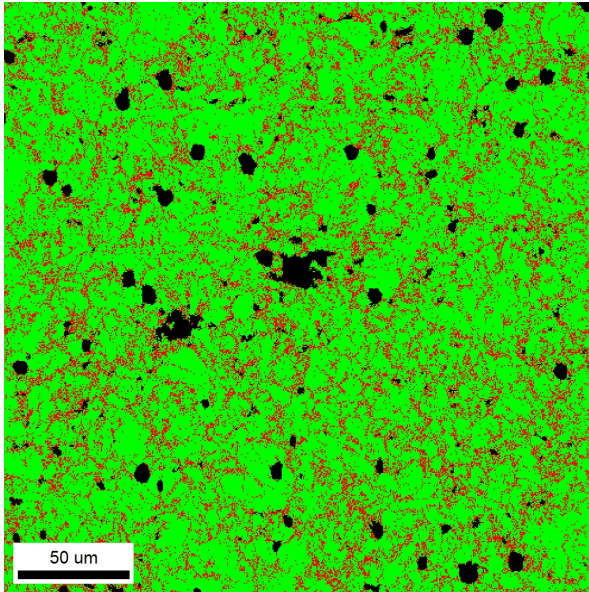


Figure 67: EBSD image of austempered 27Mn-SiCrVB6 (7.B). The measured fraction of green α was 0.773 and the fraction of red γ was 0.189. The image was taken with magnification of 400x.

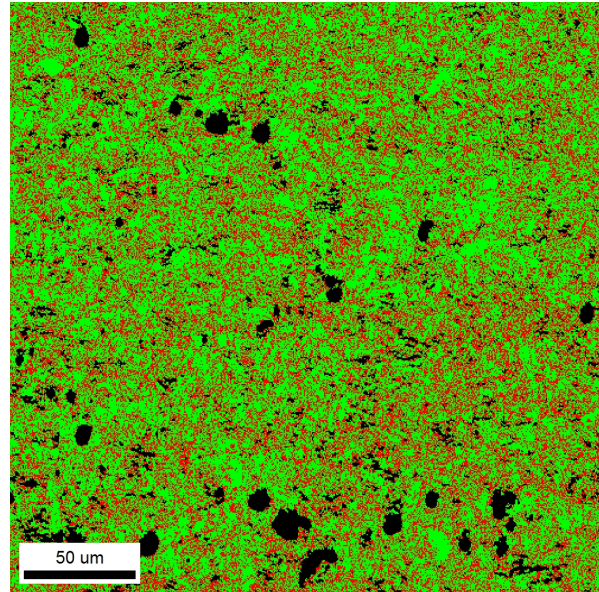


Figure 68: EBSD image of austempered 35Mn-CrMoVB5 (8.B). The measured fraction of green α was 0.588 and the fraction of red γ was 0.341. The image was taken with magnification of 400x.

4.3 Notch-impact test

4.3.1 Key data

Table 21 gives the average dial values [kgm] directly read after notch-impact testing and the read total energy [J] calculated from Equation 5. Standard deviation is included for the dial values. All tested samples of 42M13B showed higher read total energy than the other samples. For each alloy, the samples austenitized at 1200 °C followed by a lower temperature show lower energy values than the samples austenitized at only one lower temperature, an exception was 50CrMo4. Read total energy was highest for direct hardened 42M13B (1.N) and lowest for austempered 100CrSiMn6-5-4 austenitized at 1200 °C (4.B*). Dial values for all notch-impact tested samples are given in Table 30, Appendix C.

Table 21: Average dial value [kgm] and read total energy [J] for direct hardening (N), martempering (M) and austempering (B) of 42M13B (1), 50CrMo4 (2), 100Cr6 (3) and 100CrSiMn6-5-4 (4). The values are an average from three or four samples of each type.

Samples	Dial Value [kgm] ± standard deviation	Read Total Energy [J]
1.N	1.59 ± 0.08	19.09
1.N*	1.11 ± 0.04	12.5
1.M*	1.05 ± 0.05	11.67
2.N	0.88 ± 0.03	9.29
2.N*	0.83 ± 0.05	8.61
2.M*	0.89 ± 0.02	9.52
3.B	0.9 ± 0.01	10.16
3.B*	0.51 ± 0.02	4.76
4.B	0.75 ± 0.14	8.07
4.B*	0.42 ± 0.03	3.53

Table 22 gives the average dial values [kgm] directly read after notch-impact testing and the read total energy [J] calculated from Equation 5. Standard deviation is included for the dial values. For 18MnCrSiMoVB6 and 27MnSiCrVB6, read total energy was highest for the martempered samples, lower for the direct hardened samples and lowest for the austempered samples. For 35MnCrMoVB5 the energy value was quite similar, but the value was highest for austempering and lowest for direct hardening. Read total energy was highest for direct hardened 11M13CB (5.N) and lowest for austempered 27MnSiCrVB6 (7.B). Dial values for all notch-impact tested samples are given in Table 31, Appendix C.

Table 22: Average dial value [kgm] and read total energy [J] for direct hardening (N), martempering (M) and austempering (B) of 11M13CB (5), 18MnCrSiMoVB6 (6), 27MnSiCrVB6 (7) and 35MnCrMoVB5 (8). The values are an average from three or four samples of each type.

Samples	Dial Value [kgm] ± standard deviation	Read Total Energy [J]
5.N	5.26 ± 0.12	70
6.N	4.51 ± 0.57	59.78
6.M	4.76 ± 0.97	63.14
6.B	3.5 ± 0.1	45.87
7.N	2.87 ± 0.35	37.22
7.M	3.21 ± 0.18	41.93
7.B	1.51 ± 0.09	18.59
8.N	2.23 ± 0.13	28.43
8.M	2.37 ± 0.08	30.31
8.B	2.46 ± 0.14	31.59

4.3.2 Fracture surfaces

Figure 69 to 88 show SEM (scanning electron microscope) images of fracture surfaces after notch-impact testing of direct hardened, martempered and austempered 42M13B, 50CrMo4, 100Cr6, 100CrSiMn6-5-4, 11M13CB, 18MnCrSiMnVB6, 27MnSiCrVB6 and 35MnCrMoVB5.

The images were taken with a magnification of 500x. Appendix D shows images of the same fracture surfaces taken at 100x, 500x, 5000x and 10000x magnification.

42M13B

Figure 69 shows characteristics of a dimpled fracture surface. The fracture in Figure 70 seems to have occurred partly from intercrystalline fracture. Figure 71 shows a higher contribution from cleavage.

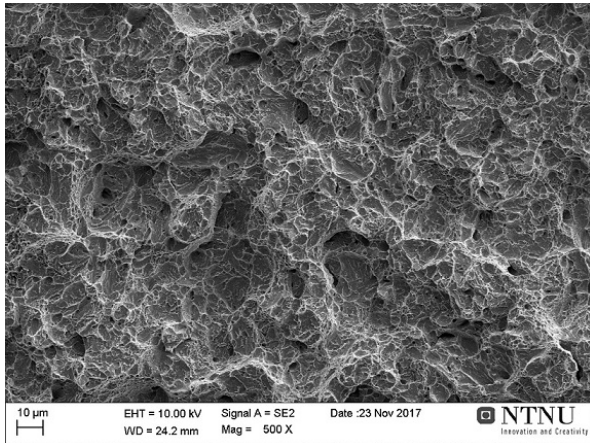


Figure 69: Direct hardened 42M13B (1.N). Magnification: 500x.

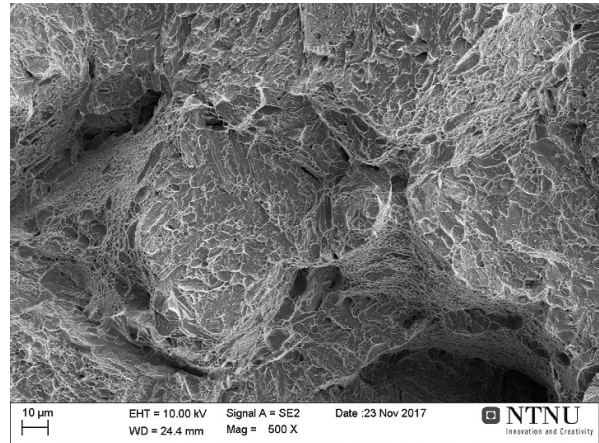


Figure 70: Direct hardened 42M13B (1.N*). Magnification: 500x.

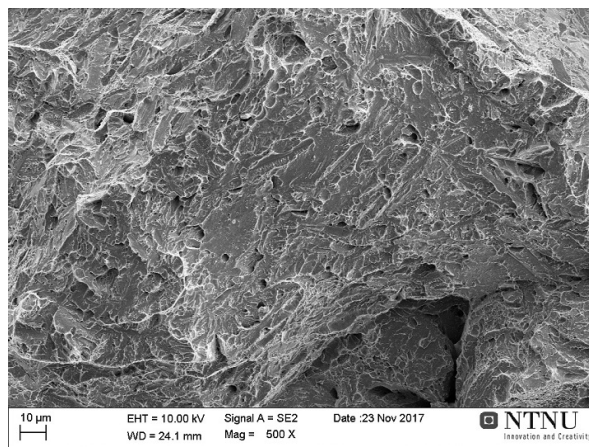


Figure 71: Martempered 42M13B (1.M*). Magnification: 500x.

50CrMo4

Figure 72 to 74 show characteristics of intercrystalline fracture surfaces. From images of higher magnification given in Appendix D, it looks like there are particles precipitated at the surfaces. Figure 72 shows smaller grains than the other samples.

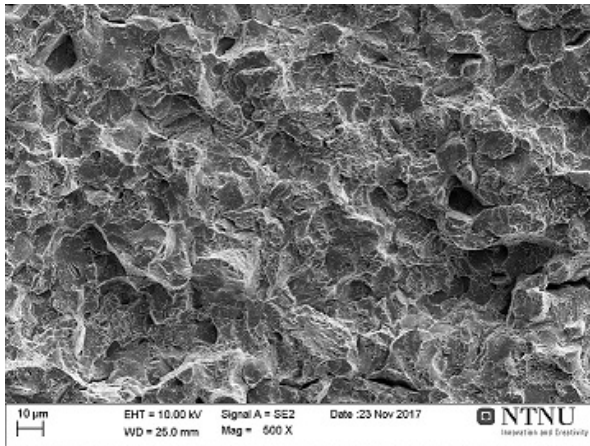


Figure 72: Direct hardened 50CrMo₄ (2.N). Magnification: 500x.

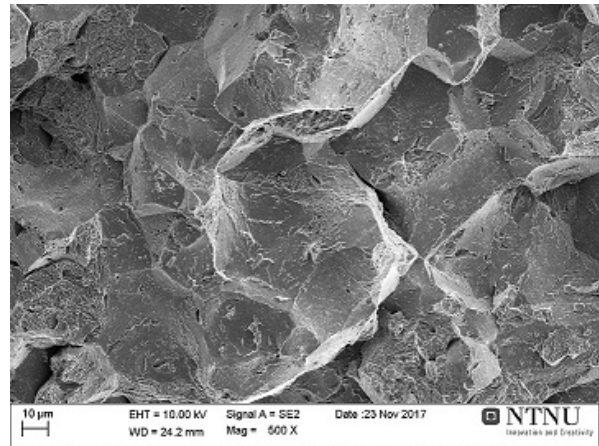


Figure 73: Direct hardened 50CrMo₄ (2.N*). Magnification: 500x.

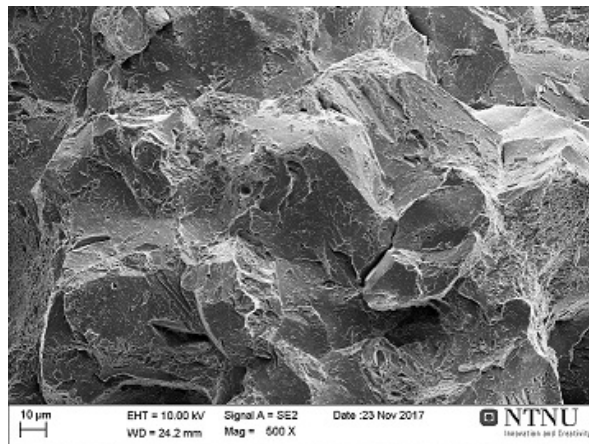


Figure 74: Martempered 50CrMo₄ (2.M*). Magnification: 500x.

100Cr6

Figure 75 and 76 show characteristics of brittle intercrystalline fracture. Smooth grain surfaces of a coarse grained steel are shown in Figure 76.

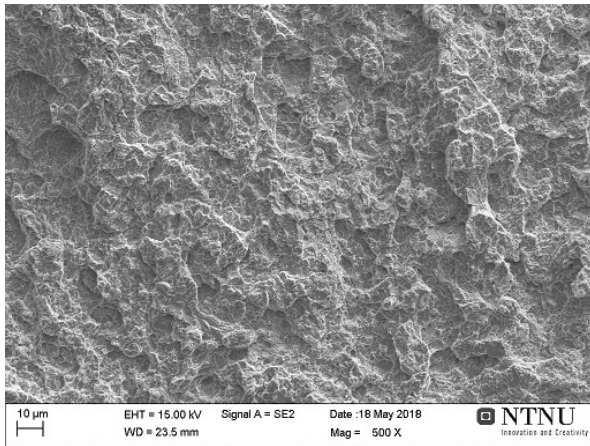


Figure 75: Austempered 100Cr6 (3.B). Magnification: 500x.

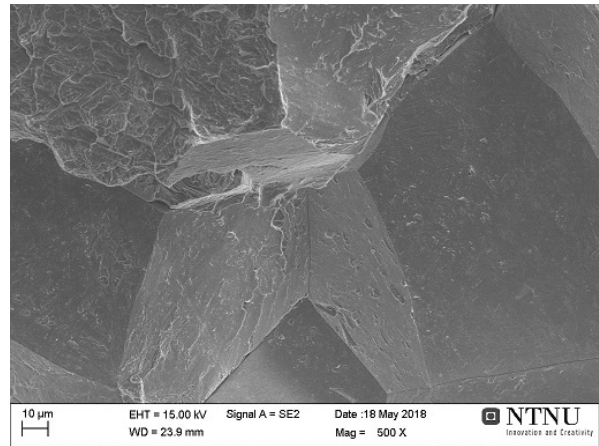


Figure 76: Austempered 100Cr6 (3.B*). Magnification: 500x.

100CrSiMn6-5-4

Figure 77 and 78 show characteristics of brittle intercrystalline fracture. Smooth grain surfaces of a coarse grained steel are shown in Figure 78.

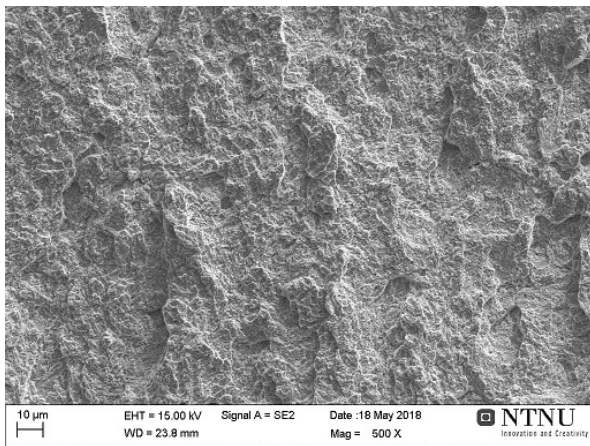


Figure 77: Austempered 100CrSiMn6-5-4 (4.B). Magnification: 500x.

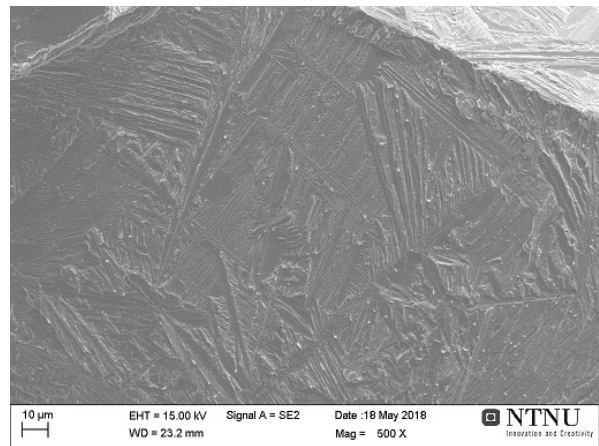


Figure 78: Austempered 100CrSiMn6-5-4 (4.B*). Magnification: 500x.

11M13CB

Figure 79 shows a dimpled surface, which is associated with ductile fracture.

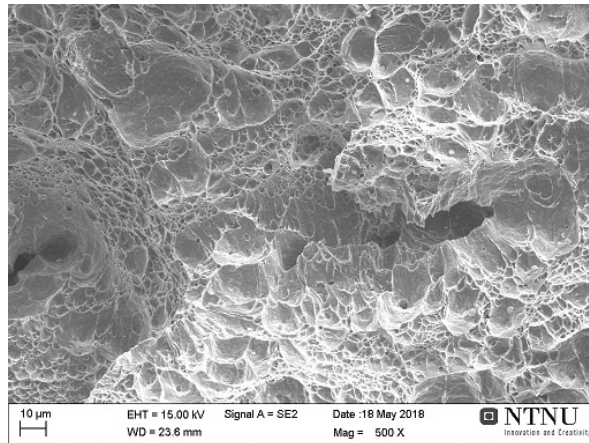


Figure 79: *Direct hardened 11M13CB (5.N). Magnification: 500x.*

18MnCrSiMoVB6

Figure 80 to 82 show contribution from cleavage fracture and some dimples.

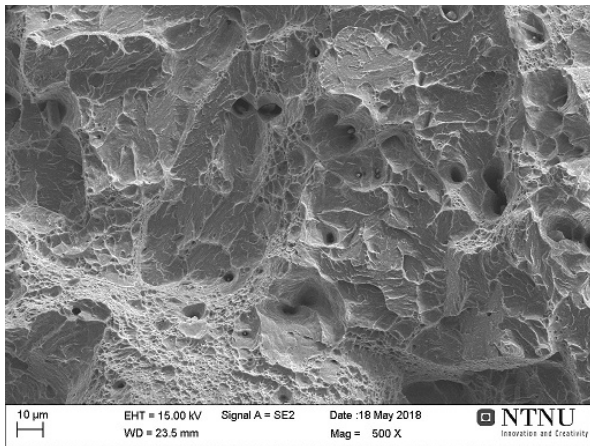


Figure 80: *Direct hardened 18MnCrSiMoVB6 (6.N). Magnification: 500x.*

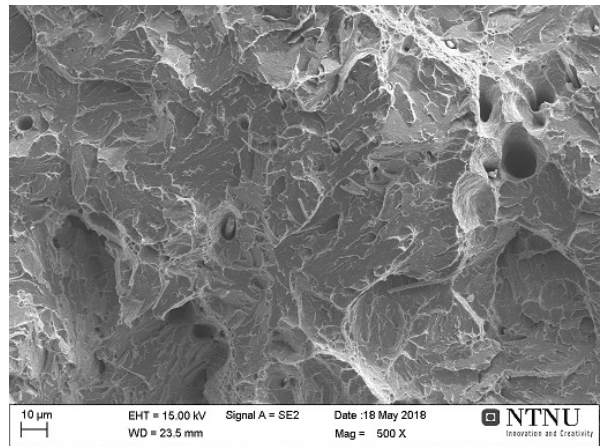


Figure 81: *Martempered 18MnCrSiMoVB6 (6.M). Magnification: 500x.*

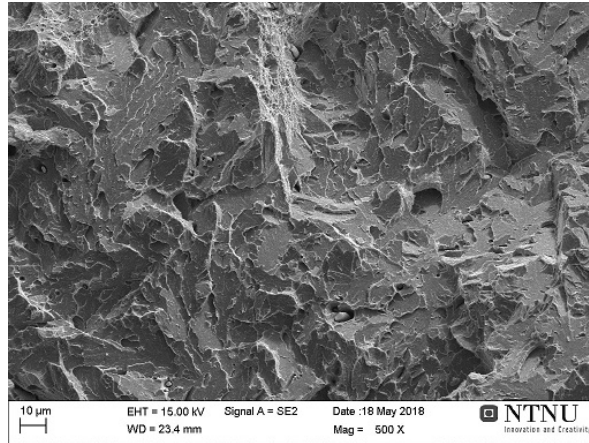


Figure 82: *Austempered 18MnCrSiMo VB6 (6.B).*
Magnification: 500x.

27MnSiCrVB6

Figure 83 to 85 show characteristics of dimples, especially for the two first samples. It looks like Figure 85 has a some contribution of cleavage.

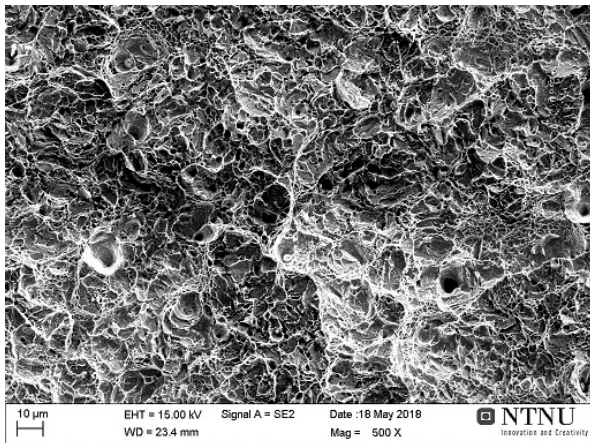


Figure 83: *Direct hardened 27MnSiCrVB6 (7.N).*
Magnification: 500x.

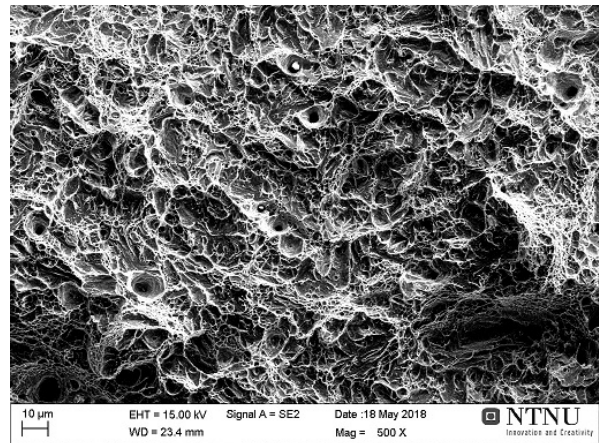


Figure 84: *Martempered 27MnSiCrVB6 (7.M).*
Magnification: 500x.

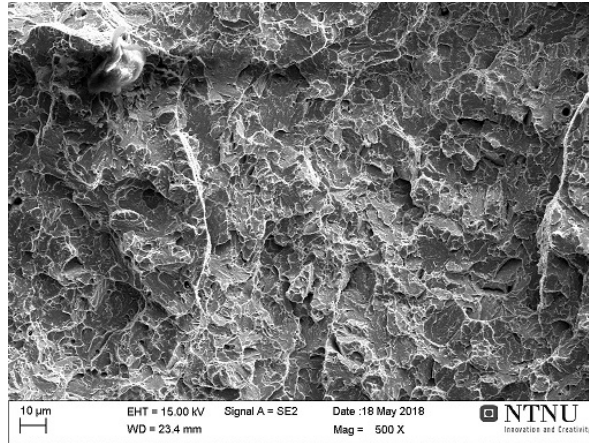


Figure 85: *Austempered 27MnSiCrVB6 (7.B).*
Magnification: 500x.

35MnCrMoVB5

It seems like the fractures in Figure 86 to 88 occurred with contribution partly from dimples and partly from cleavage. By looking at the surfaces at higher magnification, as given in Appendix D, relatively large cracks can be observed.

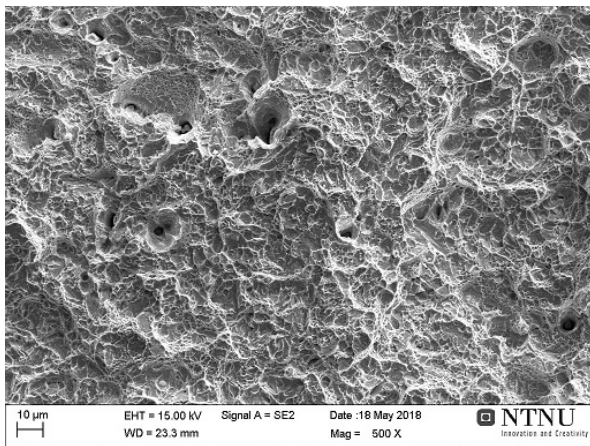


Figure 86: *Direct hardened 35MnCrMoVB5 (8.N).*
Magnification: 500x.

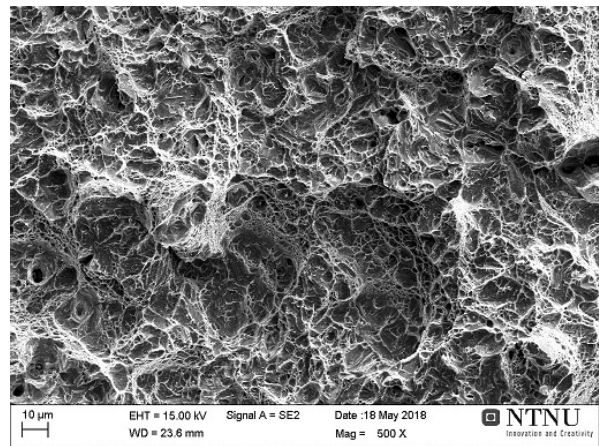


Figure 87: *Martempered 35MnCrMoVB5 (8.M).*
Magnification: 500x.

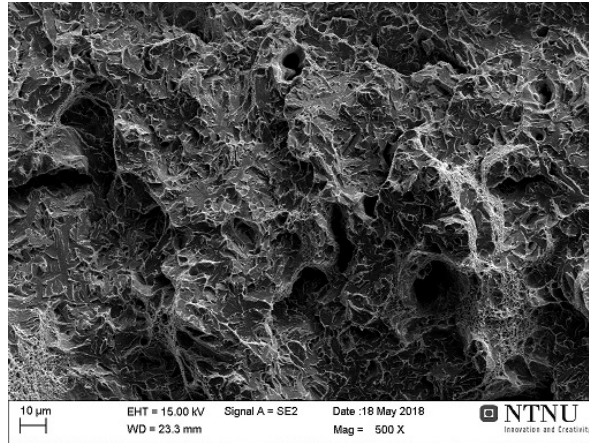


Figure 88: *Austempered 35MnCrMoVB5 (8.B).*
Magnification: 500x.

4.4 Tension test

4.4.1 Stress-strain curves

Engineering stress-strain curves for direct hardening from different austenitizing temperatures (1.N and 1.N*) and martempering (1.M*) of 42M13B are shown in Figure 89. Direct hardened 42M13B, which have not been austenitized at 1200 °C (1.N), shows a higher stress at offset yield and peak stress than the other heat treatments. Most of the tested samples for 42M13B seem to have reached peak stress.

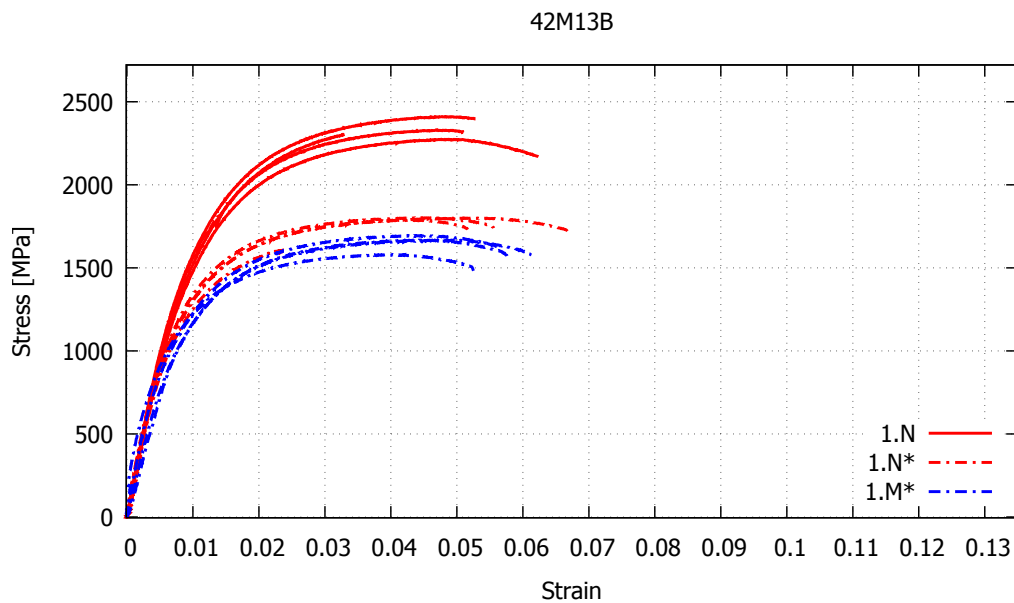


Figure 89: *Engineering stress-strain curves of direct hardened (1.N and 1.N*) and martempered (1.M*) 42M13B.*

Engineering stress-strain curves for direct hardening from different austenitizing temperatures (2.N and 2.N*) and martempering (2.M*) of 50CrMo4 are shown in Figure 90. Direct hardened 50CrMo4, which have not been austenitized at 1200 °C (2.N), shows a higher stress at offset yield than the other heat treatments. None of the direct hardened samples seems to have reached peak stress. Most of the martempered samples seem to have reached peak stress and show a better elongation than the direct hardened samples.

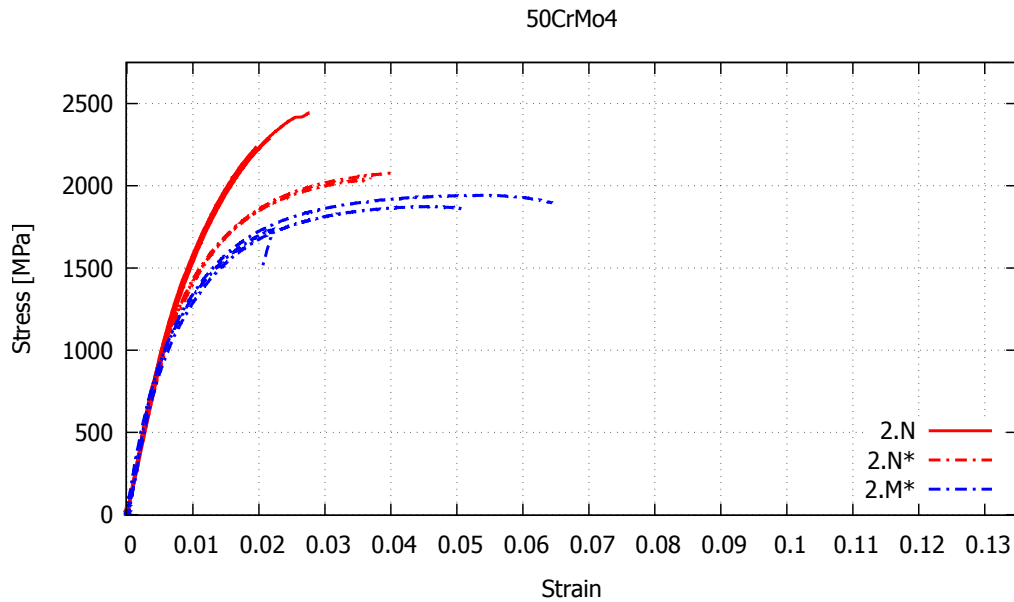


Figure 90: Engineering stress-strain curves of direct hardened (2.N and 2.N*) and martempered (2.M*) 50CrMo4.

Engineering stress-strain curves for austempering from different austenitizing temperatures (3.B and 3.B*) of 100Cr6 are shown in Figure 91. The austempered samples, which have been austenitized at 1200 °C (3.B*) seems to be very brittle. They fractured immediately outside the extensometer during testing. The austempered samples austenitized at a lower austenitizing temperature show a brittle behavior, with only little plastic deformation before fracture.

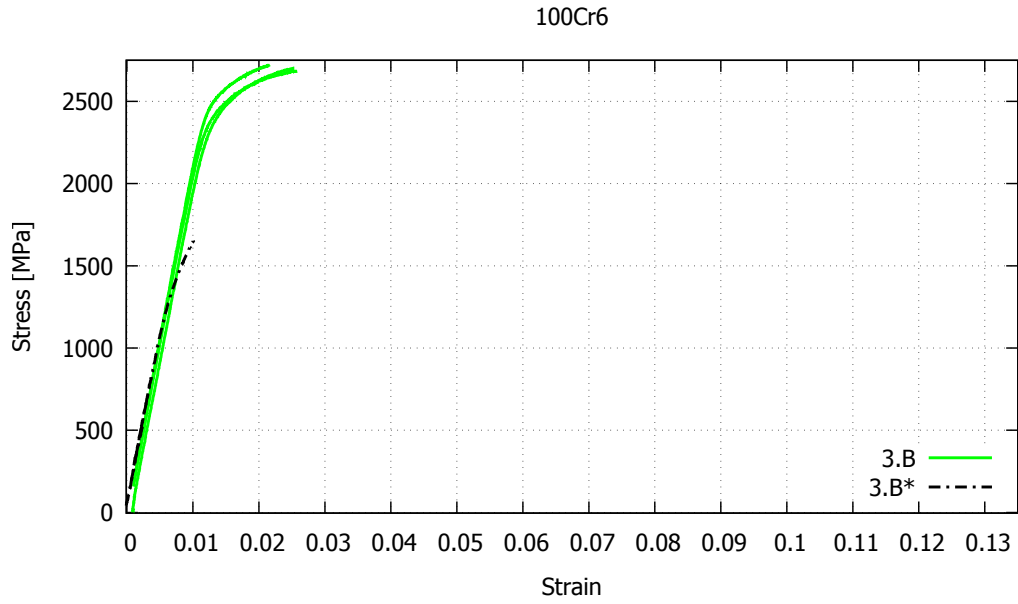


Figure 91: *Engineering stress-strain curves of austempered (3.B and 3.B*) 100Cr6.*

Engineering stress-strain curves for austempering from a low austenitizing temperature (4.B) of 100CrSiMn6-5-4 are shown in Figure 92. The curves shows a brittle behavior, with only some deformation before fracture. The samples austenitized at a higher austenitizing temperature before cooling (4.B*) could not be tested because they fractured during rough machining.

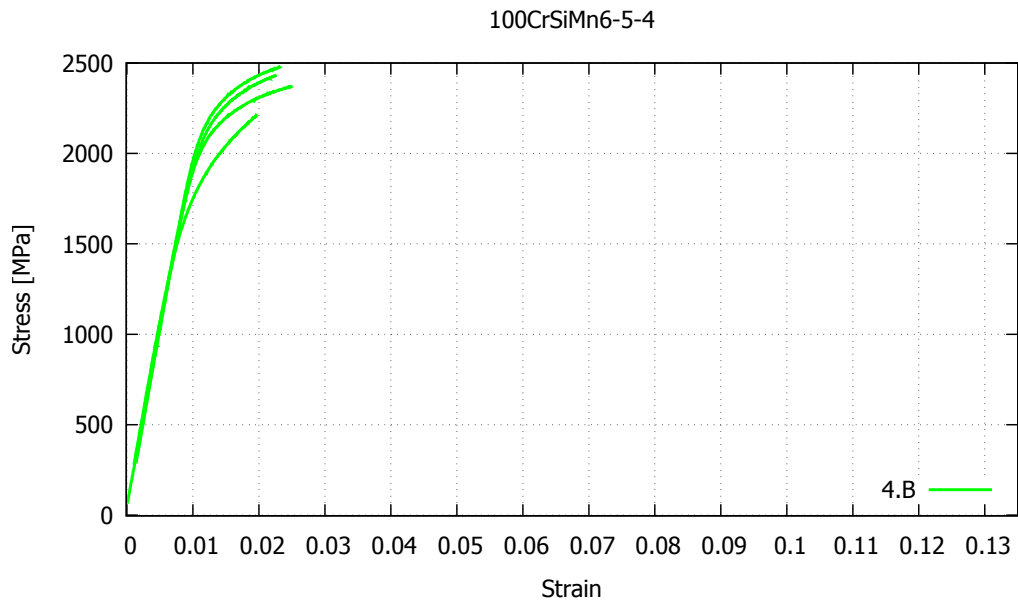


Figure 92: *Engineering stress-strain curves of austempered (4.B) 100CrSiMn6-5-4.*

Engineering stress-strain curves for direct hardening of 11M13CB are shown in Figure 93. These samples show good ductile properties.

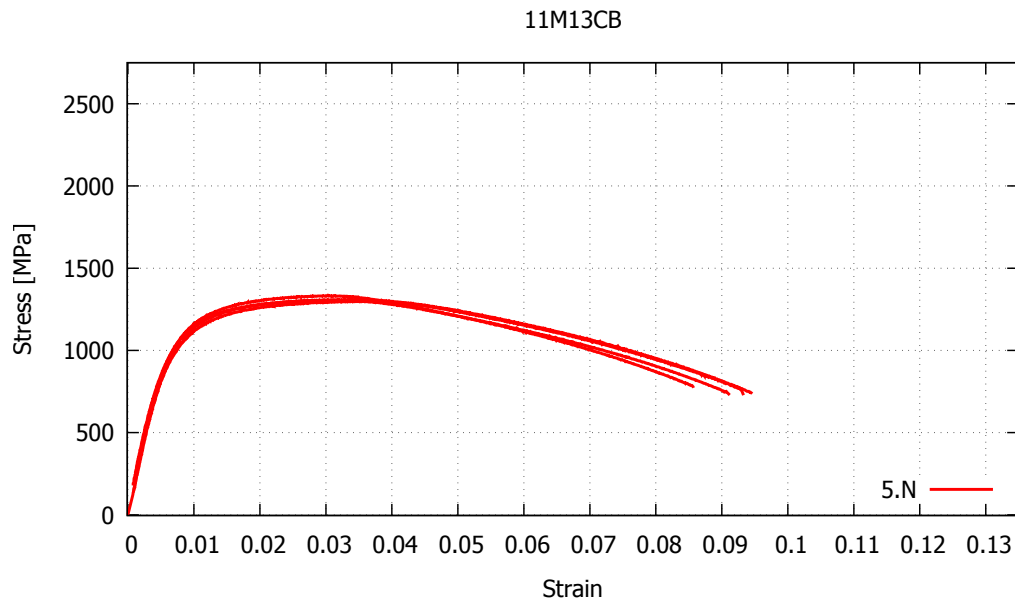


Figure 93: Engineering stress-strain curves of direct hardened (5.N) 11M13CB.

Engineering stress-strain curves for direct hardening (6.N), martempering (6.M) and austempering (6.B) of 18MnCrSiMoVB6 are shown in Figure 94. The direct hardened samples (6.N) show the highest values for stress at offset yield and peak stress and the austempered samples (6.B) the lowest. The ductility was highest for the austempered samples (6.B) and lowest for the direct hardened samples (6.N).

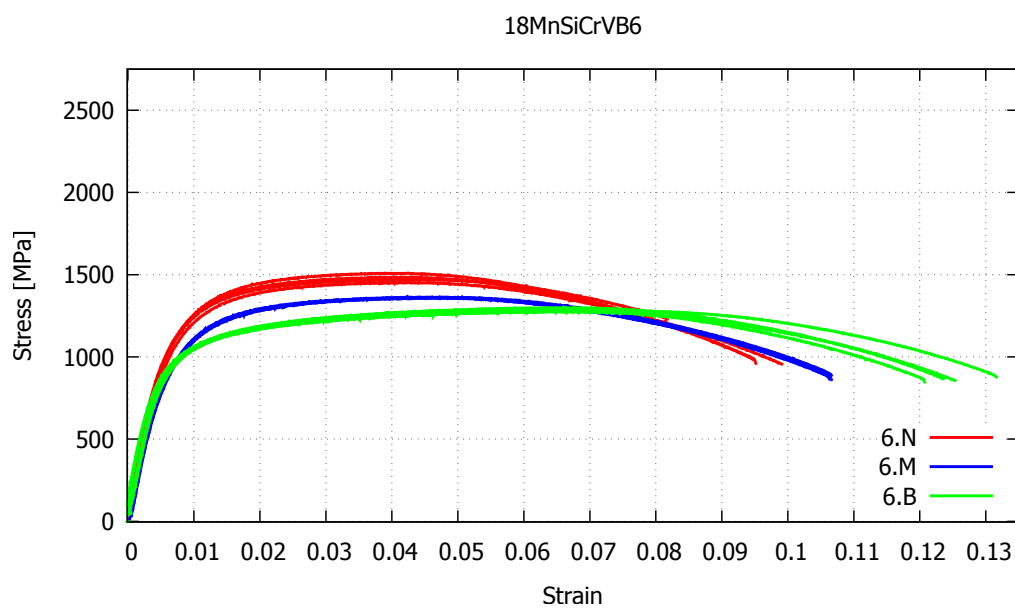


Figure 94: Engineering stress-strain curves of direct hardening (6.N), martempering (6.M) and austempering (6.B) of 18MnCrSiMoVB6

Engineering stress-strain curves for direct hardening (7.N), martempering (7.M) and austempering (7.B) of 27MnSiCrVB6 are shown in Figure 95. The direct hardened samples (7.N) show the highest values for stress at offset yield and peak stress and the austempered samples (7.B) the lowest. The ductility was highest for the austempered samples (7.B), lower for the martempered samples (7.M) and a bit lower for the direct hardened (7.N) samples.

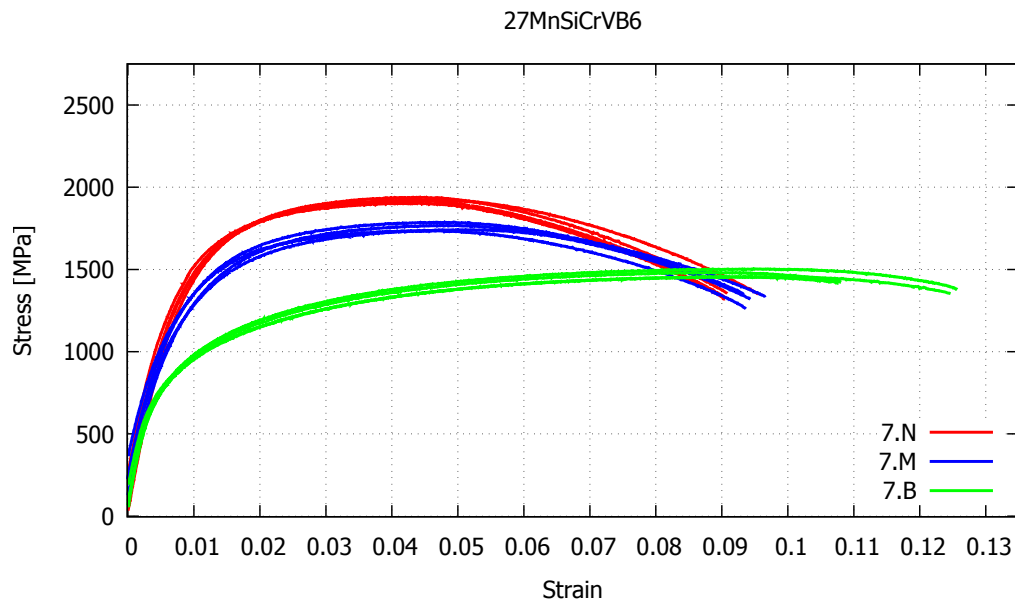


Figure 95: Engineering stress-strain curves of direct hardening (7.N), martempering (7.M) and austempering (7.B) of 27MnSiCrVB6.

Engineering stress-strain curves for direct hardening (8.N), martempering (8.M) and austempering (8.B) of 35MnCrMoVB5 are shown in Figure 96. The direct hardened samples (8.N) show the highest values for stress at offset yield and peak stress and the austempered samples (8.B) the lowest. The ductility was a bit higher for the austempered samples (8.B) than for the direct hardened (8.N) and martempered (8.M) samples.

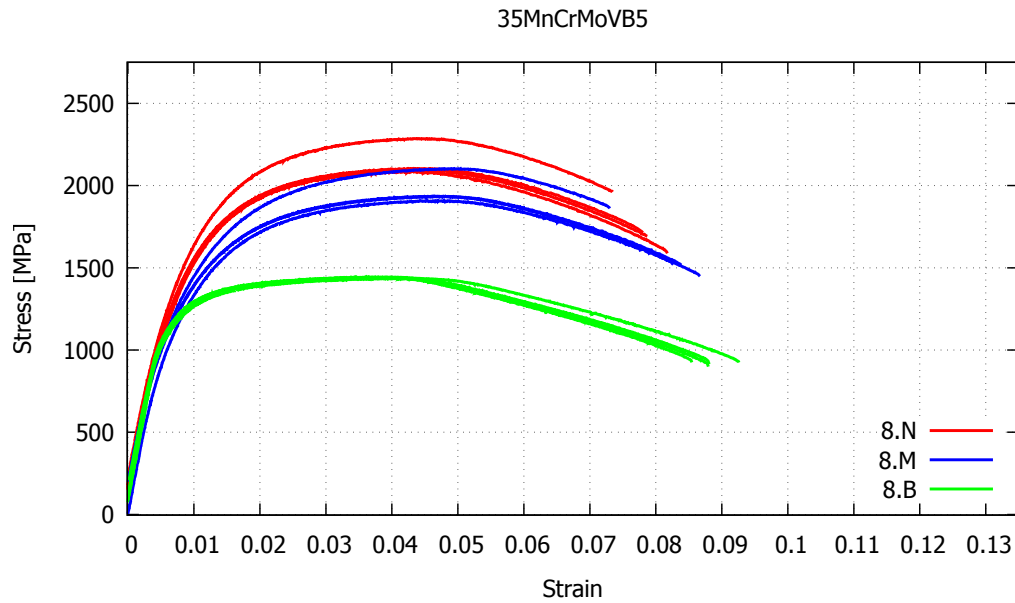


Figure 96: Engineering stress-strain curves of direct hardening (8.N), martempering (8.M) and austempering (8.B) of 35MnCrMoVB5.

4.4.2 Key data

The average engineering values for stress at offset yield [MPa] and peak stress [MPa] from tensile testing are listed in Table 23. The values for peak stress are only included for those samples that reached the top value of the stress-strain curve. Austempered 100Cr6 (3.B*) austenitized at 1200 °C fractured immediately outside the extensometer during testing, so only few data were measured. Austempered 100CrSiMn6-5-4 (4.B*) austenitized at 1200 °C, fractured during rough machining. The samples austenitized at 1200 °C seems to have lower stress at offset yield than the samples austenitized at only one lower austenitizing temperature. The stress at offset yield was highest for austempered 100Cr6 (3.B), but these samples did not reach peak stress. Stress at offset yield was lowest for martempered 42M13B (2.M*) austenitized at 1200 °C. Peak stress was highest for direct hardened 42M13B (1.N).

Table 23: Average engineering values for stress at offset yield [MPa] and peak stress [MPa] for direct hardening (N), martempering (M) and austempering (B) of 42M13B (1), 50CrMo4 (2), 100Cr6 (3) and 100CrSiMn6-5-4 (4). The values are an average from three or four parallels. Only some of the samples reached peak stress. Sample 3.B* fractured outside the extensometer and sample 3.B* fractured during rough machining.

Samples	Stress At Offset Yield [MPa]	Peak Stress [MPa]
1.N	1568	2339
1.N*	1201	1797
1.M*	1107	1653
2.N	1642	-
2.N*	1353	-
2.M*	1191	1909
3.B	2469	-
3.B*	-	-
4.B	2068	-
4.B*	-	-

The average engineering values for stress at offset yield [MPa] and peak stress [MPa] from tensile testing are given in Table 24. For 18MnCrSiMoVB6, 27MnSiCrVB6 and 35MnCrMoVB5, the stress at offset yield and peak stress were highest after direct hardening, lower after martempering and lowest after austempering. Stress at offset yield was highest for direct hardened 35MnCrMoVB5 (8.N) and lowest for austempered 27MnSiCrVB6 (7.B). Peak stress was highest for direct hardened 35MnCrMoVB5 (8.N) and lowest for austempered 18MnCrSiMoVB6 (6.B).

Table 24: Average engineering values for stress at offset yield [MPa] and peak stress [MPa] for direct hardening (N), martempering (M) and austempering (B) of 11M13CB (5), 18MnCrSiMoVB6 (6), 27MnSiCrVB6 (7) and 35MnCrMoVB5 (8). The values are an average from four parallels.

Samples	Stress At Offset Yield [MPa]	Peak Stress [MPa]
5.N	1069	1312
6.N	1174	1480
6.M	1030	1362
6.B	937	1288
7.N	1437	1922
7.M	1300	1759
7.B	911	1476
8.N	1565	2143
8.M	1376	1971
8.B	1169	1441

Table 25 show the change in cross section diameter or necking during testing of the tension rods and ductility, as percent reduction in area (RA). Necking in particular shows that the given material is ductile and will not fail suddenly. Rather it will give some indication before failure. It seems like the samples austenitized at 1200 °C show a higher change in diameter and area than the samples austenitized at only one lower temperature. The measured change in diameter and area was highest for direct hardened 42M13B austenitized at 1200 °C (1.N*) and lowest for direct hardened 50CrMo4 (2.N).

Table 25: Diameter [mm] before and after tension testing, change in diameter [mm] and percent reduction in area (RA) for direct hardening (N), martempering (M) and austempering (B) of 42M13B (1), 50CrMo4 (2), 100Cr6 (3) and 100CrSiMn6-5-4 (4). The values are measured from the first sample in each sample set.

	Diameter [mm] before testing	Diameter [mm] after testing	Change in diameter [mm]	RA [%]
1.N	2.97	2.86	0.11	7.27
1.N*	3	2.67	0.33	20.79
1.M*	2.98	2.69	0.29	18.52
2.N	3.04	3.01	0.03	1.96
2.N*	2.99	2.93	0.06	3.97
2.M*	2.99	2.75	0.24	15.41
3.B	2.95	2.9	0.05	3.36
3.B*	-	-	-	-
4.B	2.95	2.86	0.09	6.01
4.B*	-	-	-	-

Table 26 show the change in cross section diameter or necking during testing of the tension rods and ductility, as percent reduction in area (RA). The measured change in diameter and area for the bainitic samples were highest for the samples made by 18MnCrSiMiVB6. Direct hardened 11M13CB (5.N) showed the highest change in diameter and area, and austempered 27MnSiCrVB6 (7.B) the lowest.

Table 26: Diameter [mm] before and after tension testing, change in diameter [mm] and percent reduction in area (RA) for direct hardening (N), martempering (M) and austempering (B) of 11M13CB (5), 18MnCrSiMoVB6 (6), 27MnSiCrVB6 (7) and 35MnCrMoVB5 (8). The values are measured from the first sample in each sample set.

	Diameter [mm] before testing	Diameter [mm] after testing	Change in diameter [mm]	RA [%]
5.N	2.98	1.71	1.27	67.07
6.N	3	1.86	1.14	61.56
6.M	2.99	1.87	1.12	60.89
6.B	2.96	1.84	1.12	61.36
7.N	2.95	1.98	0.97	54.95
7.M	2.96	2.12	0.84	48.70
7.B	3	2.67	0.33	20.79
8.N	2.96	2.2	0.76	44.76
8.M	2.94	2.48	0.46	28.84
8.B	2.95	1.95	1	56.31

4.5 Hardness testing

The average bulk hardness [HV10] for the notch-impact and tension tested 42M13B, 50CrMo4, 100Cr6 and 100CrSiMn6-5-4 are given in Table 27. Each value is an average from five indentations in the first sample in each set. These values, together with standard deviation and minimum required hardness of current plough shears are shown in Figure 97. The samples austenitized at 1200 °C for each alloy have lower hardness than the samples austenitized at

only one lower austenitizing temperature. For 42M13B and 50CrMo4, the martempered samples are softer than the direct hardened samples. Austempered 100CrSiMn6-5-4 (4.B) showed the highest average hardness and martempered 42M13B austenitized at 1200 °C (1.M*) the lowest. This was the only sample that had hardness values lower than the minimum hardness of current plough shears.

Table 27: Average hardness for direct hardening (N), martempering (M) and austempering (B) of 42M13B (1), 50CrMo4 (2), 100Cr6 (3) and 100CrSiMn6-5-4 (4) samples used for notch-impact testing and tension testing. The given values are an average from five indentations in the first sample in each set.

Samples	Hardness [HV10]	
	Notch-impact test	Tension test
1.N	643	664
1.N*	643	632
1.M*	570	595
2.N	728	749
2.N*	721	726
2.M*	685	678
3.B	702	727
3.B*	684	644
4.B	740	725
4.B*	634	617

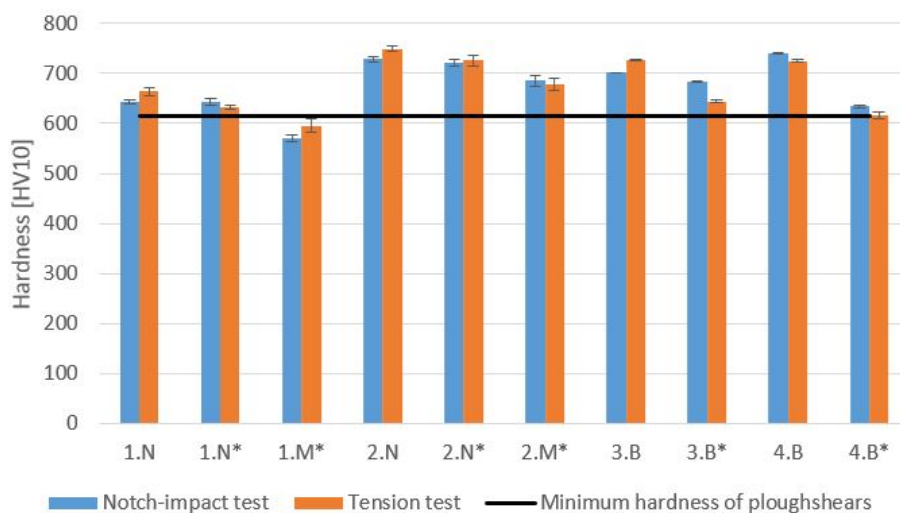


Figure 97: Average hardness, as given in Table 27, measured on notch-impact and tension tested samples. The figure includes a horizontal line for the minimum hardness of current plough shears.

The average bulk hardness [HV10] for the notch-impact and tension tested 11M13CB, 18MnCrSiMoVB6, 27MnSiCrVB6 and 35MnCrMoVB5 are given in Table 28. Each value is an average from five indentations in the first sample in each set. These values, together with standard deviation and minimum required hardness of chains are shown in Figure 98. The minimum required hardness of chains should be between 350 and 400 HV. The average hardness from notch-impact and tensile testing for 18MnCrSiMoVB6, 27MnSiCrVB6 and 35MnCrMoVB5

show highest hardness for the direct hardened samples, lower for the martempered samples and lowest for the austempered samples. Austempered 35MnCrMoVB5 (8.B) showed the highest average hardness of the austempered samples and 18MnSiCrVB6 (6.B) the lowest. This was the only one of the austempered sample where the average hardness was close to be lower than the minimum required hardness of chains.

Table 28: Average hardness for direct hardening (N), martempering (M) and austempering (B) of 11M13CB (5), 18MnCrSiMoVB6 (6), 27MnSiCrVB6 (7) and 35MnCrMoVB5 (8) samples used for notch-impact testing and tension testing. The given values are an average from five indentations in the first sample in each set.

Samples	Hardness [HV10]	
	Notch-impact test	Tension test
5.N	396	365
6.N	452	434
6.M	362	370
6.B	329	376
7.N	557	533
7.M	511	517
7.B	429	396
8.N	621	597
8.M	550	585
8.B	422	431

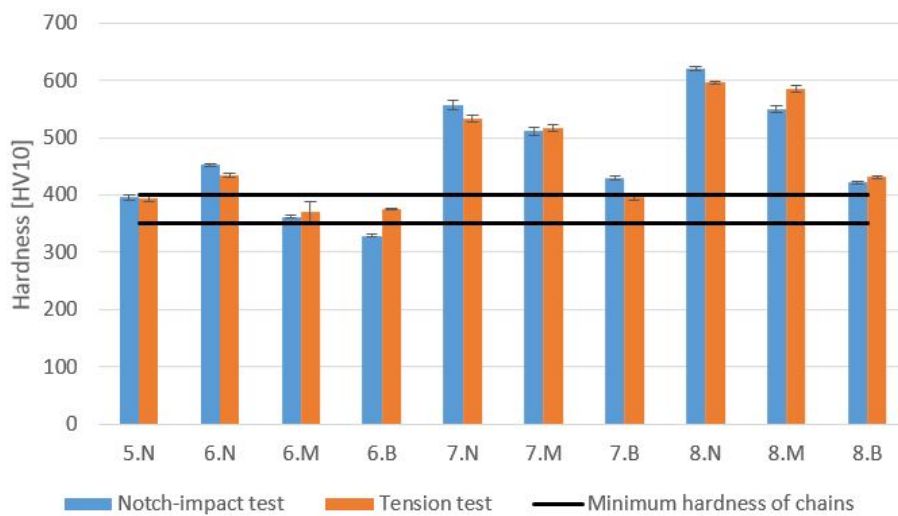


Figure 98: Average hardness, as given in Table 28, measured on notch-impact and tension tested samples. The figure includes two horizontal lines which defines the minimum hardness for chains, between 350 and 400 HV.

4.5.1 Microhardness testing

Values after microhardness testing of austempered 100Cr6 (3.B*) austenitized at 1200 °C are listed in Table 29. Microhardness testing of this microstructure was done for determination of the different regions. Hardness testing showed that the light areas were harder than the dark sheaves. The different regions tested are shown with arrows in Figure 99.

Table 29: *Microhardness of different areas in the microstructure of austempered 100Cr6 (3.B*). The values given are an average from five indentations in each microstructure area.*

Area in microstructure	Load [g]	Hardness [HV]
Dark needles	50	506
Cling of needles	100	578
Light areas	100	593

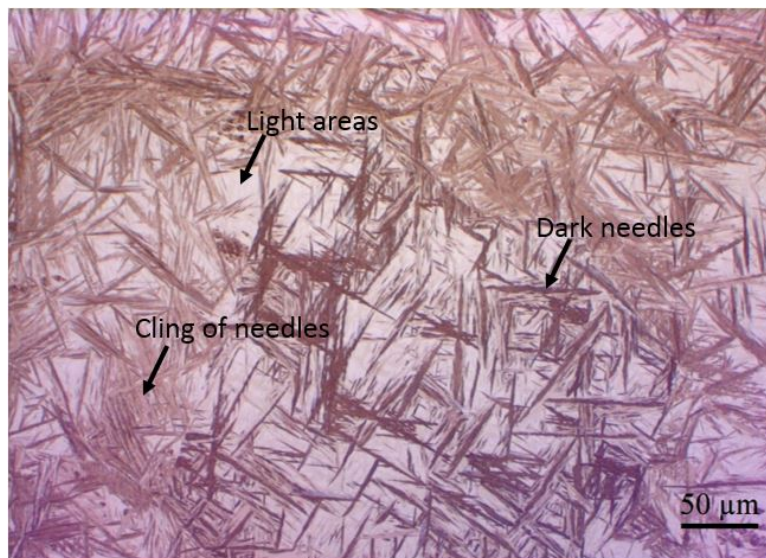


Figure 99: *Microhardness testing was performed in three different regions of the microstructure, as shown with arrows.*

5 Discussion

The mechanical properties of eight high strength bainitic and martensitic steel alloys in the hardened and untempered state have been looked at in this work. The steel covers a wide specter of alloy content, e.g the carbon content vary from a hypoeutectoid composition of 0.11 wt.% C to a hypereutectoid composition of 1.04 wt.% C.

Three types of hardening methods have been performed. These are direct hardening and martempering where martensite was the preferred microstructure and austempering where bainite was the desired microstructure. The performed hardening methods were adjusted to the specific alloys based on alloy content and per-testing.

Mechanical testing was performed to be able to understand the effect the different heat treatments had on the mechanical properties of the steel. The goal was to investigate if bainite could be used as an alternative to martensite. The mechanical properties for the performed heat treatments will contribute to a decision basis.

This part of the report will first discuss the mechanical properties of martensite compared to bainite for steels at a similar hardness. The effect of prior austenite grain size on mechanical properties of bainite will then be compared to the effect on martensite. Further, the tendency in mechanical properties across hardness levels will be looked at. Finally, the effect of silicon on mechanical properties of austempered steels will be discussed. The test results from notch-impact testing and tension testing will be the basis of the discussion, in addition to subjects like alloy content, grain size, microstructure, fracture surface and hardness.

5.1 Mechanical properties of bainite vs. martensite at similar hardness

The following sections are discussing mechanical properties of steels with hardnesses at two different levels, around 700 and 400 HV. 700 HV are relevant for plough shears produced by Kverneland, and Trygg are interested in chains with a hardness around 400 HV.

Austempering with isothermal transformation of austenite to bainite is a more time consuming process compared to direct hardening and martempering, as illustrated in Figure 25. Especially austempering of 100Cr6 and 100CrSiMn6-5-4 were time consuming with a holding time of 10 and 16 hours in the salt bath. An increase in time will most likely lead to a more expensive industrial production process [13, p. 25].

5.1.1 700 HV

The mechanical properties of the current plough shears are given by the properties of direct hardened 42M13B and should have a minimum hardness of 615 HV. A sufficient hardness is needed to achieve abrasion resistance. Precise geometry is also important for these parts to avoid tensile stress in the shears during assembling. Two austenitizing cycles are today used in the production of plough shears. The steel is first austenitized at 1200 °C, which is required for the forging operation. A lower temperature will give higher strength of the steel, which lead to higher rate of wear on the forging tool and the required forging force will increase. The parts are then cooled to room temperature before a second austenitizing to 870 °C is performed. The shears are then quenched from this temperature. The hardening processes discussed blow have to be performed after the second austenitizing if they are going to be used in the production

of plough shears, since these samples have only been austenitized at one lower temperature between 840 and 900 °C.

The hardening procedure for direct hardened 42M13B (1.N) and 50CrMo4 (2.N), in addition to austempered 100Cr6 (3.B) and 100CrSiMn6-5-4 (4.B) were adjusted to reach a final hardness of approximately 700 HV to have sufficient abrasive resistance for use as plough shears. All these samples had a higher hardness than the minimum required hardness of current plough shears, as can be seen in Figure 97.

The read total energy values from notch-impact testing are important for parts exposed to sudden impacts during use, as plough shears. Direct hardened 42M13B had a read total energy of 19 J, which was better than for both austempered 100Cr6 and 100CrSiMn6-5-4, which were 10 J and 8 J, respectively. Direct hardened 50CrMo4 had a read total energy of 9 J. The hardness value of direct hardened 42M13B was 643 HV10, which is substantially lower than the other samples. Austempered 100Cr6 and 100CrSiMn6-5-4 had a hardness of 702 and 740 HV10, while the hardness of direct hardened 50CrMo4 was 728 HV10, as listed in Table 27. These samples would probably have sufficient abrasion resistance due to the high hardness values, but the low energy values will likely make them unsuitable to use as plough shear material. The fracture surface of direct hardened 42M13B in Figure 69 shows some degree of ductility or dimples [25, p. 90-91], while austempered 100Cr6 and 100CrSiMn6-5-4 show characteristics of brittle fracture, as can be seen in Figure 75 and 77. This is in agreement with a smaller change in cross section diameter during tensile testing of the austempered samples, as shown in Table 25.

Tensile testing of the samples showed that the stress at offset yield was higher for the austempered samples than for the direct hardened samples at a hardness of about 700 HV as can be seen from Figure 100. The stress at offset yield was 2469 MPa for austempered 100Cr6 and 2068 MPa for austempered 100CrSiMn6-5-4, while the values were 1568 MPa and 1642 MPa for direct hardened 42M13B and 50CrMo4, respectively as given in Table 23. A stress higher than the yield strength or stress at offset yield, showed in Figure 12 [7, p. 164-145], will lead to plastic deformation of the material. An explanation of the different stress-strain properties can be the dissimilarity in the microstructure. Micrographs of direct hardened 42M13B and 50CrMo4 are shown in Figure 47 and 50. The microstructure of these samples shows larger plates and/ or needles which grew from austenite grain boundaries [5, p. 31-32] than for austempered 100Cr6 and 100CrSiMn6-5-4, as shown in Figure 53 and 55. The measured hardness values after tensile testing were in good agreement with the fact that a higher hardness contributes to a more brittle behavior [24, p. 178]. Direct hardened 42M13B was the only one of these sample series that reached peak stress and showed the highest degree of necking, as can be seen in Table 25.

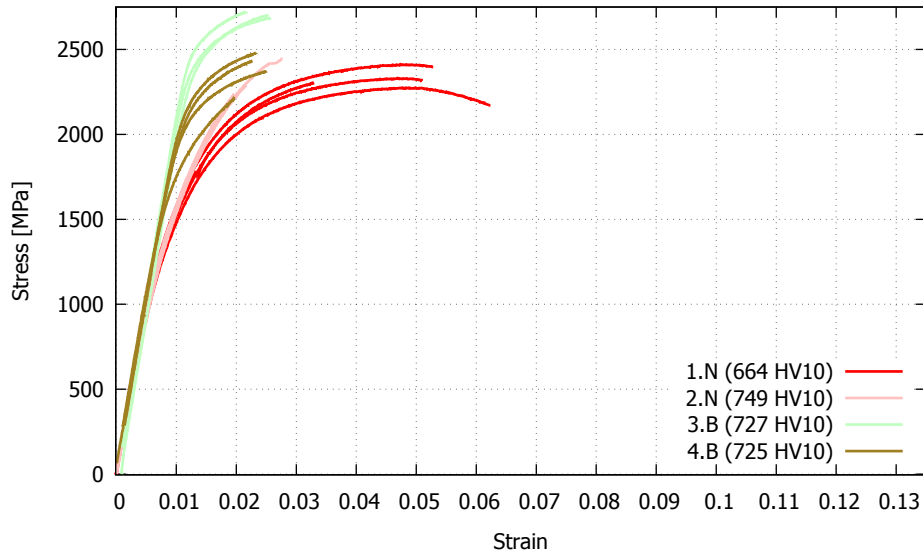


Figure 100: Engineering stress-strain curves for direct hardened 42M13B (1.N), direct hardened 50CrMo4 (2.N), austempered 100Cr6 (3.B) and austempered 100CrSiMn6-5-4 (4.B) with a hardness in the region of 700 HV10.

5.1.2 400 HV

Trygg have not fully characterized the mechanical properties of the current chain, but a minimum hardness in the range of 350-400 HV is required. One of the most important properties is the ultimate tensile strength or peak stress, as shown in Figure 12 [7, p. 164-145]. The chains are produced from coils or bars, which are cold deformed to a smaller cross section. The reduction ratio of the cross section area can be up to 30 %. The actual shaping of the chains are performed by cold deformation or by heating the steel to 500-700 °C. Further, the chains are welded, hardened and tempered.

The hardening procedure for direct hardened 11M13CB (5.N), in addition to austempered 18MnCrSiMoVB6 (6.B), 27MnSiCrVB6 (7.B) and 35MnCrMoVB5 (8.B) were adjusted to reach a final hardness of approximately 400 HV. All these samples had an average hardness higher than the minimum required hardness of current chains. The average hardness of austempered 18MnCrSiMoVB6 was on the lower limit, as can be seen in Figure 98.

Notch-impact testing, as given in Table 22, shows a read total energy of 70 J for direct hardened 11M13CB and 46, 19 and 32 J for austempered 18MnCrSiMoVB6, 27MnSiCrVB6 and 35MnCrMoVB5, respectively. All of the austempered samples showed a considerable lower energy than the direct hardened samples at similar hardness. The fracture surface of direct hardened 11M13CB is shown in Figure 79. The surface seem to be dimpled, which indicates that plastic deformation was a part of the fracture process [25, p. 90-91]. This property was here more clear than for the austempered samples which seem to have a higher contribution of cleavage fracture where crack propagation corresponds to successive and repeated breaking of atomic bonds along specific crystallographic planes [7, p. 240-241], as can be seen in Figure 82, 85 and 88. The change in diameter during tensile testing was highest for direct hardened 11M13CB as given in Table 26, which also support this observation.

EBSD was performed on austempered 27MnSiCrVB6 and 35MnCrMoVB5 to see the effect

different distributions of α/α' and γ had on mechanical properties. 27MnSiCrVB6 and 35MnCrMoVB5 was chosen based on the different silicon content, which was [REDACTED] respectively. Addition of silicon enhances the toughness, since it has a negligible solubility in cementite and hence greatly retards its precipitation [14]. The resulting phase maps can be seen in Figure 67 and 68. The green areas proves that the microstructure mainly consists of α phase, but it does not specify if it is martensite or bainite. Based on an isothermal transformation on the basis of the TTT diagrams [2, p. 63] in Figure 22 and 24, and the fact that the 27MnSiCrVB6 and 35MnCrMoVB5 were quenched to 420 and 360 °C, it is reasonable to believe that the α phase mainly consists of bainite. The red areas show the amount of γ phase in the steel. This phase is retained austenite, which has good ductile properties [2, p. 388]. The fraction of α and γ in 27MnSiCrVB6 was 0.773 and 0.189. In 35MnCrMoVB5 the fraction was 0.588 and 0.341. The black spots could be carbide or nitide precipitations in the microstructure since they were not indexed neither as FCC or BCC. Particles can lead to embrittlement and prevent grain growth [5, p. 73].

Tensile testing of the samples gave highest stress at offset yield for austempered 35MnCrMoVB5 and second highest for the direct hardened 11M13CB. The values were 1169 MPa and 1069 MPa, respectively as given in Table 24. Austempered 18MnCrSiMoVB6 and 27MnSiCrVB6 gave lower stress at offset yield, but a significant better elongation, which can be seen in Figure 101. Peak stress for austempered 27MnSiCrVB6 and 35MnCrMoVB5 were 1476 MPa and 1441 MPa, as listed in Table 24, which were higher than 1312 MPa, measured for direct hardened 11M13CB. Peak stress of austempered 18MnCrSiMoVB6 was 1288 MPa, which was slightly lower than for the direct hardened samples.

The measured hardness values after tensile testing of austempered 18MnCrSiMoVB6, 27MnSiCrVB6 and 35MnCrMoVB5 were 376, 396 and 431 HV10, respectively as given in Table 28. The hardness increased with increasing carbon content [6, p. 121]. It can be seen from Figure 101 that the elongation increases with reduced hardness for the austempered samples. Austempering have benefits as tougher and more ductile structure at equal hardness, compared to martensitic hardening [2, p. 485]. Austempered 18MnCrSiMoVB6 and 27MnSiCrVB6 had clearly greater areas under the stress-strain curve and were more ductile than the direct hardened 11M13CB. Austempered 35MnCrMoVB5 shows a greater area, but less ductility. This can be due to the relatively high amount of carbon in 35MnCrMoVB5 of 0.34 wt.% C, compared to 0.18 and 0.26 wt.% in 18MnCrSiMoVB6 and 27MnSiCrVB6, as given in Table 4. 35MnCrVB5 contained a higher amount of γ phase or retained austenite as given in the EBSD results, compared to 27MnSiCrVB6 as shown in Figure 67 and 68. Retained austenite itself is a ductile phase but the fact that it can transform into martensite during deformation can lead to a less ductile material in spite of increased content of retained austenite [11, p. 314]. This can therefore be an explanation of the reduced ductility in austempered 35MnCrVB5 compared to 27MnSiCrVB6.

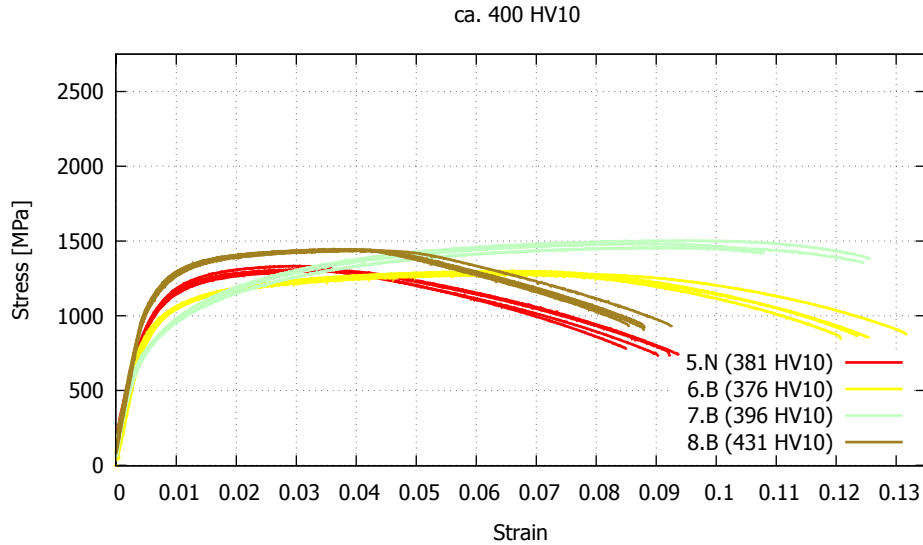


Figure 101: Engineering stress-strain curves for direct hardened 11M13CB (5.N), in addition to austempered 18MnCrSiMoVB6 (6.B), 27MnSiCrVB6 (7.B) and 35MnCrMoVB5 (8.B) at a hardness in the order of 400 HV10.

5.2 Effect of prior austenite grain size on mechanical properties of bainite vs. martensite

Austenitizing at 1200 °C followed by a lower austenitizing temperature and cooling from only one lower austenitizing temperature were performed, which resulted in varying grain sizes for the different steel grades. The following hardening procedures were adjusted for the samples to reach approximately 700 HV and can therefore be relevant for use in the production of ploughshears. It would have been cost saving for Kverneland to reduce the number of austenitizing cycles in the manufacturing process from two to only one. This can be done if the mechanical properties of the steel austenitizing at 1200 °C followed by a lower austenitizing temperature are sufficient. It would lead to reduced production time, less energy consumption and require less manufacturing storage area.

Nearly all these samples had a hardness higher than the minimum required hardness of current plough shears, as shown in Figure 97. The hardness of martempered 42M13B austenitized at 1200 °C was lower than the minimum required hardness of current plough shears. The reason for this low hardness can be self annealing due to the relatively high salt bath temperature during quenching. Another reason can be formation of some bainite in the microstructure due to inadequate hardenability [6, p. 170]. This is illustrated by the cooling curve for the core in the CCT diagram in Figure 2, where it may have occurred some bainite transformation before M_s was reached.

5.2.1 Prior austenite grain sizes

The mechanical properties of heat treated steel alloys are strongly influenced by the grain size of the parent austenite phase. Therefore, attempts have been made on determination of prior austenite grain sizes to be able to investigate the effect on the mechanical properties of bainite and martensite. Since grains could not be etched properly for all samples, a comparison of

data was done to range the prior austenite grain size for samples of 42M13B (1.N, 1.N* and 1.M*), 50CrMo4 (2.N, 2.N* and 2.M*), 100Cr6 (3.B and 3.B*) and 100CrSiMn6-5-4 (4.B and 4.B*), with a hardness around 700 HV. This comparison was based on the measured grain sizes, micrographs of etched samples for grain size determination and fracture surfaces.

100CrSiMn6-5-4 austempered from 1200 °C followed by a lower austenitizing temperature was determined to have the largest prior austenite grain size, which can clearly be seen from Figure 45. The grain size was determined to be 548 $\mu\text{m}/\text{grain}$, as shown in Table 20. 100Cr6 could not be clearly etched, but Figure 42 shows that austempering this alloy from 1200 °C followed by a lower austenitizing temperature gave second largest grains. The large grain sizes for these two samples can also be seen from the fracture surfaces in Figure 46 and 43. It looks like intercrystalline fracture had occurred along prior austenite grain boundaries [7, p. 240-241]. SEM images of the fracture surfaces in Figure 76 and 78 show smooth grain surfaces and therefore support this. Facets, as for these samples, could be seen with the naked eye on the fracture surface, were not visible in that way for other sample series. The difference in prior austenite grain size was probably mainly affected by the alloy content. The total content of microalloying elements (Nb, V and Ti) was 0.015 at.% in 100Cr6 and 0.007 at.% in 100CrSiMn6-5-4, as given in Table 3. Microalloying elements like Ti, Nb and V can lead to reduction in grain size if they are precipitated as carbides or nitrides [2, p. 226]. According to Figure 9 [5, p. 104] vanadium carbide dissolve at relatively low temperatures and will therefore contribute little to the grain boundary pinning during the heating process. TiN have low solubility in austenite and since the amount of titanium was higher in 100Cr6 than in 100CrSiMn6-5-4, this can be an explanation on the difference in grain size.

Third largest grain sizes were determined for 42M13B direct hardened and martempered from 1200 °C followed by a lower austempering temperature. The prior austenite grain size was determined to be 119 $\mu\text{m}/\text{grain}$, as shown in Table 18. The micrograph in Figure 38 shows the grains, which were clearly smaller than for the mentioned samples. For 50CrMo4 direct hardened and martempered from 1200 °C followed by a lower austenitizing temperature, the grain size was determined to be 54 $\mu\text{m}/\text{grain}$ as given in Table 19, and was therefore the fourth largest grain size. Microalloying elements like Ti, Nb and V can lead to reduction in grain size [2, p. 226] and can be an explanation on the reduced grain size. The amount of Ti was quite similar in 42M13B and 50CrMo4, and probably had a small effect. 50CrMo4 contains V and Nb, these microalloying elements were not found in 42M13B and are therefore a possible explanation. In addition, particles were observed on fracture surfaces for 50CrMo4, as can be seen in Appendix D, and can be an explanation of the smaller grain size [5, p. 73].

The grain sizes of the samples austenitized at only one lower austenitizing temperature were assumed to have smaller prior austenite grains than the samples austenitized at 1200 °C. This was assumed since grain size increase with increasing temperature and time in the austenite area, according to Equation 3 [18]. Direct hardened 42M13B was the only one of these samples where the prior austenite grains were clear enough after etching for determination of the grain size. The grain size was determined to be 8 $\mu\text{m}/\text{grain}$, as shown in Table 17 and Figure 37. Based on the measured grain sizes for the coarse grained samples it were assumed that the grain size of direct hardened 50CrMo4 was smaller than for direct hardened 42M13B. It was also assumed that austempered 100Cr6 had a smaller grain size than austempered 100CrSiMn6-5-4, based on the observations from the same alloys autenitized at 1200 °C followed by a lower austenitizing temperature.

The prior austenite grain sizes can be summarized as follows. For austempered samples, the prior austenite grain size was increasing from 3.B, 4.B, 3.B* to 4.B*. The grain sizes for the

direct hardened and martempered samples were probably smallest for 2.N, larger for 1.N, second largest for 2.N* and 2.M*, and largest for 1.N* and 1.M*. The grain size values are given in Table 16.

5.2.2 Bainite

Figure 54 and 56 show optical micrographs of nital etched 100Cr6 and 100CrSiMn6-5-4 austempered from 1200 °C followed by a lower austenitizing temperature (3.B* and 4.B*). When nital etchant is used on a mixture of bainite and martensite, bainite etches dark because it is a mixture of ferrite and cementite, and the bainite/ cementite are easily attacked by the nital etchant. Martensite etches lighter because of the absence of carbide precipitates [24]. The images probably show a mixed microstructure of lower bainite and martensite. In which the darkest etched sheaves correspond to lower bainite and the white regions corresponding to martensite. Microhardness measurements of austempered 100Cr6 in Table 29, show that the hardness values of dark needles of lower bainite were softer than the white regions of martensite. The hardness were 506 and 593 HV10, respectively, and confirms the metallographic observation. In micrograph of 100CrSiMn6-5-4, needles of bainite seem to be most frequent along prior austenite grains. The total amount of bainite in the microstructure would probably increase with increasing holding time in the quenching bath due to isothermal transformation.

The micrographs of austempered 100Cr6 (3.B) and 100CrSiMn6-5-4 (4.B) from only one lower austenitizing temperature are shown in Figure 53 and 55. The only difference in the heat treatment procedure for these alloys were the austenitizing temperature, still the micrographs looks different. The explanation have to be the difference in prior austenite grain size. An increase in grain size will displace the curve in a CCT diagram towards right. The number of nucleation sites decrease and the hardenability increases with increasing grain size [6, p. 176].

Notch-impact testing of the austempered samples show that read total energy was decreasing with increasing grain size. The energy values were 10, 8, 5 and 4 J as given in Table 21 for increased prior austenite grain size. Fracture surfaces of 100Cr6 and 100CrSiMn6-5-4 austenitized at 1200 °C, which show coarse grained crack propagation along grain boundaries, determined as intercrystalline fracture [7, p. 240-241], were shown in Figure 76 and 78. 100Cr6 and 100CrSiMn6-5-4 austenitized at only one lower temperature also show brittle behavior, as can be seen in Figure 75 and 77.

Coarse grained 100CrSiMn6-5-4 and 100Cr6 austenitized at 1200 °C followed by a lower austenitizing temperature fractured immediately during rough machining and during tensile testing. It therefore seems like small grains gave better tensile properties, since the coarse grained samples could not be sufficiently tested. Austempered 100Cr6 austenitized at only one lower austenitizing temperature had the smallest grain size of the austempered samples and the highest stress at offset yield, according to Equation 4 [6, p. 28-30]. Stress at offset yield was 2469 MPa, as given in Table 23. Austempered 100CrSiMn6-5-4 austenitized at only one lower austenitizing temperature was found to have the second smallest grains and a stress at offset yield of 2068 MPa, as given in Table 23, which was lower than for 100Cr6.

5.2.3 Martensite

Optical micrographs of nital etched 42M13B and 50CrMo4 direct hardened (1.N and 2.N) from only one lower austenitizing temperature, direct hardened (1.N* and 2.N*) and martempered

(1.M* and 2.M*) from 1200 °C followed by a lower austenitizing temperature were shown in Figure 47 to 52. They all show plates and/or needles in the hardened microstructure, which is typical for martensite. Direct hardened 42M13B and 50CrMo4 austenitized at one lower austenitizing temperature in Figure 47 and 50 show smaller needles than the samples austenitized at 1200 °C. Since martensite grows from austenite boundaries [5, p. 31-32], the grain size can be a possible explanation.

Notch-impact testing of the direct hardened and martempered samples showed higher read total energy values for the fine grained samples of 42M13B compared to the coarser grained samples of this alloy. For 50CrMo4 these values were quite equal for all samples, as can be seen in Table 21. Direct hardened 42M13B austenitized at only one lower temperature had a read total energy of 19 J, which was the highest value for these samples. The samples of 42M13B austenitized at 1200 °C followed by one lower temperature had considerable lower energy values of 13 J and 12 J. All the samples of 50CrMo4 show lower read total energy values than for 42M13B. Fracture surfaces of direct hardened and martempered 42M13B were shown in Figure 69 to 71. These surfaces seem to be more dimpled than the fracture surfaces of direct hardened and martempered 50CrMo4, as shown in Figure 72 to 74. Fracture surfaces of 50CrMo4 show a characteristics of intercrystalline fracture. The more brittle characteristics of 50CrMo4 than for 42M13B were according to the test results.

Figure 102 shows prior austenite grain size as function of stress at offset yield for samples hardened to a martensitic microstructure with hardness around 700 HV. A trend was that the stress at offset yield increases with decreasing prior austenite grain size, which is in accordance with Equation 4 [6, p. 28-30]. Based on Figure 89 to 92, it seems like, for those of the samples that reached peak stress, the value increases with decreasing grain size. The martempered samples seem to have a bit better elongation than the direct hardened samples of 50CrMo4. For 42M13B the elongation seems to be similar. The direct hardened samples for both 42M13B and 50CrMo4 seem to be the most brittle of these samples.

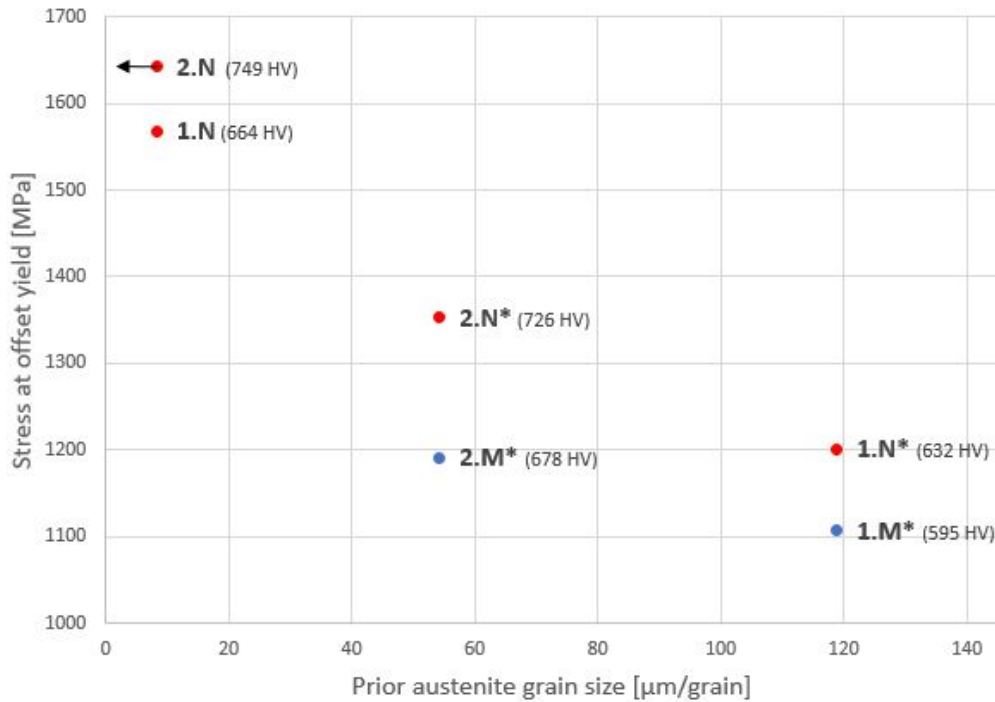


Figure 102: Prior austenite grain size [$\mu\text{m}/\text{grain}$] as a function of stress at offset yield for direct hardened and martempered 42M13B (1.N, 1.N* and 1.M*), and direct hardened and martempered 50CrMo4 (2.N, 2.N*, 2.M*). The grain size for direct hardened 50CrMo4 (2.N) was assumed to be smaller than direct hardened 42M13B (1.N), indicated by the arrow.

5.2.4 Comparison

It looks like the read total energy of bainite was more dependent on the prior austenite grain size than what martensite was. The energy of the austempered samples was decreasing with increasing grain size, while the direct hardened and martempered samples only showed this trend for the samples of 42M13B. For both bainite and martensite, the stress at offset yield will increase with decreasing grain size, according to Equation 4 [6, p. 28-30].

The difference in grain size seems to have a more significant influence on the values from tensile testing than the hardness values for both austempering and hardening to a martensitic microstructure. Austempered 100Cr6 and 100CrSiMn6-5-4 austenitized at only one lower temperature had almost equal hardness values of 727 and 725 HV10, as given in Table 27, but there was a clear difference in the stress values, Table 23. 42M13B and 50CrMo4 hardened to martensite show increasing stress values for decreasing grain size, but not a consistent trend for the hardness values, as can be seen in Figure 102.

5.3 Tendency of mechanical properties for different hardness levels

The three alloys 18MnCrSiMoVB6, 27MnSiCrVB6 and 35MnCrMoVB5 were direct hardened (6.N, 7.N and 8.N), martempered (6.M, 7.M and 8.M) and austempered (6.B, 7.B and 8.B) to be able to evaluate the mechanical properties after the different heat treatments independent of hardness levels.

The hardness testing showed a trend where the direct hardened samples got the highest hardness values, the martempered samples were second hardest and the austempered samples were softest, as given in Table 28. An explanation could be that carbon has a lower solid solution strengthening effect in bainite than martensite, due to precipitation of cementite or carbon in the austenite [9]. An exception was seen for martempered and austempered 18MnSiCrVB6 where the hardness values were quite similar. And after tensile testing, the austempered samples were even slightly harder than the martempered samples. This could be due to the relatively high and similar salt bath temperatures during cooling. The salt bath temperature was 371 °C during martempering and 385°C during austempering, as given in Table 12 and 13. In addition, the strengthening effect from carbon in the martensite was probably lower in 18MnCrSiMoVB6 than 27MnSiCrVB6 and 35MnCrMoVB5 due to a lower content of carbon.

Notch-impact testing of 18MnCrSiMoVB6 and 27MnSiCrVB6 showed a trend where read total energy was highest for the martempered samples, lower for the direct hardened samples and lowest for the austempered samples, as given in Table 22. The austempered samples were in both cases softest, but showed the lowest value of energy. For 35MnCrMoVB5 all the read total energy values were quite similar. It only differs about 3 J from highest to lowest value and the austempered samples showed the highest values and the direct hardened the lowest.

Tensile testing of the three alloys 18MnCrSiMoVB6, 27MnSiCrVB6 and 35MnCrMoVB5 were showed in Figure 94, 95 and 96. They all show the same tendency, which was that the stress at offset yield and peak stress was highest for the direct hardened samples, lower for the martempered samples and lowest for the austempered samples. An explanation of the lower yield strength for the austempered samples compared to the martempered could be that the bainite sheaf is larger than the tempered martensite plate [4]. Or it could be the difference in hardness. The ductility was best for the austempered samples, worst for the direct hardened samples and a bit better for the martempered samples.

Stress at offset yield as a function of read total energy for direct hardened, martempered and austempered 18MnCrSiMnVB6, 27MnSiCrVB6 and 35MnCrMoVB5 are shown in Figure 103. Direct hardened 11M13CB are included for comparison and shows the highest read total energy of the direct hardened samples, but also the lowest stress at offset yield and hardness.

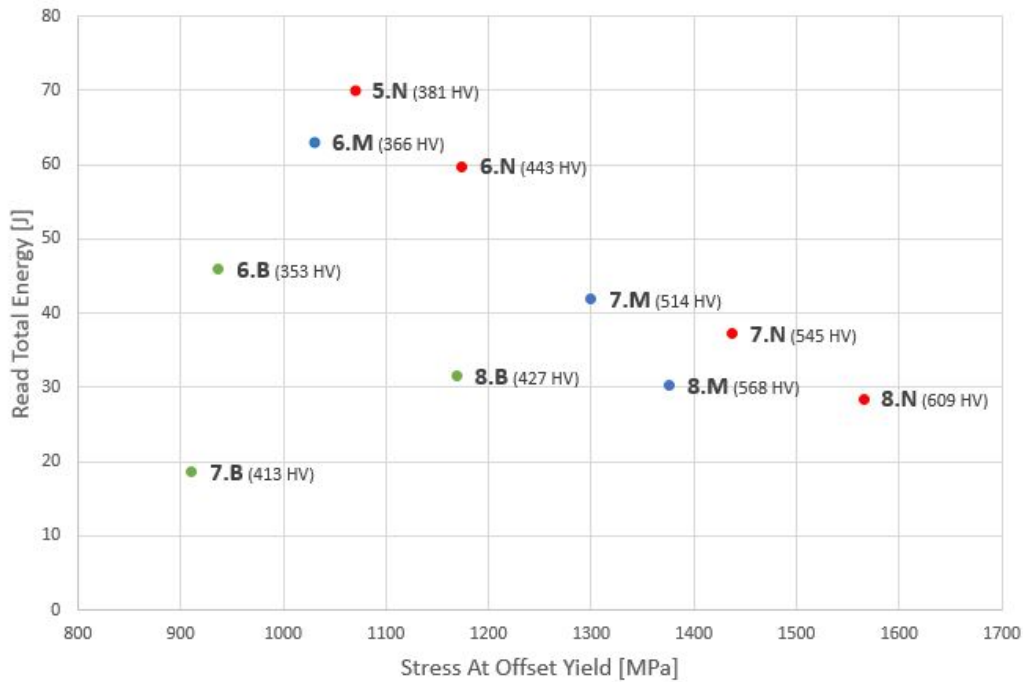


Figure 103: Stress at offset yield [MPa] as function of read total energy [J] for direct hardened (N), martempered (M) and austempered (B) 18MnCrSiMnVB6 (6), 27MnSiCrVB6 (7) and 35MnCrMoVB5 (8) are shown in Figure 103. Read dots are for direct hardening, blue dots for martempering and green dots for austempering. The hardness values are an average from the measured values after notch-impact and tensile testing.

5.4 The effect of silicon on austempered 100Cr6 and 100CrSiMn6-5-4

Austempered 100Cr6 (3.B and 3.B*) and 100CrSiMn6-5-4 (4.B and 4.B*) contains a similar amount of carbon, which was 1.044 and 0.995 wt.%, but the content of silicon was quite different. 100Cr6 contains 0.31 wt.% silicon and 100CrSiMn6-5-4 contains 1.216 wt.% silicon, according to Table 3. Toughness in bainitic steel can in principle be improved by using steels with a high silicon concentration (e.g. 1.5 wt %). Silicon has a negligible solubility in cementite and hence greatly retards its precipitation [14]. The addition of silicon enhances the toughness because the carbon that is usually precipitated as brittle cementite instead partitions into the residual austenite, allowing the latter to be retained [15].

Read total energy was higher for austempered 100Cr6 than for 100CrSiMn6-5-4. That was the case for both austenitizing at 1200 °C followed by a lower temperature and austenitizing only at one lower temperature, as given in Table 21. Tensile testing of austempered 100Cr6 and 100CrSiMn6-5-4 at only one lower austenitizing temperature showed a higher stress at offset yield for 100Cr6, as given in Table 23. It seems like the addition of silicon in 100CrSiMn6-5-4 did not have the assumed effect on the mechanical properties as described in the literature [14] [15, p. iii] for these alloys. Since the properties seemed to be worse for 100CrSiMn6-5-4 than for 100Cr6, an explanation can be that the microstructure had a higher degree of martensite compared to the microstructure of 100Cr6 [11, p. 314].

6 Conclusion

The mechanical properties of the high strength bainitic and martensitic steel alloys 42M13B, 50CrMo4, 100Cr6, 100CrSiMn6-5-4, 11M13CB, 18MnCrSiMoVB6, 27MnSiCrVB6 and 35MnCrMoVB5 in the hardened and untempered state have been studied. The main objective of the work was to investigate the possibility of using steel hardened to a bainitic microstructure instead of a martensitic microstructure. Mechanical properties resulting from the different heat treatments will contribute to a decision-basis. Conclusions from this work are summarized as follows:

Mechanical properties of bainite vs. martensite at similar hardness

- Direct hardened 42M13B and 50CrMo4, in addition to austempered 100Cr6 and 100CrSiMn6-5-4, austenitized at only one lower temperature between 840-900 °C had a hardness higher than the minimum required hardness of current plough shears.
- For a hardness of about 700 HV, direct hardened 42M13B had a read total energy from charpy testing, which was higher than for both austempered 100Cr6 and 100CrSiMn6-5-4. Direct hardened 50CrMo4 had a energy value similar to the austempered samples. All samples were austenitized at only one lower austenitizing temperature between 840-900 °C.
- For a hardness of about 700 HV, stress at offset yield was higher for austempered 100Cr6 and 100CrSiMn6-5-4 than for direct hardened 42M13B and 50CrMo4 austenitized at only one lower austenitizing temperature between 840-900 °C. Direct hardened 42M13B was the only one of these samples that reached peak stress.
- Direct hardened 11M13CB and austempered 18MnCrSiMoVB6, 27MnSiCrVB6 and 35MnCrMoVB5 had an average hardness higher than the minimum required hardness of current chains.
- For a hardness of about 400 HV, austempered 18MnCrSiMoVB6, 27MnSiCrVB6 and 35MnCrMoVB5 showed a significantly lower read total energy from charpy testing than direct hardened 11M13CB.
- For a hardness of about 400 HV, peak stress for austempered 27MnSiCrVB6 and 35MnCrMoVB5 were higher than for direct hardened 11M13CB. Austempered 18MnCrSiMoVB6 had a slightly lower peak stress than the direct hardened samples. All of the austempered samples had a grater area under the stress-stain curves than direct hardened 11M13CB. Austempered 18MnCrSiMoVB6 and 27MnSiCrVB6 had a significantly better elongation than direct hardened 11M13CB.

Effect of prior austenite grain size on mechanical properties of bainite vs. martensite

- For direct hardened and martempered 42M13B (1.N, 1.N* and 1.M*) and 50CrMo4 (2.N, 2.N* and 2.M*), in addition to austempered 100Cr6 (3.B and 3.B*) and 100CrSiMn6-5-4 (4.B and 4.B*), nearly all samples showed hardness values higher than the minimum

required hardness of current plough shears. The exception was martempered 42M13B (1.M*).

- Austempered 100Cr6 and 100CrSiMn6-5-4 austenitized at 1200 °C followed by a lower austenitizing temperature between 840-900 °C and austenitized at only one lower temperature, the read total energy was decreasing with increasing prior austenite grain size.
- Austempered 100Cr6 and 100CrSiMn6-5-4 austenitized only at one lower temperature between 840-900 °C gave better stress-strain properties than austenitizing at 1200 °C followed by a lower temperature.
- Notch-impact testing of the direct hardened and martempered samples of 42M13B and 50CrMo4 austenitized at 1200 °C followed by a lower austenitizing temperature at 870 °C and austenitizing only at one lower temperature, showed higher read total energy values for the fine grained samples of 42M13B compared to the coarser grained samples of this alloy. For 50CrMo4 the energy values were quite equal for all grain sizes.
- Direct hardening and martempering of 42M13B and 50CrMo4 austenitized at 1200 °C followed by a lower austenitizing temperature at 870 °C and austenitizing only at one lower temperature, the stress at offset yield was increasing with decreasing prior austenite grain size.

Tendency of mechanical properties for different hardness levels

- Direct hardening, martempering and austempering of 18MnCrSiMoVB6, 27MnSiCrVB6 and 35MnCrMoVB5 showed a trend where the direct hardened samples were hardest, the martempered samples second hardest and the austempered samples softest.
- Read total energy from charpy testing for 18MnCrSiMoVB6 and 27MnSiCrVB6 showed a trend where the energy values were highest for the martempered sample, lower for the direct hardened samples and lowest for the austempered samples. The values for read total energy of 35MnCrMoVB5 were quite similar for all tested heat treatments.
- Direct hardening, martempering and austempering of 18MnCrSiMoVB6, 27MnSiCrVB6 and 35MnCrMoVB5 showed a trend where the stress at offset yield and peak stress were highest for the direct hardened samples, lower for the martempered samples and lowest for the austempered samples. The ductility was highest for the austempered samples, lower for the martempered samples and lowest for the direct hardened samples.

The effect of silicon on austempered 100Cr6 and 100CrSiMn6-5-4

- Austempered 100CrSiMn6-5-4 showed poorer mechanical properties compared to austempered 100Cr6. A considerable difference between these alloys was the higher content of silicon in 100CrSiMn6-5-4.

7 Further work

The following are recommendations for further work that could be conducted in order to gain a deeper understanding of the topics investigated:

- Perform autenitizing at 1200 °C in 30 min followed by 10 min at a lower austenitizing temperature for all alloys, to be able to look at the effect of prior austenite grains on mechanical properties for bainite compared to martensite.
- If picric acid is available, try to etch prior austenite grain boundaries in a picric acid based etch at temperature.
- TEM (transmission electron microscopy) or SEM can be used for safer identification of bainite in the microstructure.
- Perform notch-impact, tension and hardness testing of current chain for better comparison.

8 Reference

References

- [1] SINTEF, RoHard Robust advanced steel quenching processes, <http://www.sintef.no/en/projects/rohard-robust-advanced-steel-quenching-processes/>, 2016, Online; accessed 13 September 2017.
- [2] K. E. THELNING, *Steels and its heat treatment*, Swerea IVF, 2012.
- [3] A. S. HALAND, Mechanical properties of steels for quenching and tempering in the hardened and untempered state, Technical report, 2017.
- [4] M.-Y. TU, C.-A. HSU, W.-H. WANG, and Y.-F. HSU, *Materials Chemistry and Physics* **107** (2008) 418â425 (2007).
- [5] J. K. SOLBERG, *Teknologiske metaller og legeringer*, NTNU, Instituttet for materialteknologi, 2014.
- [6] H. BHADESHIA, *Steels : microstructure and properties*, Elsevier, Amsterdam, 3rd ed. edition, 2006.
- [7] W. D. CALLISTER and D. G. RETHWISCH, *Materials science and engineering*, Wiley, Hoboken, N.J, 8th ed., si version. edition, 2011.
- [8] H. BHADESHIA and R. HONEYCOMBE, *Steels: Microstructure and Properties*, Elsevier Science, 4 edition, 2017.
- [9] H. BHADESHIA, POSCO Lectures on Bainite - Part 3, <https://www.youtube.com/watch?v=9-KuMd4w8bI>, 2011, Online; accessed may 4 2018.
- [10] D. H. HERRING, *Industrial Heating* **72** (2005).
- [11] H. BHADESHIA, *Bainite in steels: Theory and practice*, Maney Publishing, 2015.
- [12] *ASM Handbook: Heat Treating. Vol. 4*, 1991.
- [13] H. ALTENA and K. BUCHER, Process technology and plant design for bainite hardening, in *Trattamenti termici*, 2015.
- [14] H. BHADESHIA, *J PHYS. IV FRANCE 7 (1997) Colloque C5, SupplCment au Journal de Physique III de novembre 1997* (1997).
- [15] A. S. PODDER, *Tempering of a Mixture of Bainite and Retained Austenite*, PhD thesis, St. Johnâs College, Cambridge, 2011.
- [16] F. T. HAN, , B. C. HWANG, D. W. SUH, Z. C. WANG, D. L. LEE, and S. J. KIM, *Metals and Materials International (MMI)* **14** (2008).
- [17] S. N. GHALI, H. S. EL-FARAMAWY, and M. M. EISSA, *Scientific Research* (2012).
- [18] S.-J. LEE and Y.-K. LEE, *Materials and Design* **29**, 1840 (2008).
- [19] ASTM E112 Standard Test Methods for Determining Average Grain Size.
- [20] Metallic materials - Charpy pendulum impact test - Part 1: Test method (ISO 148-1:2016).

- [21] N. E. DOWLING, *Mechanical behavior of materials : engineering methods for deformation, fracture, and fatigue*, Pearson Education, Boston, Mass, 4th ed. edition, 2013.
- [22] G. E. DIETER, *Mechanical metallurgy*, McGraw-Hill series in materials science and engineering, McGraw-Hill, London, si metric ed. edition, 1988.
- [23] Metallic materials - Tensile testing - Part 1: Method of test at room temperature (ISO 6892-1:2016).
- [24] H. BHADESHIA, Interpretation of the Microstructure of Steels, <https://www.phase-trans.msm.cam.ac.uk/2008/SteelMicrostructure/SM.html>, 2008, Online; accessed 15 April 2018.
- [25] V. J. COLANGELO, *Analysis of metallurgical failures*, Wiley, New York, 2nd ed. edition, 1987.
- [26] OVAKO, 50CrMo4, <https://steelnavigator.ovako.com/steel-grades/50crmo4/>, Online; accessed 6 February 2018.
- [27] OVAKO, 100Cr6, <https://steelnavigator.ovako.com/steel-grades/100cr6/>, Online; accessed 2 February 2018.
- [28] T. SOURMAIL, F. MOUDIAN, M. BILLET, and M. MILLOT-MEHEUX, *Bearing steel technologies: 11th volume* (2017).
- [29] T. SOURMAIL, *Email correspondence*, R&D Section Manager - Metallurgy (Ascometal).
- [30] ASTM E407-07(2015) Standard Practice for Microetching Metals and Alloys.
- [31] G. PETZOW, *Metallographic Etching*, American society for metals.
- [32] Metallic materials - Charpy V-notch pendulum impact test - Instrumented test method (ISO 14556:2015).

9 Appendix

A Converting weight percent to atomic percent

Equation 6 shows how to convert weight percent (wt.%) to atom percent (at.%). A_x is the atomic weight [g/mol] of element x and x,y,z.... are the different elements in the steel.

$$at.\%(x) = \frac{wt.\%(x)/A_x}{wt.\%(x)/A_x + wt.\%(y)/A_y + wt.\%(z)/A_z.....} * 100 \quad (6)$$

B Control measurement of notch-impact samples

Control measurement of notch-impact samples were done using measuring tools on Leica MEF4M light microscope, as shown in Figure 104.

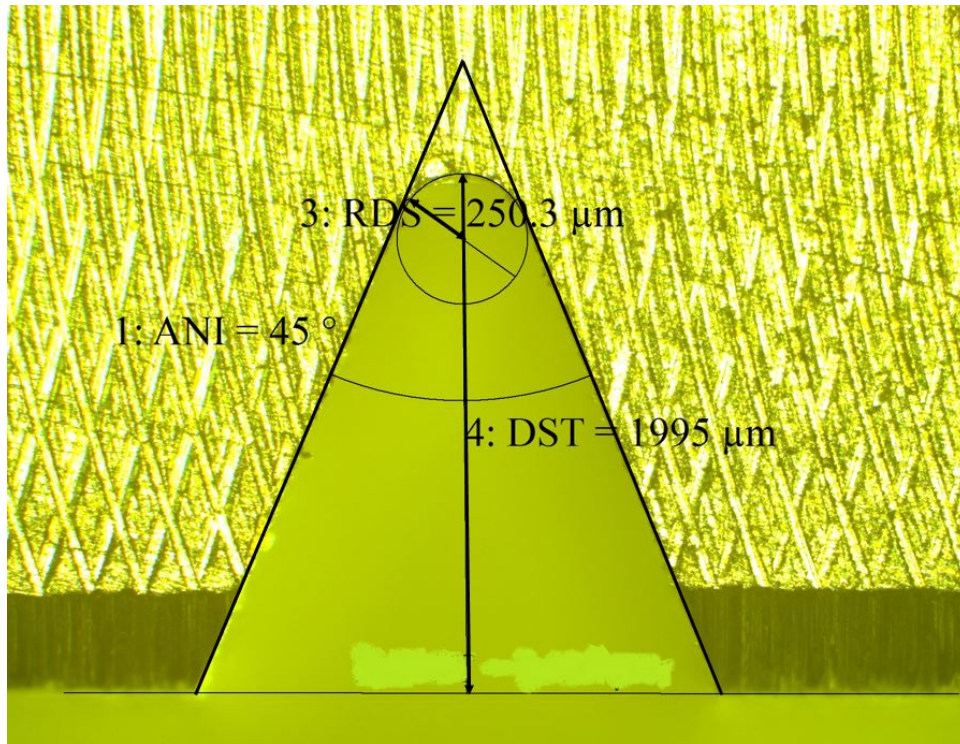


Figure 104: Control measurement of the notch in the samples for notch-impact testing. The image was taken using Leica MEF4M with magnification of 25x.

C Key data for all tested notch-impact samples

The energy used in breaking the samples or the dial value [kgm] that were read directly from the dial on the notch-impact machine, are given for all tested samples in Table 30 and 31.

Table 30: *The dial value [kgm] of 42M13B, 50CrMo4, 100Cr6 and 100CrSiMn6-5-4.*

Sample	Dial Value [kgm]
1.N1	1.62
1.N2	1.65
1.N3	1.5
1.N1*	1.08
1.N2*	1.15
1.N3*	1.1
1.M1*	1.1
1.M2*	1.05
1.M3*	1
2.N1	0.85
2.N2	0.88
2.N3	0.9
2.N1*	0.8
2.N2*	0.88
2.N3*	0.8
2.M1*	0.88
2.M2*	0.88
2.M3*	0.92
3.B1	0.91
3.B2	0.89
3.B3	0.9
3.B1*	0.5
3.B2*	0.49
3.B3*	0.53
4.B1	0.72
4.B2	0.95
4.B3	0.63
4.B4	0.69
4.B1*	0.4
4.B2*	0.4
4.B3*	0.45

Table 31: *The dial value [kgm] of 11M13CB, 18MnCrSiMoVB6, 27MnSi-CrVB6 and 35MnCrMoVB5.*

Sample	Dial Value [kgm]
5.N1	5.35
5.N2	5.12
5.N3	5.3
6.N1	4.33
6.N2	5.1
6.N3	3.8
6.N4	4.82
6.M1	4.33
6.M2	4.38
6.M3	6.2
6.M4	4.12
6.B1	3.6
6.B2	3.5
6.B3	3.4
7.N1	3
7.N2	2.43
7.N3	3.25
7.N4	2.8
7.M1	3.19
7.M2	3.05
7.M3	3.4
7.B1	1.62
7.B2	1.47
7.B3	1.45
8.N1	2.35
8.N2	2.09
8.N3	2.25
8.M1	2.35
8.M2	2.3
8.M3	2.45
8.B1	2.5
8.B2	2.3
8.B3	2.58

D Fracture surfaces

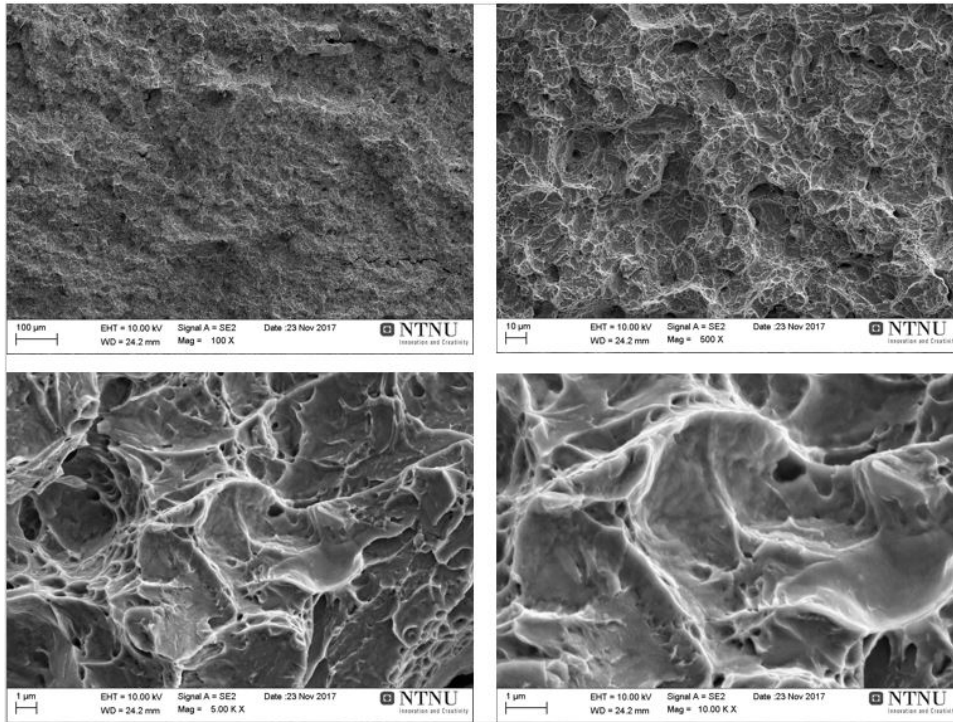


Figure 105: Scanning electron microscopy image from fracture surface of notch-impact tested direct hardened 42M13B (1.N). The images were taken with magnification 100x, 500x, 5000x and 10000x.

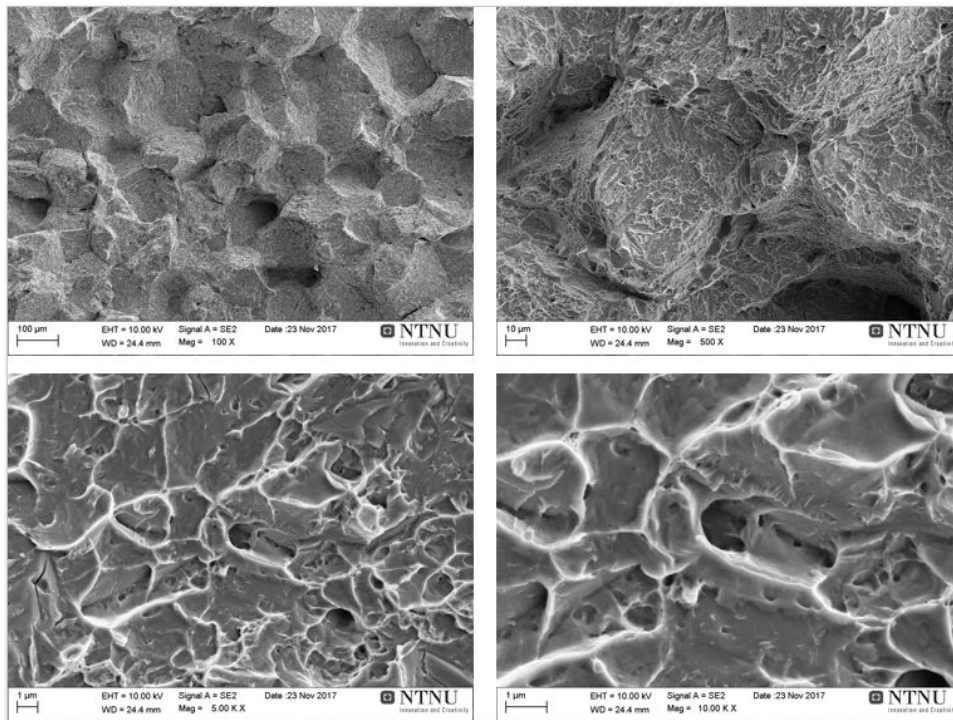


Figure 106: Scanning electron microscopy image from fracture surface of notch-impact tested direct hardened 42M13B (1.N*). The images were taken with magnification 100x, 500x, 5000x and 10000x.

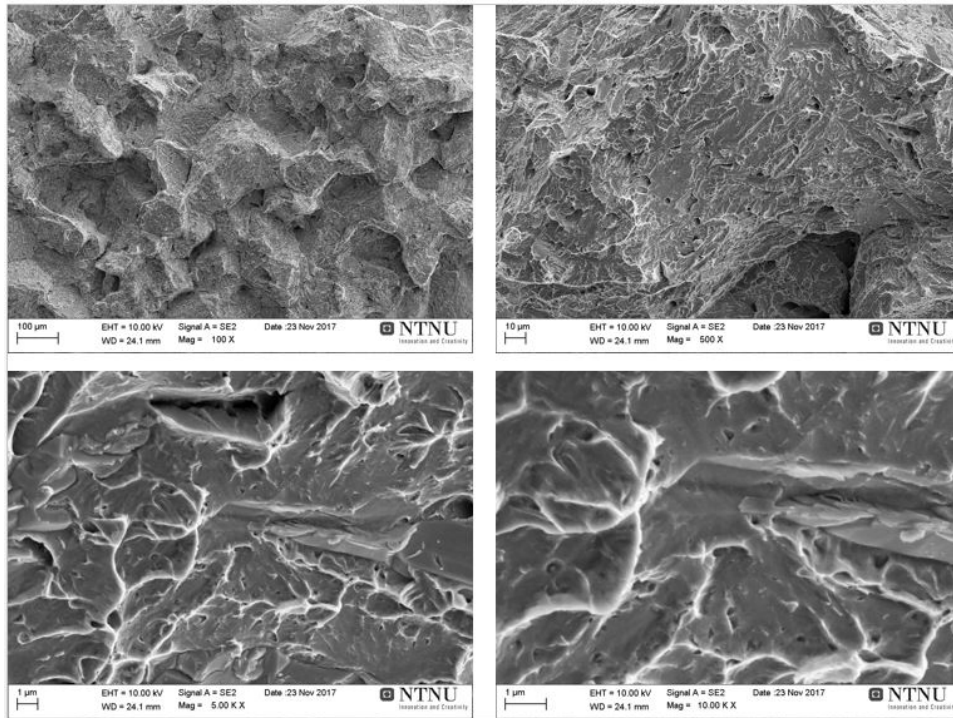


Figure 107: Scanning electron microscopy image from fracture surface of notch-impact tested martempered 42M13B (1.M*). The images were taken with magnification 100x, 500x, 5000x and 10000x.

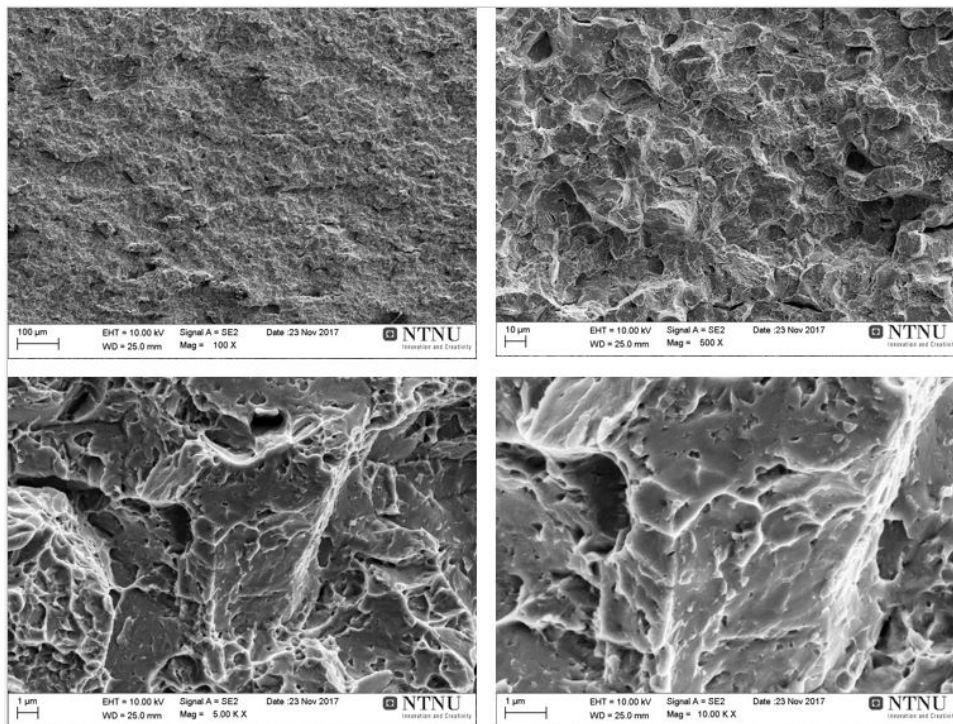


Figure 108: Scanning electron microscopy image from fracture surface of notch-impact tested direct hardened 50CrMo4 (2.N). The images were taken with magnification 100x, 500x, 5000x and 10000x.

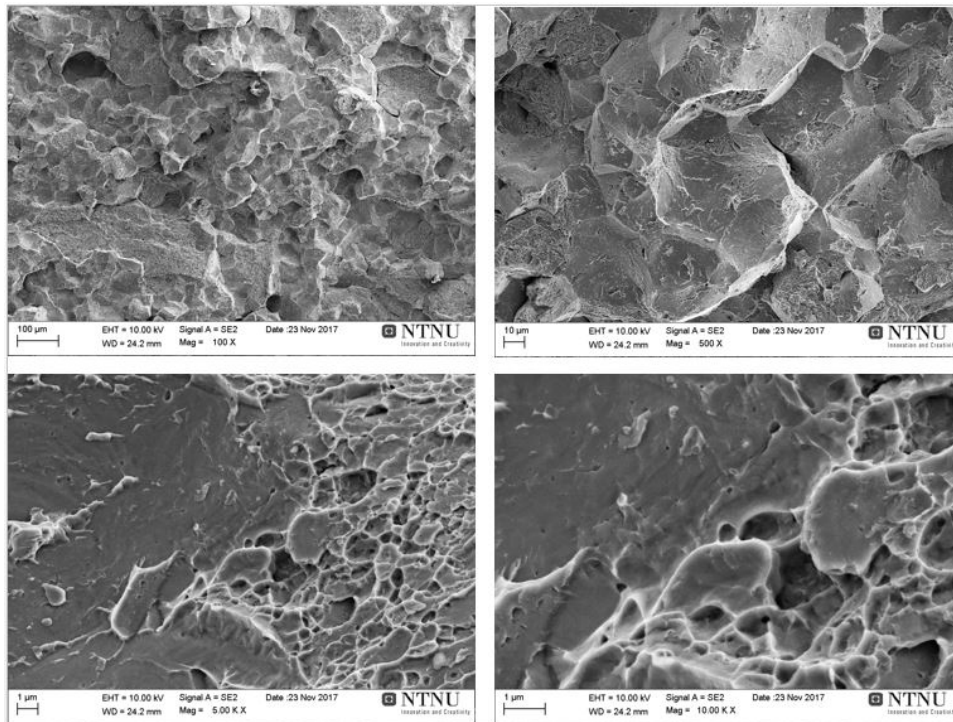


Figure 109: Scanning electron microscopy image from fracture surface of notch-impact tested direct hardened 50CrMo₄ (2.N*). The images were taken with magnification 100x, 500x, 5000x and 10000x.

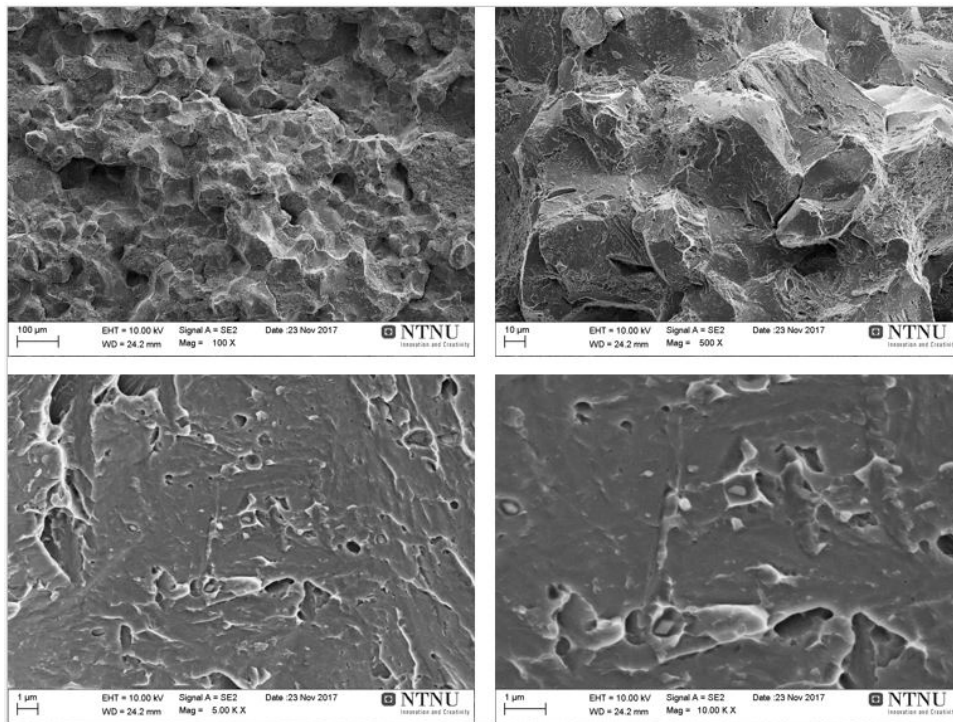


Figure 110: Scanning electron microscopy image from fracture surface of notch-impact tested martempered 50CrMo₄ (2.M*). The images were taken with magnification 100x, 500x, 5000x and 10000x.

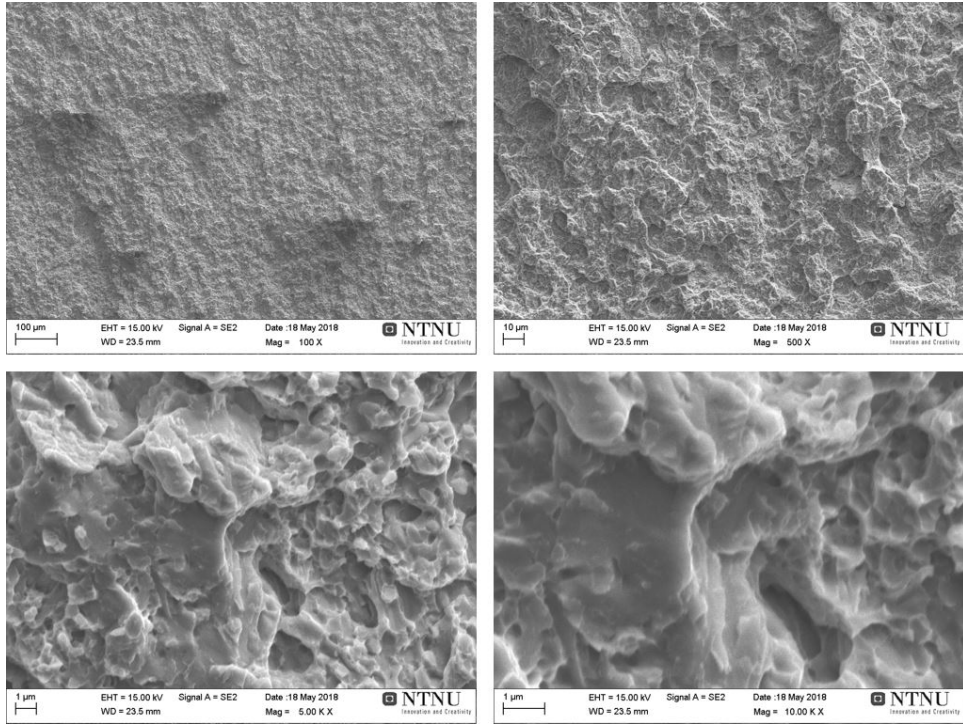


Figure 111: Scanning electron microscopy image from fracture surface of notch-impact tested austempered 100Cr6 (3.B). The images were taken with magnification 100x, 500x, 5000x and 10000x.

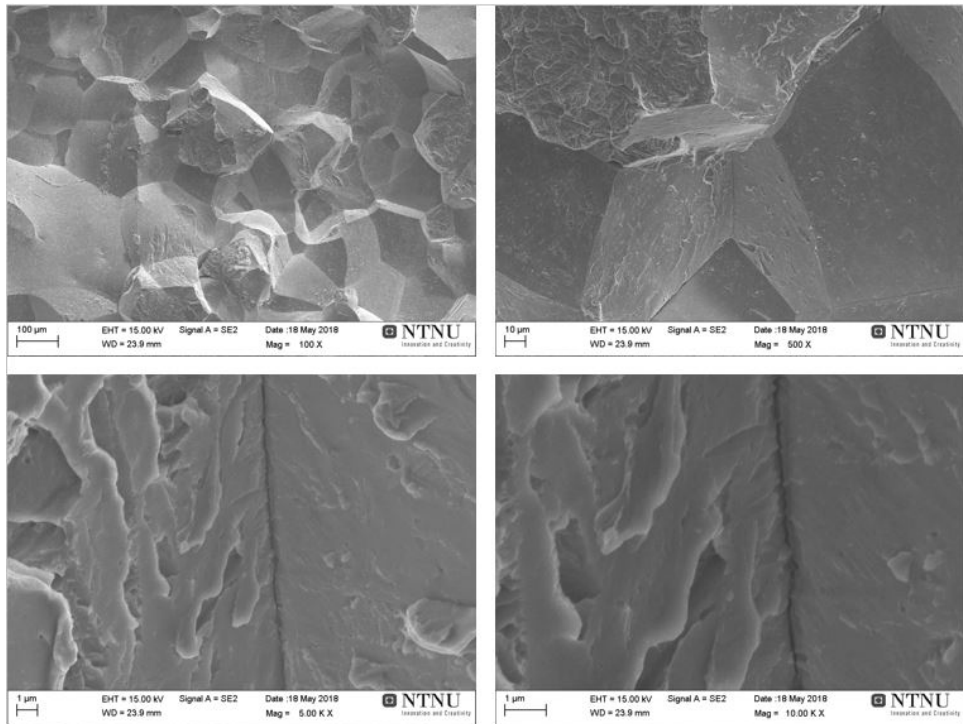


Figure 112: Scanning electron microscopy image from fracture surface of notch-impact tested austempered 100Cr6 (3.B*). The images were taken with magnification 100x, 500x, 5000x and 10000x.

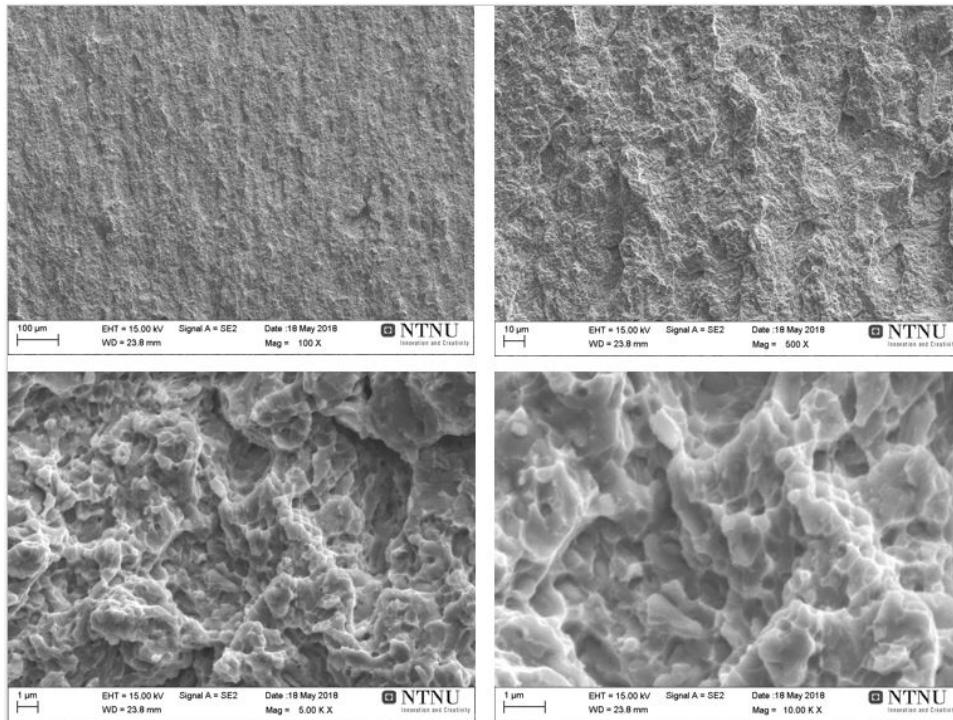


Figure 113: Scanning electron microscopy image from fracture surface of notch-impacted austempered 100CrSiMn6-5-4 (4.B). The images were taken with magnification 100x, 500x, 5000x and 10000x.

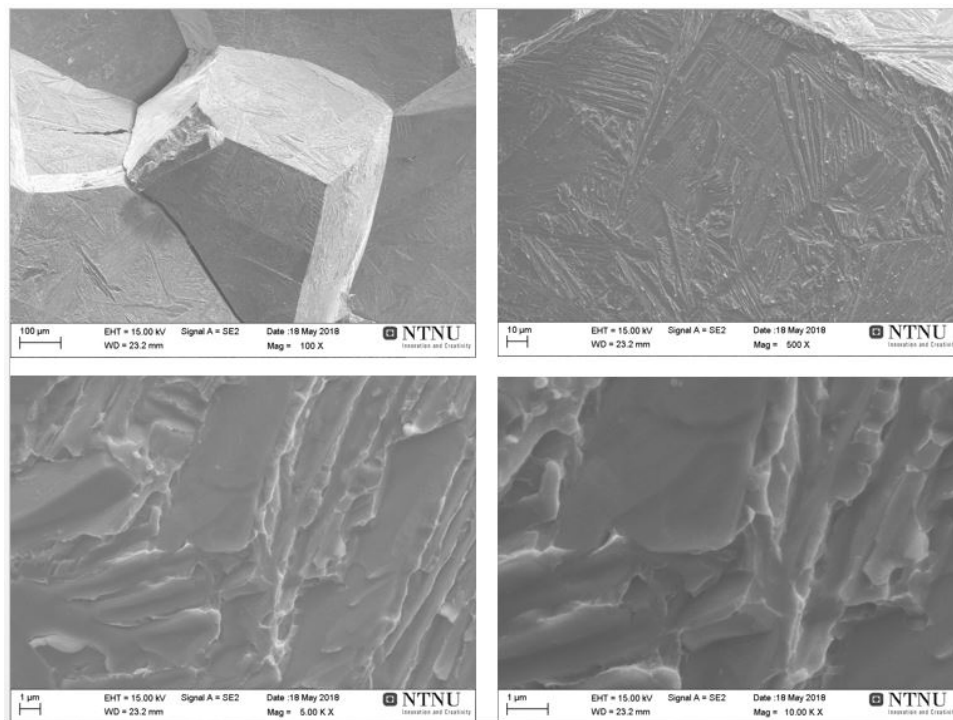


Figure 114: Scanning electron microscopy image from fracture surface of notch-impacted austempered 100CrSiMn6-5-4 (4.B*). The images were taken with magnification 100x, 500x, 5000x and 10000x.

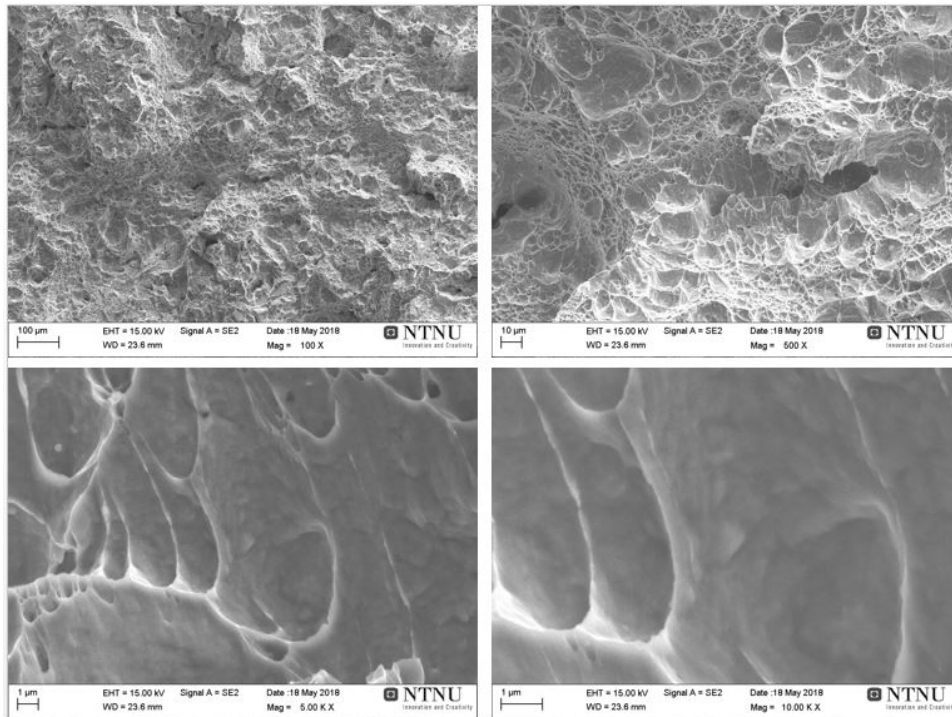


Figure 115: Scanning electron microscopy image from fracture surface of notch-impact tested direct hardened 11M13CB (5.N). The images were taken with magnification 100x, 500x, 5000x and 10000x.

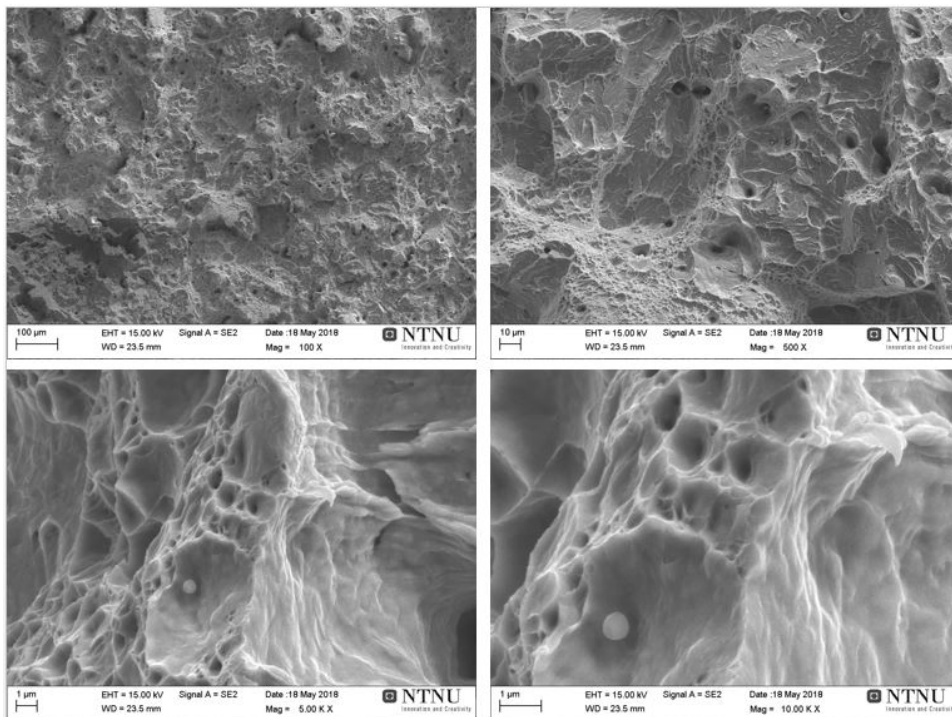


Figure 116: Scanning electron microscopy image from fracture surface of notch-impact tested direct hardened 18MnCrSiMoVB6 (6.N). The images were taken with magnification 100x, 500x, 5000x and 10000x.

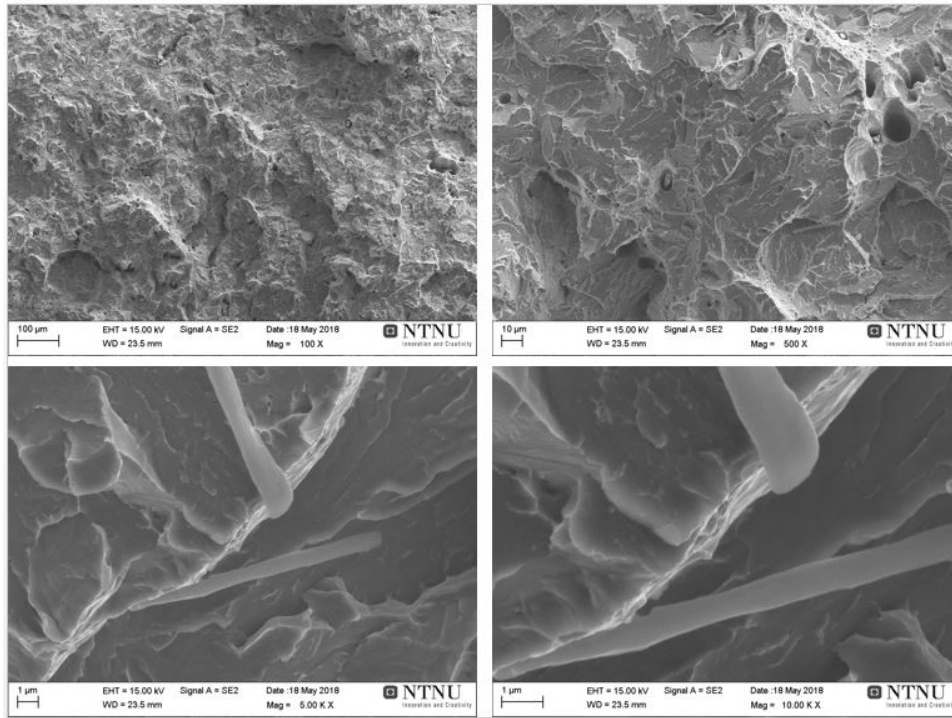


Figure 117: Scanning electron microscopy image from fracture surface of notch-impact tested martempered 18MnCrSiMoVB6 (6.M). The images were taken with magnification 100x, 500x, 5000x and 10000x.

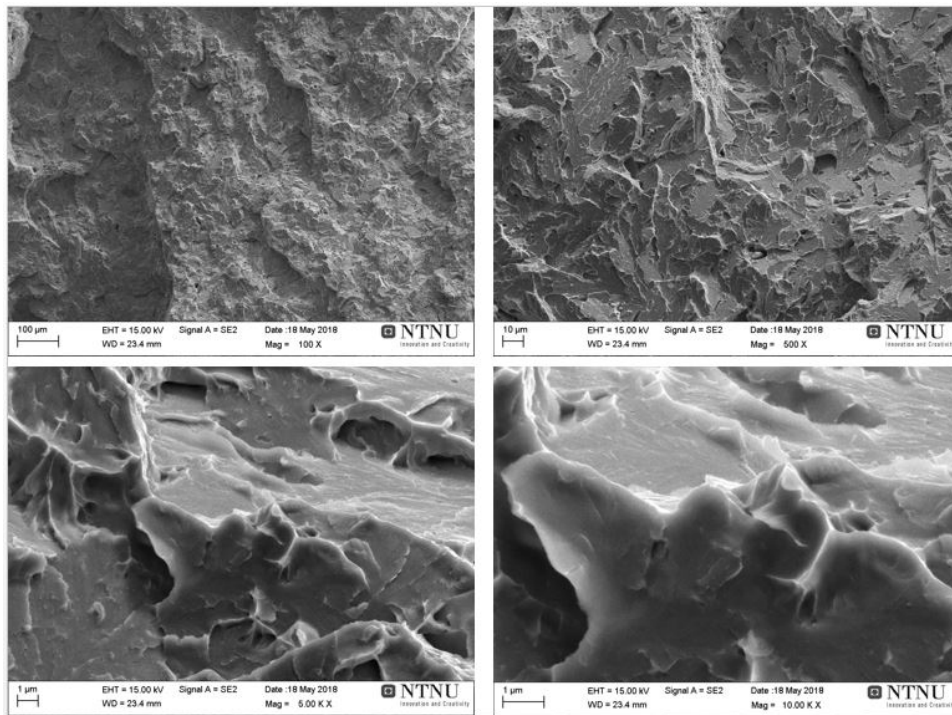


Figure 118: Scanning electron microscopy image from fracture surface of notch-impact tested austempered 18MnCrSiMoVB6 (6.B). The images were taken with magnification 100x, 500x, 5000x and 10000x.

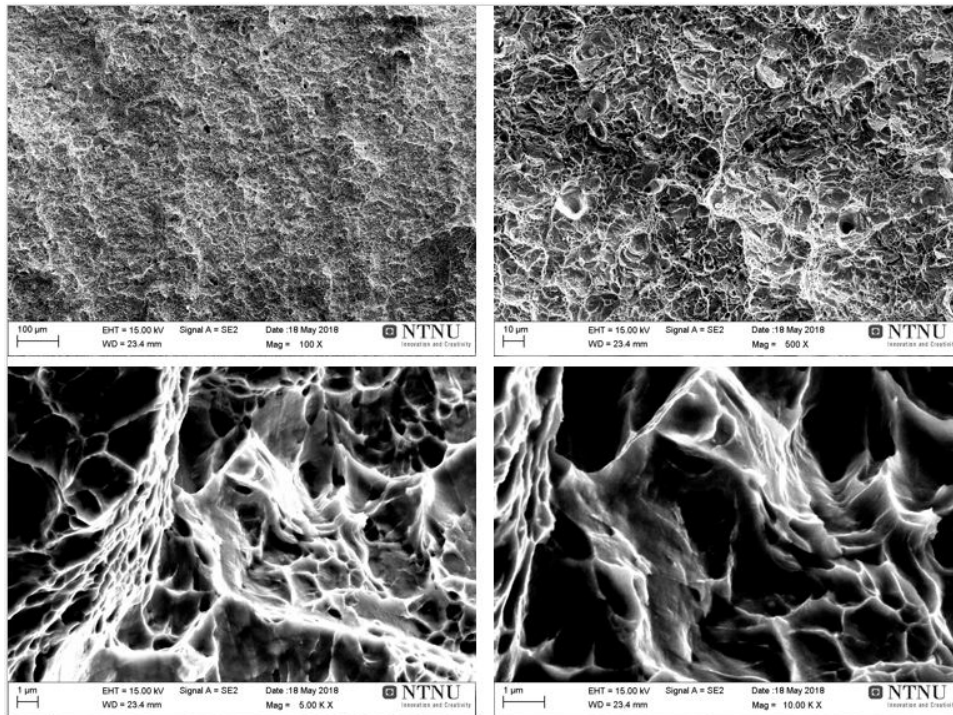


Figure 119: Scanning electron microscopy image from fracture surface of notch-impact tested direct hardened 27MnSiCrVB6 (7.N). The images were taken with magnification 100x, 500x, 5000x and 10000x.

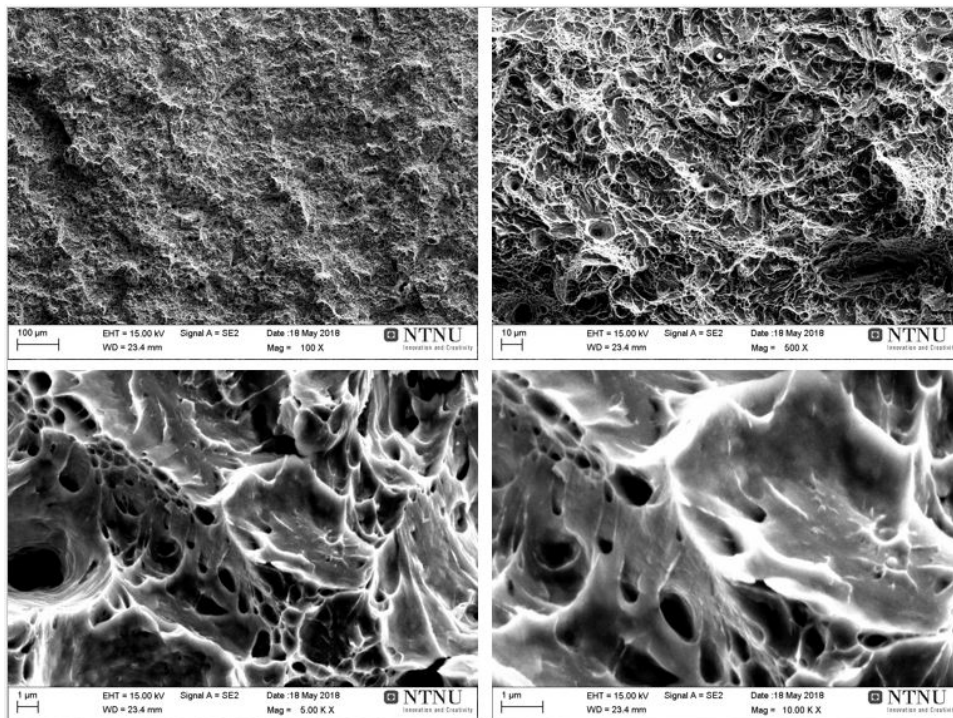


Figure 120: Scanning electron microscopy image from fracture surface of notch-impact tested martempered 27MnSiCrVB6 (7.M). The images were taken with magnification 100x, 500x, 5000x and 10000x.

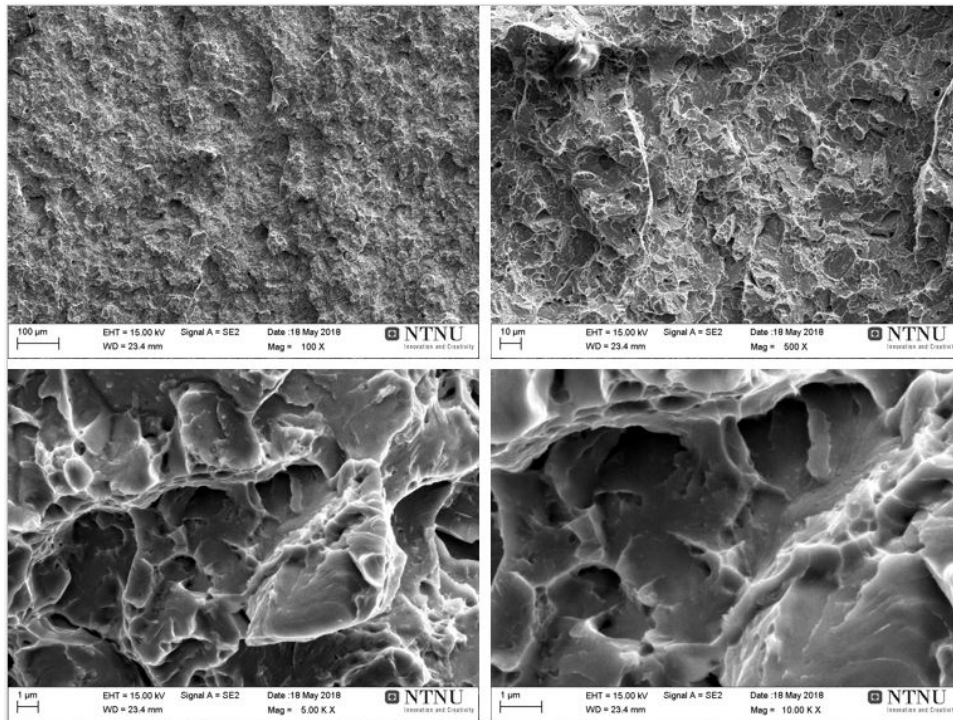


Figure 121: Scanning electron microscopy image from fracture surface of notch-impact tested austempered 27MnSiCrVB6 (7.B). The images were taken with magnification 100x, 500x, 5000x and 10000x.

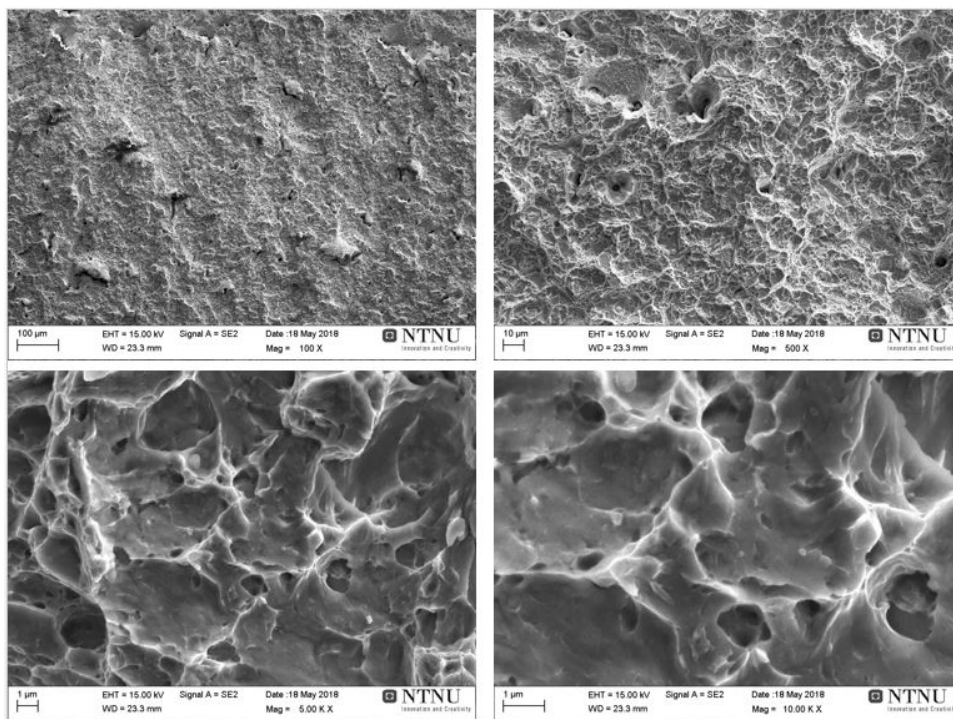


Figure 122: Scanning electron microscopy image from fracture surface of notch-impact tested direct hardened 35MnCrMoVB6 (8.N). The images were taken with magnification 100x, 500x, 5000x and 10000x.

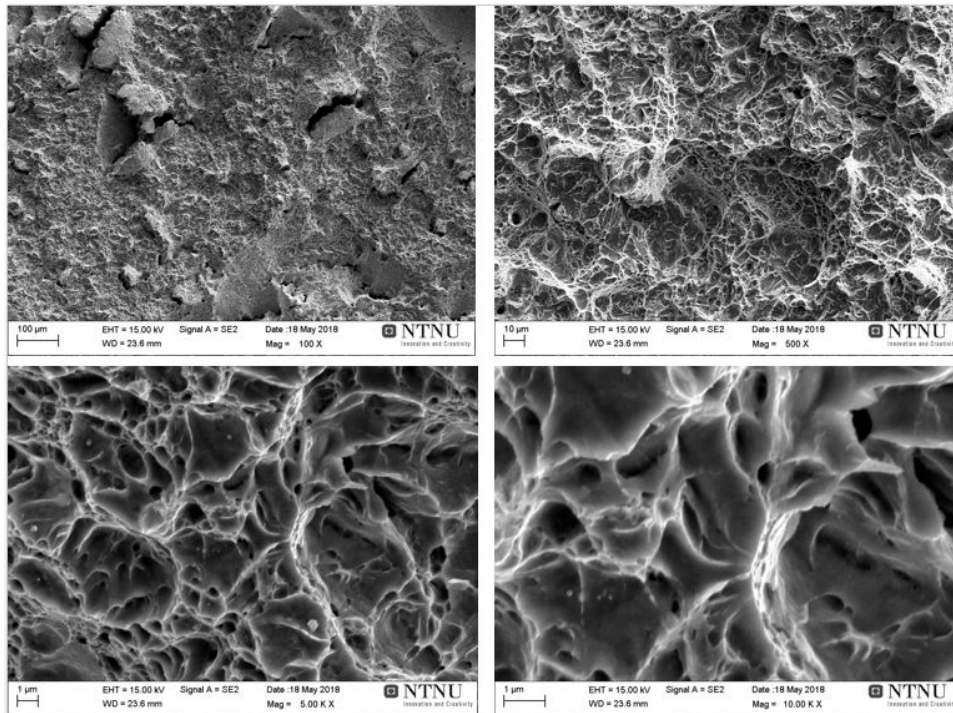


Figure 123: Scanning electron microscopy image from fracture surface of notch-impact tested martempered 35MnCrMoVB6 (8.M). The images were taken with magnification 100x, 500x, 5000x and 10000x.

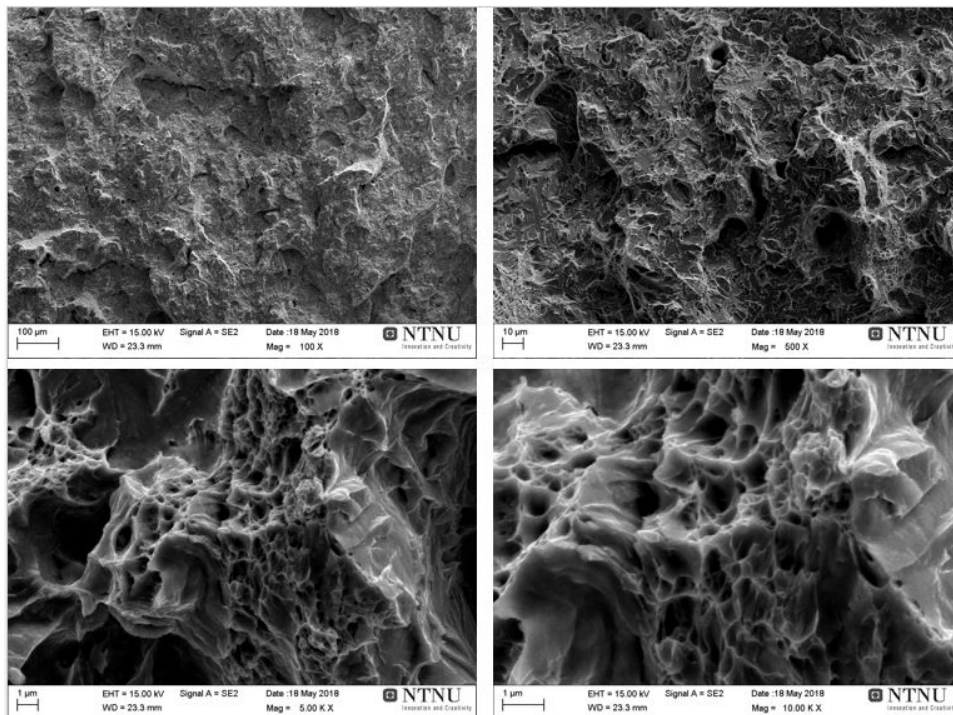


Figure 124: Scanning electron microscopy image from fracture surface of notch-impact tested austempered 35MnCrMoVB6 (8.B). The images were taken with magnification 100x, 500x, 5000x and 10000x.